

UNIVERSITY OF MANITOBA

THE COARSENING BEHAVIOUR OF
 γ'' AND γ' PARTICLES IN INCONEL 718

BY

HAN YA FANG

A THESIS SUBMITTED TO THE
FACULTY OF GRADUATE STUDIES IN
PARTIAL FULFILLMENT OF THE
REQUIREMENTS FOR THE DEGREE
OF MASTER OF SCIENCE IN MECHANICAL ENGINEERING

DEPARTMENT OF MECHANICAL ENGINEERING
WINNIPEG, MANITOBA

November 1981

THE COARSENING BEHAVIOUR OF
"γ AND γ' PARTICLES IN INCONEL 718

BY

HAN YAFANG

A thesis submitted to the Faculty of Graduate Studies of
the University of Manitoba in partial fulfillment of the requirements
of the degree of

MASTER OF SCIENCE

© 1982

Permission has been granted to the LIBRARY OF THE UNIVER-
SITY OF MANITOBA to lend or sell copies of this thesis, to
the NATIONAL LIBRARY OF CANADA to microfilm this
thesis and to lend or sell copies of the film, and UNIVERSITY
MICROFILMS to publish an abstract of this thesis.

The author reserves other publication rights, and neither the
thesis nor extensive extracts from it may be printed or other-
wise reproduced without the author's written permission.

ABSTRACT

The coarsening behaviour of disc-shaped B.C.T. (DO_{22}) γ'' phase and spherically ordered F.C.C. (LI_2) γ' phase, both of which are coherent with F.C.C. matrix in Inconel 718 has been investigated by transmission electron microscopy. The growth kinetics of both γ'' and γ' precipitates has been observed to follow the Lifshitz-Wagner theory of lattice diffusion controlled growth at the aging temperatures of 973 K, 998 K and 1023 K. The activation energies of 298 KJ mol^{-1} for γ'' and 271 KJ mol^{-1} for γ' growth process obtained during the present investigation are in reasonable agreement with previously published data for the activation energies for the diffusion of solute atoms present in Inconel 718. However, the particle-size distribution of γ'' and γ' phase is significantly broader than the distribution predicted by the Lifshitz-Wagner theory, especially for γ'' precipitate. This discrepancy could be due to the effect of an "encounter" process between growing particles or to a relatively large lattice misfit between the precipitates and the matrix.

ACKNOWLEDGEMENTS

I would like to express my appreciation to my supervisor, Dr. M.C. Chaturvedi, for his precious guidance and sincere help. I am grateful for his financial support.

I am also grateful to Dr. J. Cahoon and Dr. P. Deb for their helpful suggestions and discussion, and I would like to thank Mr. John Van Dorp and Mr. Don Mardis for their very useful technical assistance.

I would also like to thank the Government of Peoples Republic of China for the financial support and Institute of Aeronautical Materials, Beijing, China for giving me leave-of-absence, and finally, I would like to express my thanks to my husband for his endless encouragement and help throughout my studies.

TABLE OF CONTENTS

	<u>Page</u>
ABSTRACT	i
ACKNOWLEDGEMENTS	ii
TABLE OF CONTENTS	iii
LIST OF TABLES	v
LIST OF FIGURES	vi
 <u>CHAPTER</u>	
1 INTRODUCTION	1-2
2 LITERATURE REVIEW	3-51
2.1 The influence of precipitate size on the yield strength . . .	4-17
2.2 Precipitation in a solid solution	17-46
2.2.1 Nucleation of precipitates from supersaturated solid solution	18-22
2.2.2 Growth of precipitates from supersaturated solid solution	22-23
2.2.3 The general coarsening process	24-46
2.2.3.1 The lattice diffusion controlled coarsening	28-35
2.2.3.2 Time-dependent of particle-size distribution	35-39
2.2.3.3 Effect of volume fraction on coarsening behaviour	39-46
2.3 Experimental observation of precipitate coarsening	46-49
2.4 Precipitates in nickel-base superalloys	49-51

<u>CHAPTER</u>	<u>Page</u>
3	EXPERIMENTAL TECHNIQUES 52-56
3.1	Materials 52
3.2	Rolling and heat treatment 52
3.3	Preparation of thin foils and electron microscopy 54
3.4	Volume fraction determination 54-55
3.5	X-ray diffraction technique 56
4	RESULTS 57-103
4.1	Precipitation behaviour of Inconel 718 57-74
4.1.1	Microstructure of solution treated specimens 57-62
4.1.2	Structures of aged specimens 67-70
4.1.3	The volume fraction of precipitates 70-74
4.2	Growth rate of precipitates 75-79
4.3	Activation energy 79-88
4.4	Distribution of precipitate particle size 88-103
5	DISCUSSION 104-117
5.1	Precipitation behaviour 104
5.1.1	The presence of precipitates in solution treated condition 104-105
5.1.2	Lattice parameter of γ matrix 106
5.1.3	Volume fraction of precipitates 106-107
5.1.4	Interaction between γ' and γ'' phases 107-109
5.2	Growth kinetics 110-112
5.3	The distribution of particle size 112-115
6	CONCLUSION 116-117
	REFERENCES 118-120

LIST OF TABLES

<u>Table</u>		<u>Page</u>
1	Chemical composition of Inconel 718	53
2	X-ray results of the lattice parameter of solution treated Inconel 718	61
3	Volume fraction of γ' and γ'' precipitates measured by electron micrographs	72
4	Experimentally determined volume fraction $f_v (\gamma' + \gamma'')$	73
5	Measured average particle size	78
6	Experimentally determined values of rate constants K and mean onset particle size \bar{d}_0	80
7	Slopes of log (particle size) vs. log (aging time) plots	81
8	Data for the determination of activation energy Q	89

LIST OF FIGURES

<u>Figure</u>		<u>Page</u>
1	Dislocation held up at obstacles	5
2	The relationship between γ' particle size and shear proof stress increase	11
3	The theoretical and experimentally observed particle size/proof stress increase relationships for V1682 aged at 975K	12
4	Dependence of initial flow-stress upon Ni_3Al particle size for Ni-12.7 at % Al; $f=0.057$	13
5	Variation in Δt with $r^{1/2}$ in Co-Ni-Cr superalloy	15
6	The relationship between yield strength and aging time for γ Inconel 718	16
7	Free energy-compositional relationship for a conventional nucleation and growth process	19
8	Schematic representation of the free energy of a nucleus plotted against its radius	20
9	Two spherical β precipitates of radius r_1 and r_2 in an α matrix	27
10	a) An array of precipitates around a particular precipitate of radius r b) Variation in concentration around this particle	30
11	Variation in precipitate growth rate dr/dt with precipitate radius r for diffusion controlled grow for two different values of the mean radius \bar{r}	33

<u>Figure</u>		<u>Page</u>
12	Expected distribution of particle size for diffusion controlled coarsening of LSW theory	37
13	Variation in the rate constant, $K(\phi)$, for diffusion-controlled coarsening with the volume fraction ϕ	41
14	The dependence of the theoretical distribution of particle sizes on the volume fraction ϕ	42
15	The effect of volume fraction on the parameter γ and on the ratio of the rate constant, K_e	44
16	LSEM particle size distribution as a function of volume fraction of precipitate	45
17	Typical experimental result for particle coarsening for γ' precipitate in Ni-Al alloys	47
18	Microstructure of solution treated Inconel 718 annealing for 1 hour at 1200°C and water quenching. Bright field	58
19	The selected area diffraction pattern of structure shown in Fig. 18. a) regular project lens current b) reduced project lens current	59
20	Thin film structure of a specimen aged for 200 hours at 998K. Bright field	63
21	The selected area diffraction pattern of structure shown in Fig. 20	64
22	The dark field micrographs of structure for 1023K, 30 hours aged specimen. (001) orientation	66

<u>Figure</u>	<u>Page</u>	
23	Unit cell showing ordering a) BCT (DO_{22}) structure b) FCC (LI_2) structure	67
24	Typical Morphology of γ' and γ'' precipitates	69
25	The difference in shape of γ'' particles for different aging time	71
26	The variation in the total volume fraction $f_v(\gamma' + \gamma'')$ with aging time of Inconel 718 .	74
27	The variation in γ' (diameter) ³ with aging time at different aging temperature	82
28	The variation in γ'' (diameter) ³ with aging time at different aging temperature	83
29	Log plots of mean diameter of γ'' vs. aging time at different aging temperature	84
30	Log plots of mean thickness of γ'' vs. aging time at different aging temperature .	85
31	Log plots of mean diameter of γ' vs. aging time at different aging temperature .	86
32	Arrhenius plots for the determination of the activation energy for coarsening of γ' and γ'' phases	90
33	Comparison of the experimental histograms for γ' particles with the theoretical distribution function $\rho^2 h(\rho)$	94
34	Comparison of the experimental histograms for γ'' particles with the theoretical distribution function $\rho^2 h(\rho)$	95
35	Observed and theoretical distribution of γ' particle size for different aging temperature after various aging time A) 973 K; B) 998 K; C) 1023 K	96-99

<u>Figure</u>		<u>Page</u>
36	Observed and theoretical distribution of γ'' particle size for different aging temperature after various aging time A) 973 K B) 998 K C) 1023K	100-103
37	Microstructure of the specimen aged for 100 hours at 998 K, showing the inter- action between γ' and γ'' phases	109

CHAPTER 1

INTRODUCTION

The growth kinetics of second phase particles in precipitation strengthened alloys has been extensively studied, as the particle size and distribution significantly effect the mechanical properties of these alloys. For most cases precipitation strengthening superalloys operate at high temperatures where rapid diffusion occurs and therefore the coarsening of precipitates can not be avoided. γ' phase is the most widely used strengthening phase in nickel-base and some of the cobalt-base superalloys, and its coarsening behaviour has been widely investigated during the past twenty years⁽¹⁻⁶⁾. The growth of γ' precipitate particles has been confirmed to follow the theory of lattice diffusion controlled growth developed by Lifshitz and Slyozov⁽⁷⁾ and Wagner⁽⁸⁾ (LSW theory). The main points of the LSW theory are as follows: 1) the driving force for the coarsening process is the reduction in the interfacial energy due to a decrease in the particle-matrix interfacial area; 2) the mean particle size is proportional to the cube root of aging time; 3) the activation energy for the coarsening process is equal to that for the diffusion of solute atoms in the

matrix; 4) the particle size distribution at aging time t is independent of the distribution at the onset of the coarsening process and maximum particle size is 1.5 times the mean particle size.

Another strengthening phase commonly observed in nickel base superalloys is γ'' phase. This phase has a B.C.T. structure, is disc shaped and precipitates coherently with F.C.C. matrix. The growth process of γ'' phase has been observed to follow the $t^{1/3}$ law in some alloy systems^(9,10) and the $t^{1/2}$ law in others^(11,12). Inconel 718 is a commercial nickel-iron base superalloy and has excellent strength at room temperature as well as at the intermediate temperature of about 920 K. Two major strengthening phase γ'' and γ' , exist simultaneously in this alloy.

This thesis is concerned with the coarsening behaviour of γ'' and γ' precipitates in Inconel 718 within the temperature range of 973 - 1023 K.

CHAPTER 2
LITERATURE REVIEW

The yield strength of two-phase or precipitation hardening alloys depends upon the following factors: volume fraction of precipitates, particle size and distribution of precipitates, antiphase boundary energy of precipitates, lattice misfit between precipitates and matrix, and solid solution strengthening of both matrix and precipitates. Most of these factors depend on the composition of the alloy systems and are not very sensitive to the aging (or operating) temperature and time, except for the first two factors. Furthermore, in general, the volume fraction of precipitate reaches a constant value very soon during aging. Therefore only particle size and distribution will generally change during the heat treatment or during service, which can greatly influence the mechanical properties of alloys. Therefore studies of the growth characteristics of precipitate particles are of great importance. In this chapter the influence of particle size on the yield strength of two phase alloys is reviewed, which is followed by a review of precipitate particle coarsening.

2.1 The influence of precipitate size on the yield strength

Second-phase particles can increase the strength of an alloy in one or two ways. The particles may act as impenetrable barriers to dislocation motion and force the glide dislocations to bow-out and by-pass them following the Orowan mechanism. Alternatively, the second-phase particles may be cut or sheared by the glide dislocations at stresses below the Orowan stress.

The stress required to initiate plastic flow, i.e., critical resolved shear stress, is the stress required to send a dislocation a large distance through the array of precipitates. This stress is a threshold stress for plastic flow, and the theoretical treatment of second-phase particle strengthening is based on the following model. The glide dislocation bows out between the particles as shown in Figure 1 and, when the included angle ϕ between the two arms of the dislocation reaches a certain critical value, the dislocation breaks away from the obstacle. This value of angle ϕ is referred to as the breaking angle, and at this critical point the obstacle strength, F , is related to the dislocation line tension, T , by

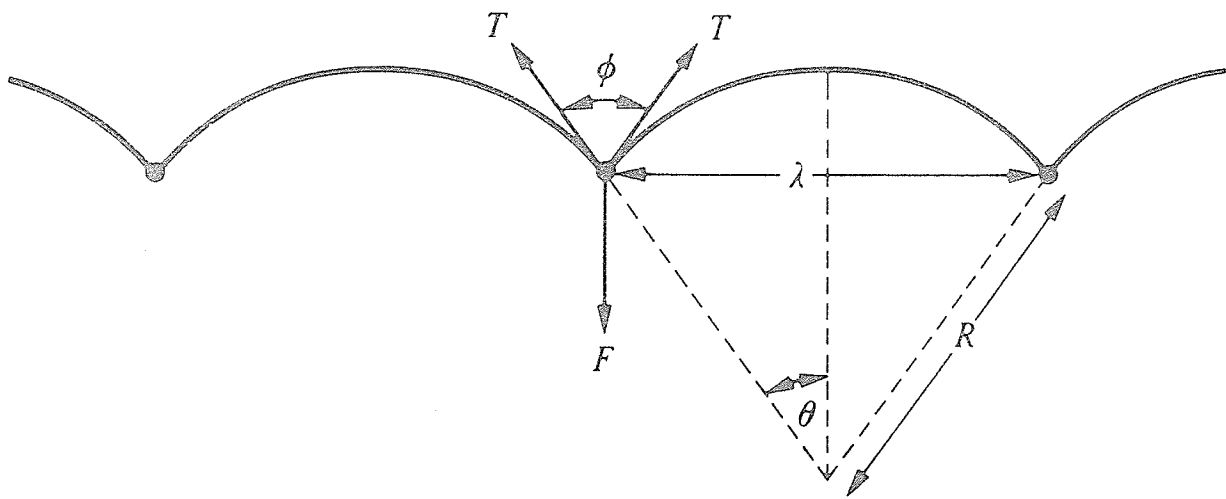


Figure 1. Dislocation held up at obstacles. The bowing angle ϕ is defined as shown¹⁶.

$$F = 2T \cos \left(\frac{\phi}{2} \right) \quad . \quad (2.1)$$

When the breaking angle $\phi = 0$, the particle behaves as an impenetrable obstacle (Orowan hardening), while for values of $\phi > 0$, the particle can be sheared by the glide dislocation with the required shearing force, τ , equal to F .

For the case of particle shearing, the shear stress τ needed to cause the dislocation to break away from the particle may be related to F as follows. The applied shear stress, τ , causes the dislocation of Burgers vector b to bow into a loop of radius of curvature R , where

$$\tau b = T/R \quad . \quad (2.2)$$

From Figure 1 it can be seen that

$$2R \sin\theta = \lambda$$

$$\text{Therefore } \tau b = 2T \sin\theta/\lambda \quad (2.3)$$

$$\text{as } \theta = 90 - \frac{1}{2} \phi \quad \text{hence from (2.1)}$$

$$\tau b = F/\lambda$$

$$\text{i.e. } \tau = F/b\lambda = \frac{2T \cos\left(\frac{\phi}{2}\right)}{b\lambda} \quad (2.4)$$

$$\text{or } \tau = \frac{2T}{bL} \left[\cos\left(\frac{\phi}{2}\right) \right]^{3/2} (0.8 + \phi/5\pi) \quad (2.5)$$

where λ is the effective interparticle spacing, L is the average spacing of particles in the slip plane, $L = 1/N_A^{1/2}$ and N_A is the number of particles per unit area of slip plane.

It can be seen that the interparticle spacing L , which depends on the particle size and distribution, influences the yield strength significantly.

There are a number of possible sources for the additional shearing force F due to the presence of precipitates, which have been discussed in a number of recent review articles (13, 14, 15, 16).

1. Coherency hardening

Coherency hardening arises from the elastic coherency strain surrounding a particle that does not fit the matrix exactly and is given by⁽¹³⁾

$$\tau = \beta G (\epsilon)^{3/2} (R/b)^{1/2} (f)^{1/2} \quad (2.6)$$

where, G = matrix shear modulus, ϵ = misfit between particle and matrix, R = particle radius, f = volume fraction of

precipitate particles, and β is a constant (3 for edge dislocations and 1 for screw dislocations).

2. Surface or chemical hardening

Surface hardening arises from the energy required to create an additional particle/matrix interface when the particle is sheared by the dislocation. This component is given by⁽¹⁶⁾

$$\tau = 2(3/\pi)^{1/2} G (\sigma_s/Gb)^{3/2} (b/R) f^{1/2} \quad (2.7)$$

where σ_s is the particle/matrix interfacial energy and other terms are as defined above.

3. Order hardening

Order hardening is due to the additional work required to create an antiphase boundary in the case of dislocation passing through precipitates which have an ordered lattice. For a paired dislocation, this is given by^(15, 16)

$$\tau = \frac{\sigma_{APb}}{2b} \left[\left(\frac{4 \sigma_{APb} R f}{T} \right)^{1/2} - f \right] \quad (2.8)$$

where σ_{APb} is antiphase boundary energy and T is the dislocation line tension, $T = \frac{1}{2} G b^2$.

4. Stacking-fault hardening

Stacking-fault hardening occurs when there is a difference between the stacking-fault energies of the particle and that of the matrix when these are both F.C.C. or both H.C.P. in structure and is expressed by⁽¹³⁾

$$\tau = \left(\frac{8}{\pi}\right)^{1/2} G \left(\frac{\Delta\gamma}{Gb}\right)^{3/2} \left(\frac{R}{b}\right)^{1/2} f^{1/2} I_m \quad (2.9)$$

where, $\Delta\gamma = \gamma_m - \gamma_p$, γ_m is the stacking-fault energy of matrix and γ_p is that of precipitate, I_m is a complex function of R and the stacking-fault energy of the precipitate.

5. Modulus hardening

Modulus hardening arises from the difference between the elastic modulus of matrix and particle. This can be obtained by the following expression^(13, 14)

$$\tau = \frac{\Delta G}{4\pi^2} \left(\frac{3\Delta G}{Gb}\right)^{1/2} [0.8 - 0.143 \ln(R/b)]^{3/2} R^{1/2} f^{1/2} \quad (2.10)$$

Where ΔG = difference in shear modulus between matrix and precipitate.

From the above strengthening expression it can be seen that for a number of mechanisms, when particles are sheared by dislocations τ increases as R increases because of the increase of F with R .

However, as F increases the breaking angle ϕ decreases, and eventually becomes zero. Therefore the maximum strengthening effect of second-phase particles occurs when precipitates act as impenetrable obstacles and force the dislocation to bow-out and by-pass the particles, leaving dislocation loops around the particles. The strengthening expression in this case follows the Orowan original equation.

$$\tau = 2T/bL = Gb/L \quad . \quad (2.11)$$

Many investigations on the relationship between the increased yield strength due to the presence of precipitates and particle size have been conducted^(17, 18, 19). Raynor and Silcock⁽¹⁷⁾ studied five $LI_2 \gamma'$ [$Ni_3(Al.Ti)$] precipitates containing Fe-Ni-Cr alloys. Their results are shown in Figures 2 and 3. The dependence of increased critical resolved shear stress on Ni_3Al particle size for Ni-12.7 at % Al alloy system was investigated by Davies and Stollof⁽¹⁸⁾ and the results are shown in Figure 4.

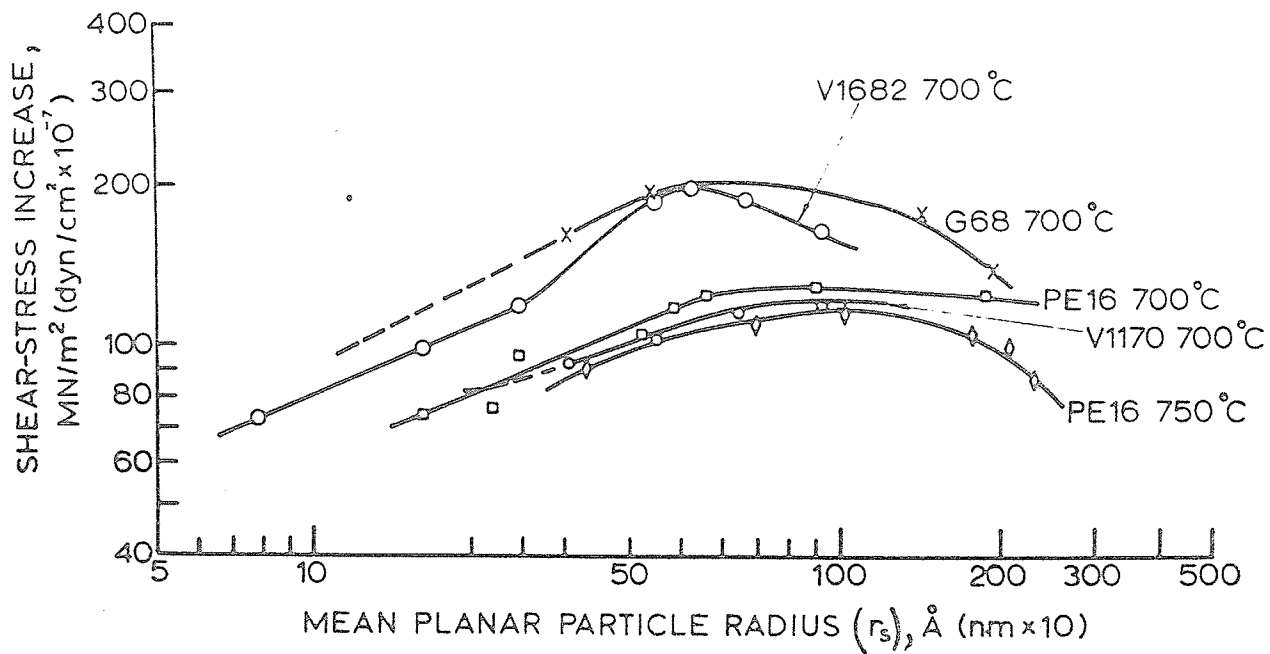


Figure 2. The relationship between γ' particle size and shear proof stress increase¹⁷.

Broken lines indicate values obtained from extrapolated particle sizes.

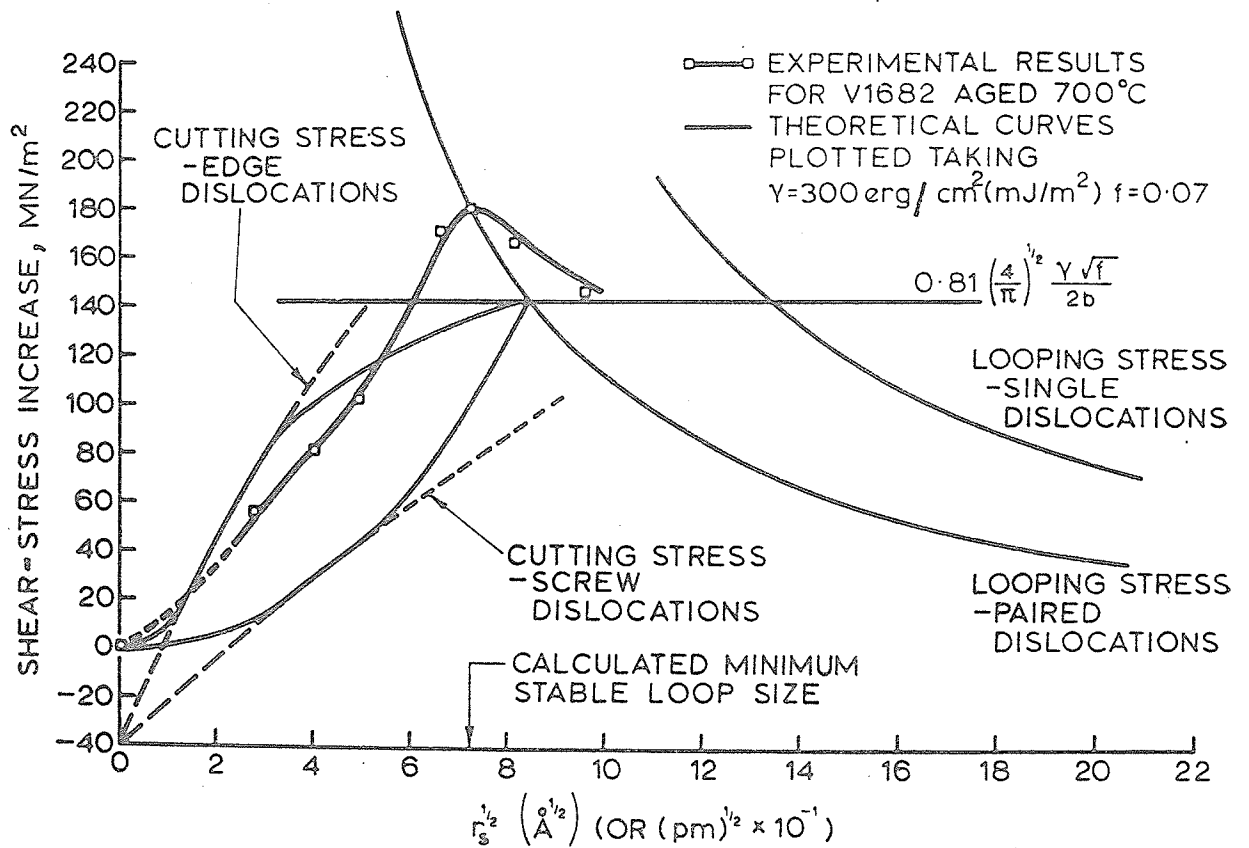


Figure 3. The theoretical and experimentally observed particle size/proof stress increase relationships for V1682 aged at 700°C (975 K)¹⁷.

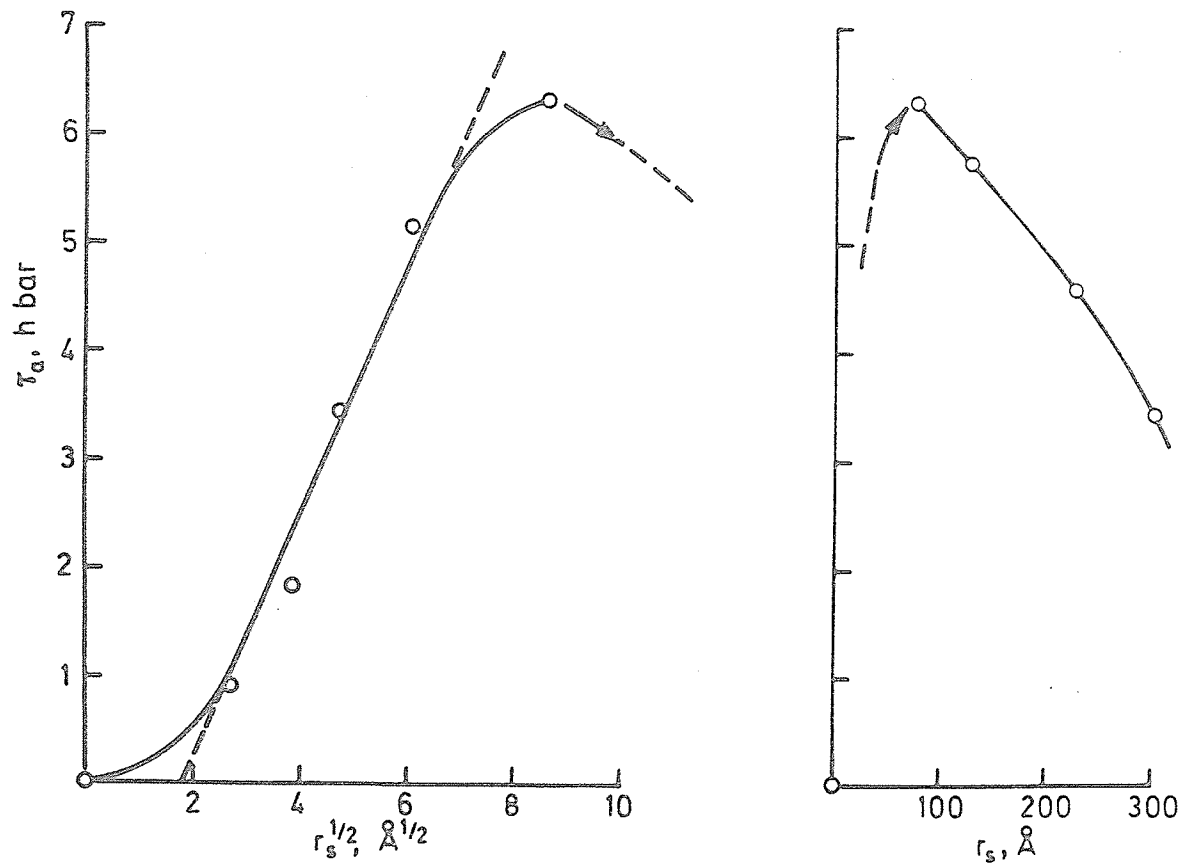


Figure 4. Dependence of initial flow-stress upon Ni_3Al particle size for $\text{Ni}=12.7 \text{ at.}\% \text{ Al}$; $f = 0.057^{14}$.

Chaturvedi et al⁽¹⁹⁾ have recently studied the yielding behaviour of γ' -phase precipitation-strengthening Co-Ni-Cr superalloys containing various volume fraction of the ordered Ni_3Ti phase and their results are shown in Figure 5. The relationship between yield strength and aging time in present alloy Inconel 718 is shown in Figure 6⁽²⁰⁾.

All these studies found that when the γ' particle size was small the strengthening was due to the shearing of the precipitates. However, as the particle size increased the strengthening of the alloys was due to the dislocation by-passing mechanism.

Based on the discussion above it can be concluded that as long as particles are being cut, the flow stress increases with increasing particle size and there is a critical particle size for peak hardness or peak strength at which dislocation by-passing mechanism begins. Any further increase in particle size or interparticle spacing causes a decrease in the strength of the alloys.

The creep strength of the γ' precipitation hardened superalloys is also related the particle size. It has been reported that⁽²¹⁾ particle size is more important than volume fraction in determining creep life and the smallest

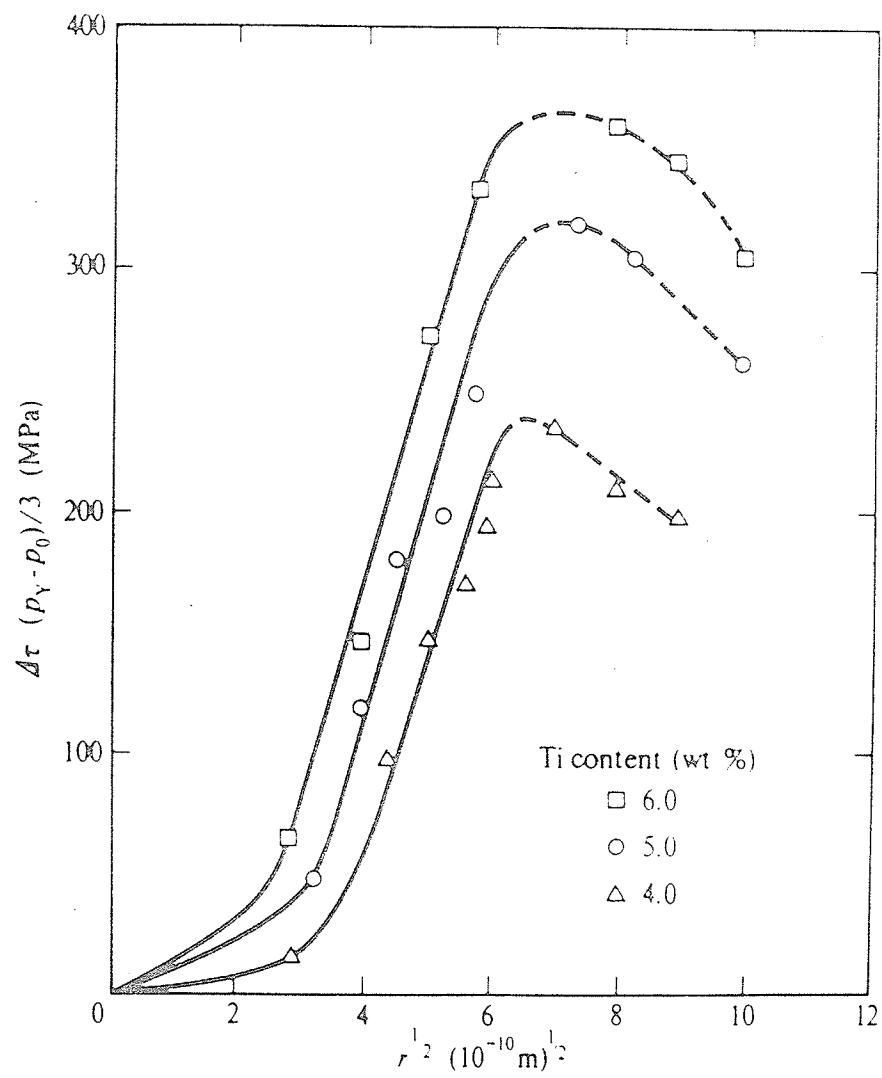


Figure 5. Variation in $\Delta\tau$ with $r^{1/2}$ in Co-Ni-Cr superalloy¹⁹.

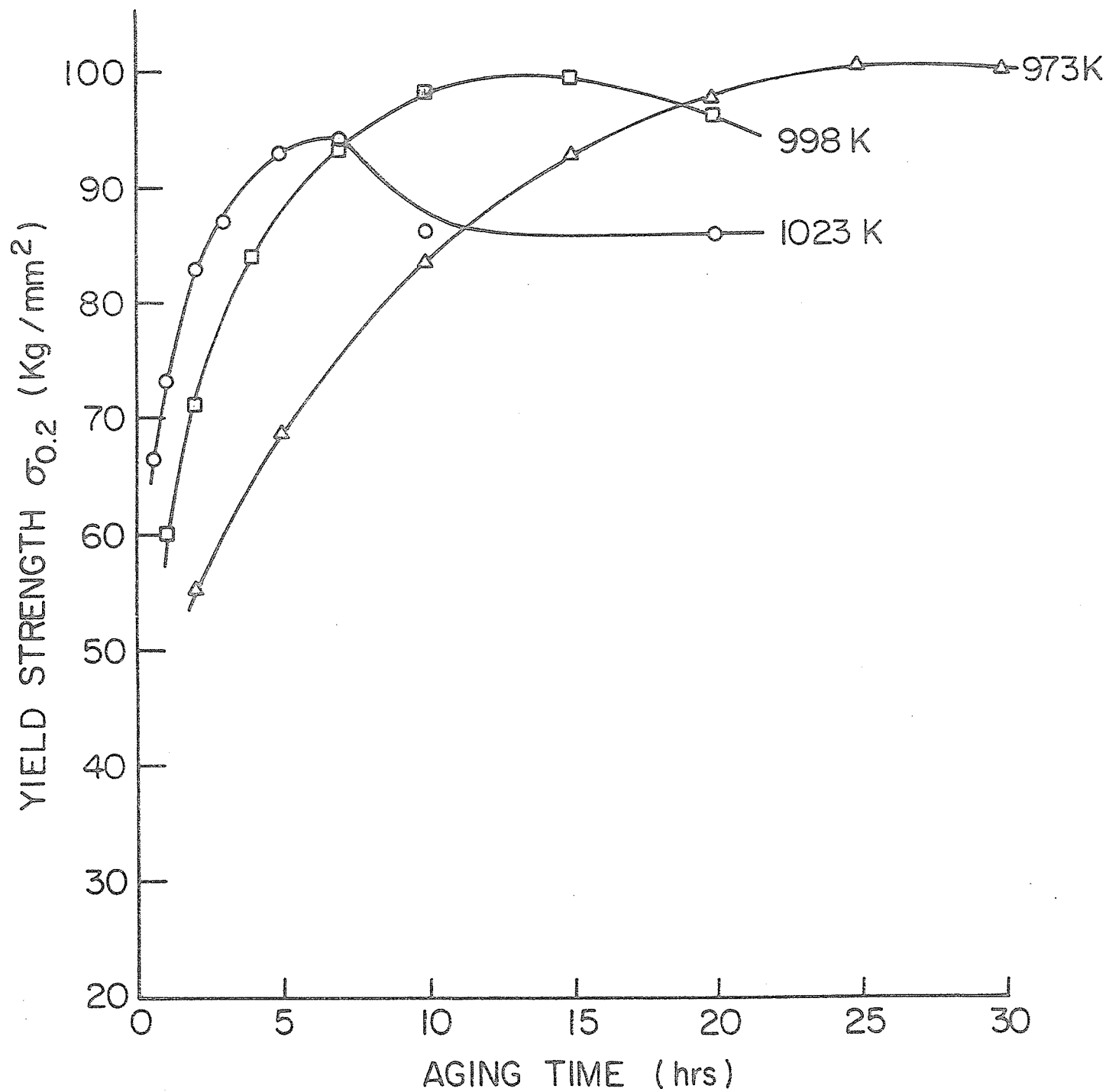


Figure 6. The relationship between yield strength and aging time for Inconel 718.

γ' particles gave optimum creep resistance at 973 K for Ni-Cr-Al-Ti alloys containing 10-20% γ' .

The above discussion has demonstrated the importance of particle size in determining the mechanical properties of an alloy. A study of the growth or coarsening behaviour will not only establish the optimum heat treatment but will also help design alloys which are resistant to particle coarsening and therefore, have better elevated temperature properties.

2.2 Preceipitation in a solid solution

In a supersaturated solid solution, precipitate particles of new phase may form at the temperature where diffusion occurs. The precipitation reaction can be divided into three stages. In the first stage, concentration and structural fluctuations produce nuclei of the new phase. In the second stage, the nuclei grow directly from supersaturated medium. In the third stage, when the particles have reached an appreciable size and degree of supersaturation in matrix has become negligible. the larger particles grow at the expense of the smaller ones.

2.2.1 Nucleation of precipitates from supersaturated solid solution

There are two types of phase change in solid solution. One is called spinodal decomposition, i.e., a small concentration fluctuation may occur spontaneously and there are no barriers for nucleation such as at composition C_1 in Figure 7A. Another is the normal precipitation reaction such as at composition C_3 in Figure 7B, where there exists a nucleation barrier.

A more general case of nucleation process, i.e. normal precipitation reaction, and the situation of the homogeneous nucleation without the benefit of pre-existing heterogeneities in the system is discussed first. The change in free energy ΔF associated with homogeneous nucleation of an embryo of the new phase is equal to the sum of the change in volume free energy, ΔF_v , the interfacial energy, σ , required to form the new surface and the elastic strain energy, ϵ , due to the lattice distortions during nucleation (16, 22).

$$\Delta F = \Delta F_v + \sigma + \epsilon . \quad (2.12)$$

For a spherical nucleus of radius r

$$\Delta F = 4\pi r^2 + \frac{4}{3} \pi r^3 (\Delta F_v + \epsilon) . \quad (2.13)$$

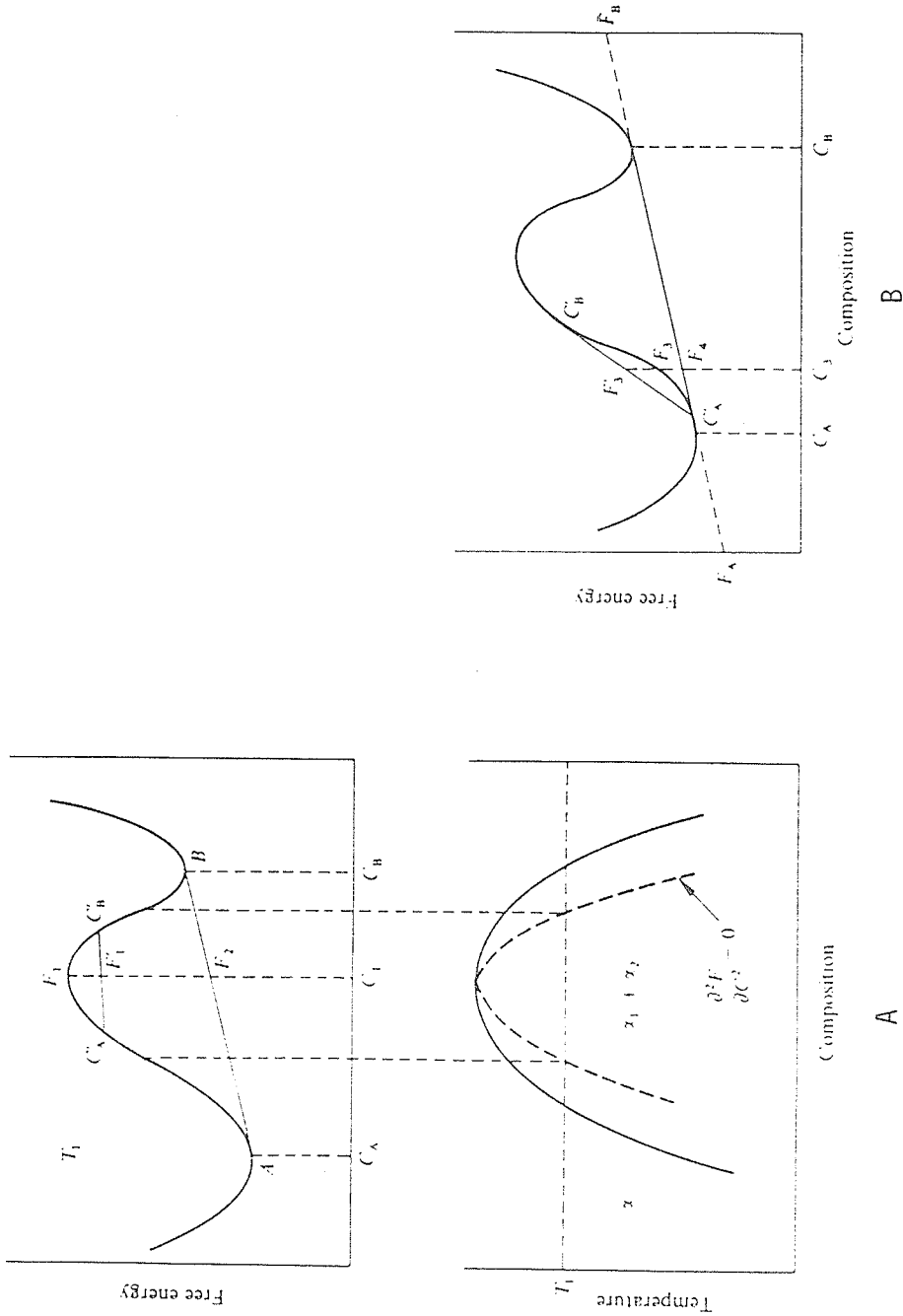


Figure 7. (A) Free energy-compositional relationship corresponding to spinodal decomposition. (B) Free energy-compositional relationship for a conventional nucleation and growth process²².

The variation of ΔF with radius, r , is shown in Figure 8. The condition for continued growth of an embryo is that its radius should exceed r_0 , where $d(\Delta F)/dr = 0$. i.e.

$$r_0 = \frac{2\sigma}{-(\Delta F_V + \epsilon)} \quad (2.14)$$

and the critical free energy, or activation energy for nucleation is given by

$$\Delta F^* = \frac{16\pi}{3} \frac{\sigma^3}{(\Delta F_V + \epsilon)^2} \quad (2.15)$$

A steady-state nucleation rate, the number of stable nuclei produced in unit time in unit volume of untransformed solid, \dot{N}_V , is proportional to $\exp(-\Delta F^*/KT)$. The rate at which individual nuclei grow will also depend on the frequency with which atoms adjacent to the nucleus can join it. This is proportional to $\exp(-\Delta F_D/KT)$, where ΔF_D is the activation energy for diffusion. Therefore the rate of nucleation of precipitates is given by

$$\dot{N}_V = K \exp\left(\frac{-\{A\sigma^3/(\Delta F_V + \epsilon)\} + \Delta F_D}{KT}\right) \quad (2.16)$$

In supersaturated solid solutions some types of lattice defects can be expected, such as vacancies, interstitials, dislocations, grain or twin boundaries, stacking faults,

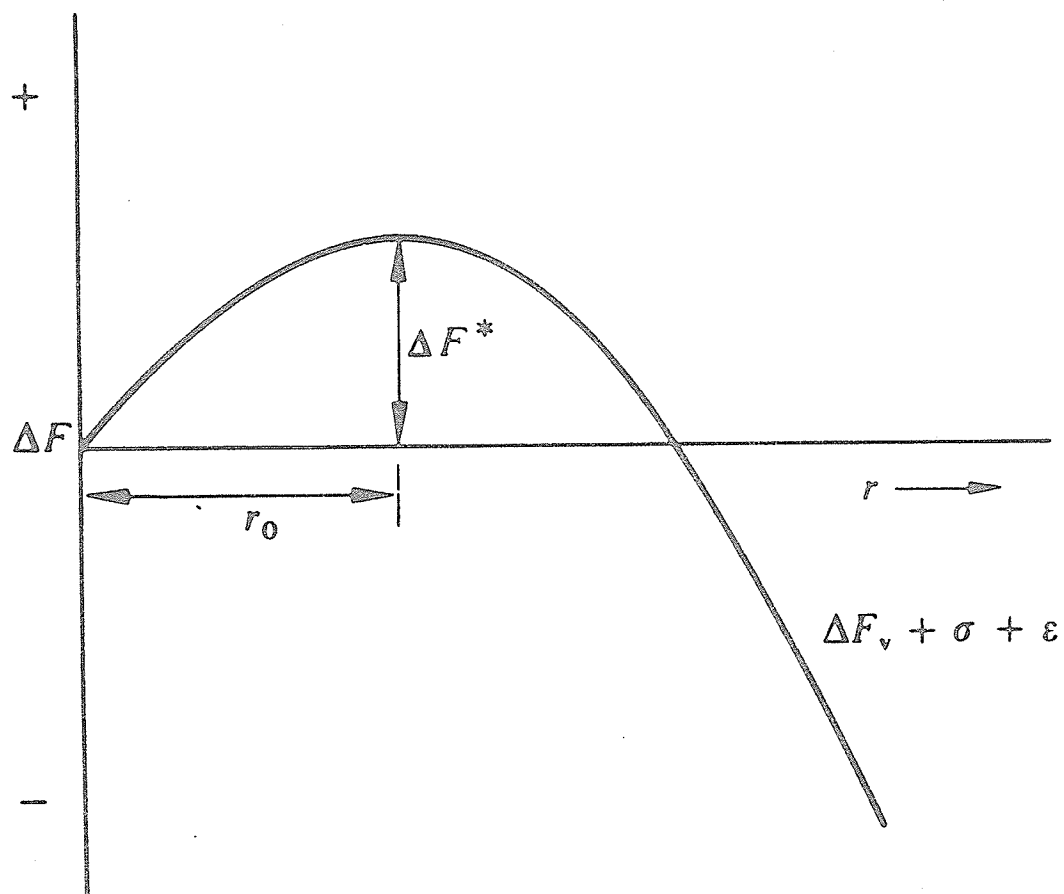


Figure 8. Schematic representation of the free energy of a nucleus plotted against its radius²².

antiphase domain boundaries. Therefore instead of homogeneous nucleation of an equilibrium phase, heterogeneous nucleation is usually encountered. In the regions of lattice defects the free energy will be higher than the average free energy, which will facilitate the nucleation of precipitates. These kinds of lattice defects are called nucleation catalysts. The rate of heterogeneous nucleation, \dot{N}_s , is again proportional to $\exp(-\Delta F^*/KT)$ and the ΔF^* for heterogeneous nucleation is lower than that for homogeneous nucleation.

2.2.2 Growth of precipitates from supersaturated solid solution

For many precipitation processes in metallic systems nucleation occurs very rapidly at the beginning of transformation at sites of catalysts. A very small amount of precipitation will change the mean concentration of solute in the matrix by one or two orders of magnitude, which will be sufficient to decrease the nucleation rate to a negligible value⁽²²⁾. The growth of nuclei from supersaturated solid solution will, however, continue.

During this type of growth two limiting factors are likely to control the reaction rate. First the movement

of atoms to the precipitate-matrix interface by diffusion and the second the movement of atoms across the interface. In the initial stage when the particle size is small the diffusion distances are likely to be very small and the movement of atoms across the interface is likely to be the rate controlling process. When particle size is large the diffusion distances are also large and the rate controlling process is generally the diffusion of atoms in the matrix to the precipitate particle-matrix interface.

Diffusion-controlled growth has been recently analysed by Martin and Doherty⁽²²⁾. For the growth of spherical precipitates, the radius R after time t is given by

$$R = \alpha (Dt)^{1/2} \quad (2.17a)$$

where D is the volume diffusion coefficient and α is a function of the supersaturation.

In the case of planar precipitates a similar expression has been deduced ,

$$S = \alpha (Dt)^{1/2} \quad (2.17b)$$

where s is the half thickness of the planar precipitates.

2.2.3 The general coarsening process

When the volume fraction of precipitate reaches almost constant value, i.e., the precipitation from solid solution is complete, further aging will lead to precipitate coarsening and the large particles will grow at the expense of the small ones. This process is called "Ostwald ripening". The driving force for this process is the reduction in the interface free energy of the system due to a decrease in particle-matrix interface area. Martin et al⁽¹¹⁾ have calculated the change in interface free energy when particle size changes from $R = 100 \text{ \AA}$ to $R = 10^4 \text{ \AA}$ for alloy containing 5 volume per cent of precipitate, with the surface free energy, σ , equal to 0.2 MJ m^{-3} . They found that when $R = 100 \text{ \AA}$ the total interface free energy is 2 MJ m^{-3} while when $R = 10^4 \text{ \AA}$, the total surface energy is only 0.02 MJ m^{-3} i.e., about 100 times less than the fine dispersion system.

Thermodynamically, for a given system, the increase in chemical potential due to a second phase particle of radius r is inversely proportional to r , i.e.

$$\Delta\mu = \mu_r - \mu_\infty = \frac{2 \sigma V_m}{r} \quad (2.18)$$

where μ_r is the chemical potential of precipitate of radius r

μ_∞ is the chemical potential of infinite size particle

V_m is the molar volume of precipitate

σ is the interfacial surface free energy.

Also for any particle of radius r , C_e can be assumed to be the equilibrium concentration of solute atoms in the matrix at infinity from the precipitate and C_r is the concentration in the matrix in equilibrium with the precipitate. If the matrix is assumed to be a dilute solution where the activity coefficient of the solute atoms is constant, then,

$$\Delta\mu = RT \ln \frac{C_r}{C_e} \quad (2.19)$$

Combining (2.18) and (2.19), the Gibbs-Thomas equation can be reduced to

$$C_r = C_e \exp \frac{2 \sigma V_m}{rRT} \quad (2.20)$$

Usually $rRT \gg 2 \sigma V_m$, i.e. $\frac{2 \sigma V_m}{rRT} \ll 1$, therefore

$$C_r = C_e \left(1 + \frac{2 \sigma V_m}{rRT} \right) \quad (2.21)$$

Equation (2.20) shows that in a system containing various particle sizes concentration gradients will exist. Therefore solute diffusion will occur in the matrix from the regions near smaller particles to the regions near larger ones, which leads to the growth of larger particles at the expense of smaller ones as shown in Figure 9.

There are three major steps in the coarsening process,

- 1) dissolution of solute from smaller particles to the matrix, i.e., transport of atoms across the interface between smaller particles and matrix;
- 2) diffusion of solute in the matrix from the region near smaller particles to the regions near larger particles;
- 3) deposition of solute onto larger ones.

The coarsening rate of a system depends on the slowest step. Therefore, when the transfer of solute atoms across the interface is much faster than the rate of diffusion of solute in the matrix the coarsening process is lattice diffusion controlled. When the rate of diffusion is faster than the rate of transfer of solute atoms across the interface, the coarsening process is interface controlled. A third mechanism, known as grain boundary diffusion controlled coarsening, operates when most of the precipitates are situated at grain boundaries and diffusion occurs

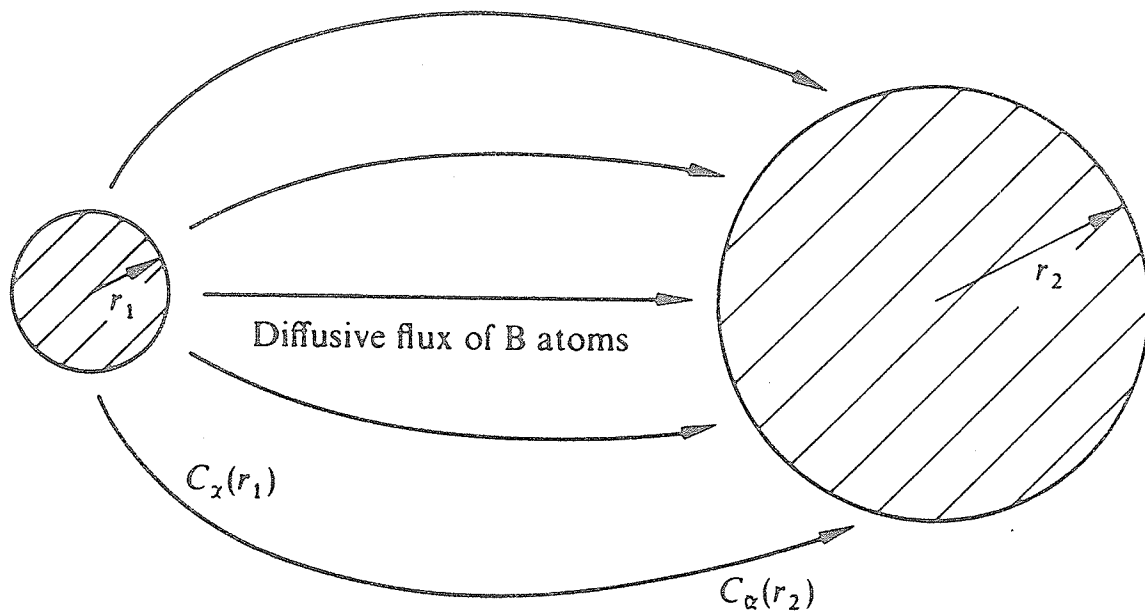


Figure 9. Two spherical β precipitates of radius r_1 and r_2 in an α matrix. Since $C_\alpha(r_1) > C_\alpha(r_2)$ there is a diffusive flux from (1) to (2)²².

along the grain boundaries.

Many studies concerning precipitate coarsening behaviour have been done, especially on the γ' precipitate-containing alloy systems, most of which revealed that the coarsening process was lattice diffusion controlled. In recent investigations it has been found that the coarsening process in both γ' and γ'' is also lattice diffusion controlled, therefore only the lattice diffusion controlled coarsening mechanism will be discussed in detail here.

2.2.3.1 The lattice diffusion controlled coarsening

The analysis of lattice diffusion controlled coarsening process is very complex and the following simplifying assumptions are made when deducing the coarsening rate of precipitates⁽⁸⁾.

- (1) There is no significant barrier to atom transfer across the precipitate/matrix interface.
- (2) Volume fraction of precipitates is very small and remains constant, i.e., the inter-particle distance is great in comparison to their radii.
- (3) The local equilibrium of particle-matrix exists.

- (4) The concentration gradients are independent of time and the diffusion coefficient is independent of concentration.
- (5) Gibbs-Thomas equation is applicable.

Any system where particles are coarsening will consist of large and small particles with an average particle radius \bar{r} . Figure 10 shows such a system where the distribution of solute atoms inside a particle of radius r is $C_\beta(r)$ which is generally assumed to be ≈ 1 . The distribution of solute atoms at the particle-matrix interface is $C_\alpha(r)$ which increases to $C_\alpha(\bar{r})$ at distance $R \gg r$. Since the concentration gradient exists in the matrix, i.e., $C_\alpha(r) \neq C_\alpha(\bar{r})$, lattice diffusion will occur.

For steady state condition of diffusion, the rate of the volume change of a precipitate of radius r should be equal to the flux of the solute.

According to Fick's first law of diffusion the flux of solute q to the precipitate is

$$q = JA = - 4 \pi R^2 D \frac{\partial C}{\partial R} \quad (2.22)$$

where $\partial C / \partial R$ is the concentration gradient across sphere at a distance R from the particle center.

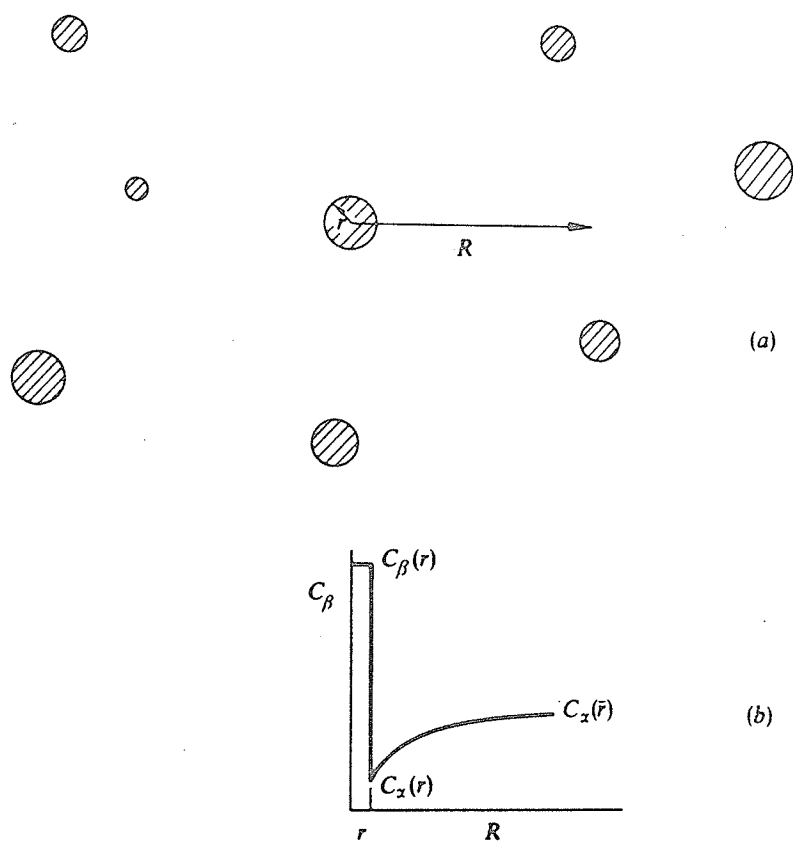


Figure 10. (a) An array of precipitates around a particular precipitate of radius r . (b) Showing variation in concentration away from the centre of this precipitate. It is assumed that the concentration rises to the average value $C_\alpha(\bar{r})$ before the nearest neighbours and their diffusive fields are approached²².

And the volume change of this particle, $\partial V/\partial t$, is

$$\frac{\partial V}{\partial t} = \frac{\partial V}{\partial r} \cdot \frac{\partial r}{\partial t} = \frac{\partial(\frac{4}{3} \pi r^3)}{\partial r} \cdot \frac{\partial r}{\partial t}$$

i.e. $\frac{\partial V}{\partial r} = 4 \pi r^2 \cdot \frac{\partial r}{\partial t}$ (2.23)

as $\frac{\partial V}{\partial t} = q$

therefore

$$4\pi r^2 \frac{\partial r}{\partial t} = - 4\pi R^2 D \frac{\partial C}{\partial R}$$
 (2.24a)

or

$$- \frac{\partial R}{R^2} = \frac{D}{r^2(\partial r/\partial t)} \partial C$$
 (2.24b)

By integrating 2.24b from the surface of the precipitate, i.e. from $R = r$ to large radial distance R and hence the concentration C from C_r to C_e , one obtains

$$\int_r^\infty - \frac{\partial R}{R^2} = \int_{C_r}^{C_e} \frac{D}{r^2(\partial r/\partial t)} \partial C$$

For a given value of r the growth rate $\partial r/\partial t$ is constant,

$$\frac{1}{r} = \frac{D}{r^2(\partial r/\partial t)} (C_e - C_r)$$
 (2.25)

$$c_r = c_e \left(1 + \frac{2 \sigma V_m}{rRT} \right)$$

$$\frac{\partial r}{\partial t} = \frac{2 D \sigma V_m}{rRT} \left(\frac{1}{\bar{r}} - \frac{1}{r} \right) \quad (2.26)$$

For two different \bar{r} values the variation in the values of $\frac{\partial r}{\partial t}$ with r is shown in Figure 11.

It is seen that particles with radius $r < \bar{r}$ are dissolving at increasing rate with decreasing values of r and all the particles of $r > \bar{r}$ are growing. The growth rate, dr/dt , for $r > \bar{r}$ increases from zero at $r = \bar{r}$ to the maximum at $r = 2\bar{r}$ and then decrease. It is also observed that as \bar{r} increases the growth rate for all precipitates decreases.

Since concentration, thermal and energy fluctuations exist in any real two-phase alloy system during aging, all the precipitates can not be of the same size at any time. Therefore the coarsening process will continue during the whole period of aging, which will make the particle size distribution wider with increasing time since all particles of $r > \bar{r}$ can grow. However the spread of the particle size distribution will be limited because of the existence of the maximum growth rate at $r = 2\bar{r}$. The particles of $r > 2\bar{r}$

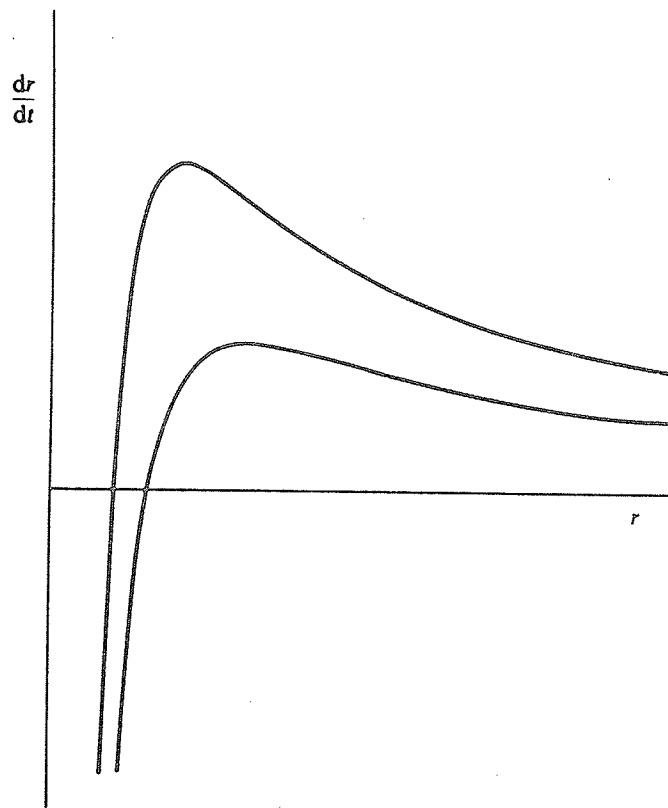


Figure 11. Variation in precipitate growth rate dr/dt with precipitate radius r for diffusion controlled for two different values of the mean radius \bar{r} - for the lower curve \bar{r} - for the lower curve \bar{r} is increased by 50%²².

will grow more slowly than those of $r = 2\bar{r}$ and the particle size will tend to become homogeneous at a radius somewhat greater than \bar{r} . Thus particles with radii much larger than $2\bar{r}$ can not exist in the system and a sharp cut-off point in the particle-size distribution curve will be observed.

As the maximum growth rate occurs for those particles of size $r = 2\bar{r}$, $d\bar{r}/dt$ can be approximately equal to $(\frac{dr}{dt})_{r=2\bar{r}}$, i.e.,

$$\frac{d\bar{r}}{dt} \quad \left(\frac{dr}{dt}\right)_{r=2\bar{r}} = \frac{D \sigma V_m C_e}{2RT\bar{r}^2} .$$

Therefore,

$$\bar{r}_t^3 - \bar{r}_0^3 = \frac{3}{2} \frac{D \sigma V_m C_e}{RT} . \quad (2.27)$$

A more detailed and rigorous analysis has shown that particles with radii $r > 1.5 \bar{r}$ can not continue to exist, i.e. the cut-off point is at $r = 1.5 \bar{r}$ rather than at $r = 2\bar{r}$. Therefore the final equation for lattice diffusion controlled coarsening process when the steady-state distribution has achieved is given by

$$\bar{r}_t^3 - \bar{r}_0^3 = \frac{8}{9} \frac{D \sigma V_m C_e t}{RT} = Kt . \quad (2.28)$$

This is called the Lifshitz-Slyozov-Wagner relationship and this theory is called LSW theory which has been widely used to study the coarsening process.

2.2.3.2 Time-dependent of particle-size distribution during lattice diffusion controlled growth

An elaborate analysis of particle size distribution has been done by Wagner⁽⁸⁾. A particle size distribution function $f(r,t)$ can be defined as the number of particles of a given radius r at time t , and the total number of particles in the system at any instant is thus given by

$$N = \int_0^{\infty} f(r,t) dr \quad (2.29)$$

where N is the number of particles per unit volume.

Wagner has shown that the distribution of particle size evolves towards a 'quasi-steady-state' distribution $f(r,t)$, which is independent of the initial distribution $f(r,0)$ while depends on the type of the rate controlling coarsening process.

In the case of lattice diffusion control

$$f(r,t) = f'(t) \rho^2 h_1(\rho) \quad (2.30)$$

$$\text{where } f'(t) = \frac{\text{const}}{(1 + t/\tau_D)^{1/3}} \quad \text{and } \tau_D = \frac{\bar{r}_0^3 RT}{2 \sigma D C_e V_m^2}$$

For a given system $\tau_D = \text{constant}$ and usually the observed $t \gg \tau_D$ hence $f'(t)$ is a function of time only.

$\rho = r/\bar{r}$ and $h_1(\rho)$ is given by

$$h_1(\rho) = \left(\frac{3}{3+\rho}\right)^{7/3} \left(\frac{3/2}{3/2-\rho}\right)^{11/3} \exp\left(\frac{-\rho}{3/2-\rho}\right), \rho < \frac{3}{2}$$

$$h_1(\rho) = 0 \quad \rho \geq \frac{3}{2}$$
(2.31)

This theoretical distribution function $\rho^2 h_1(\rho)$ has the following characteristic features:

1. a sharp cut-off at $\rho = 3/2$;
 2. a maximum at $\rho = 1.135$;
 3. $\int_0^{\infty} \rho^2 h_1(\rho) d\rho = \frac{9}{4}$.
- (2.32)

The distribution function of steady-state particle size predicted by the diffusion controlled coarsening of the LSW theory is shown in Figure 12.

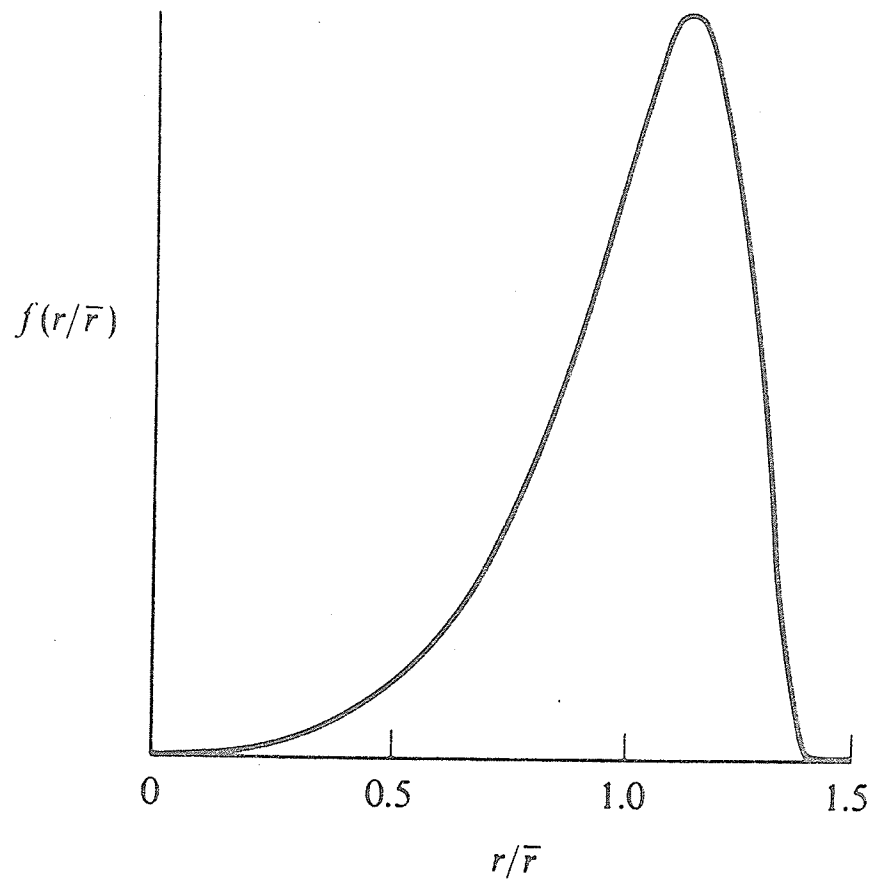


Figure 12. Expected distribution of particle size for diffusion controlled coarsening²².

The original LSW theory was applicable to a fluid matrix only. However Andell and Nicholson⁽¹⁾ have used this theory successfully to quantitatively analyse the γ' precipitate coarsening process in Ni-Al solid solution. To normalize the particle-size distribution function $f(r,t)$, they introduced a new function $g(r,t)$ such that

$$\int_0^{\infty} g(r,t) dr = 1 \quad \text{and therefore}$$

$$g(r,t) = f(r,t)/N \quad . \quad (2.33)$$

By combining equations (2.29), (2.30), (2.32) and (2.33)

$$\begin{aligned} g(r,t) &= \frac{f(r,t)}{N} = \frac{f'(t) \cdot \rho^2 h_1(\rho)}{\int_0^{\infty} f(r,t) dr} = \frac{f'(t) \cdot \rho^2 h_1(\rho)}{\int_0^{\infty} f'(t) \cdot \rho^2 h_1(\rho) dr} \\ &= \frac{f'(t) \cdot \rho^2 h_1(\rho)}{f'(t) \int_0^{\infty} \rho^2 h_1(\rho) dr} = \frac{\rho^2 h_1(\rho)}{\int_0^{\infty} \rho^2 h_1(\rho) d\rho \cdot \frac{dr}{d\rho}} \\ &= \frac{\rho^2 h_1(\rho)}{9/4 \cdot \frac{dr}{d\rho}} \end{aligned}$$

since $\rho = \frac{r}{\bar{r}}$ and $d\rho = \frac{1}{\bar{r}} dr$

i.e. $\frac{dr}{d\rho} = \bar{r}$

Therefore

$$g(r,t) = \frac{\rho^2 h_1(\rho)}{\frac{9}{4} \cdot \bar{r}} \quad (2.34)$$

For comparing the experimentally measured particle size distribution with the theoretical time-independent function $\rho^2 h_1(\rho)$, the measured function $f(r,t)$ needs only to be multiplied by $\frac{9}{4} \bar{r}$.

2.2.3.3 Effect of volume fraction on coarsening behaviour

A very important assumption in the LSW theory of lattice diffusion controlled particle coarsening is that the volume fraction, ϕ , of precipitates is very small, i.e. the interparticle spacing is very large compared to the particle size. This implies that there is no interaction between neighboring particles during the coarsening process. However, in most real two-phase alloy systems, the volume fraction is not very small (up to 0.5 ~ 0.6 for some γ' containing nickel-base alloys), which does not satisfy this assumption. Intuitively, it is expected that as the volume fraction increases the coarsening rate should increase as the diffusion paths are getting shorter for a given particle size system. The discrepancy between the experimental results and the LSW theory has been found in most of the systems studied, especially in terms of particle-size distribution. Generally, the maximum is different from the predicted value

and occurs at a different value of ρ . Also the maximum cut-off values of ρ are greater than $3/2$.

Ardell⁽²³⁾ first modified the LSW theory (MLSW) by considering the effect of the volume fraction, ϕ , on the coarsening behaviour. The central idea of MLSW theory is that when ϕ is not negligibly small the interparticle spacing R can not be considered as infinity compared with the particle size, which is different from the treatment in the LSW theory. The coarsening equation of Ardell's MLSW theory is given by

$$\bar{r} - \bar{r}_0 = K_m \frac{8}{9} \frac{D\sigma V_m C_e}{RT} t \quad (2.35)$$

where K_m is a function of ϕ only, $K_m = \frac{K(\phi)}{K(0)}$, and when $\phi = 0$, $K_m = 1$. The variation of K_m with ϕ is shown in Figure 13.

The particle-size distribution predicted by the MLSW theory is shown in Figure 14. When $\phi = 0$, the curve is the result of the LSW theory, while $\phi = 1$, the curve agrees with the interface controlled coarsening of $t^{1/2}$ law.

The Lifshitz-Slyozov encounter modified theory (LSEM) has been recently developed by Davies et. al⁽²⁴⁾. They have treated the lattice diffusion controlled coarsening

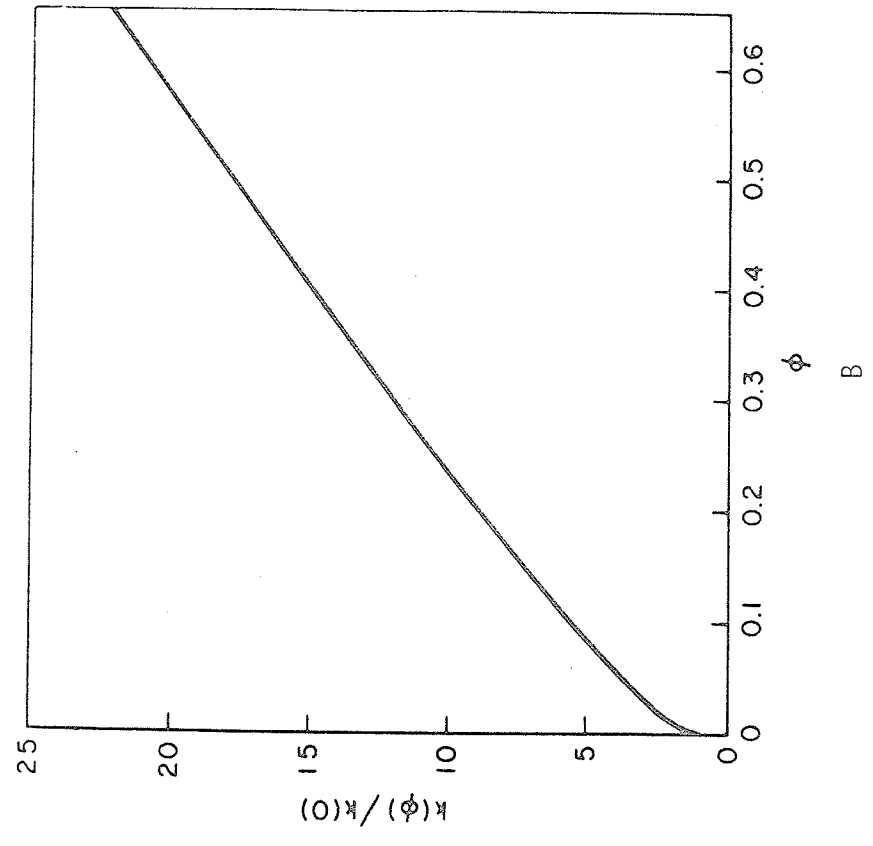
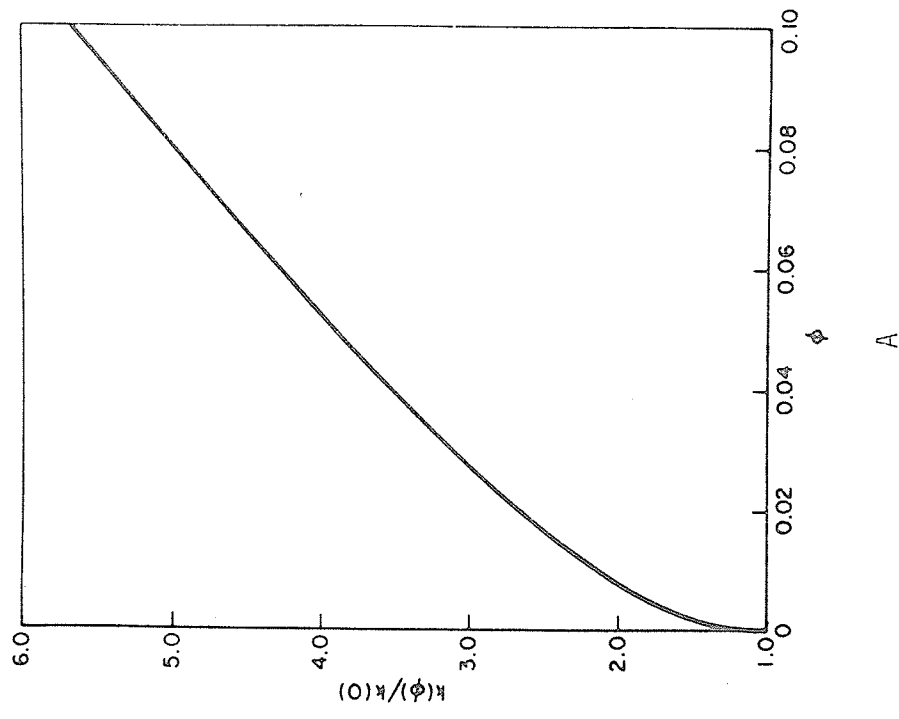


Figure 13. Illustrating how the rate constant, $k(\phi)$, for diffusion-controlled coarsening varies with the volume fraction, ϕ ; a) at small volume functions; b) at volume fraction up to $\phi = 0.65$ ²³.

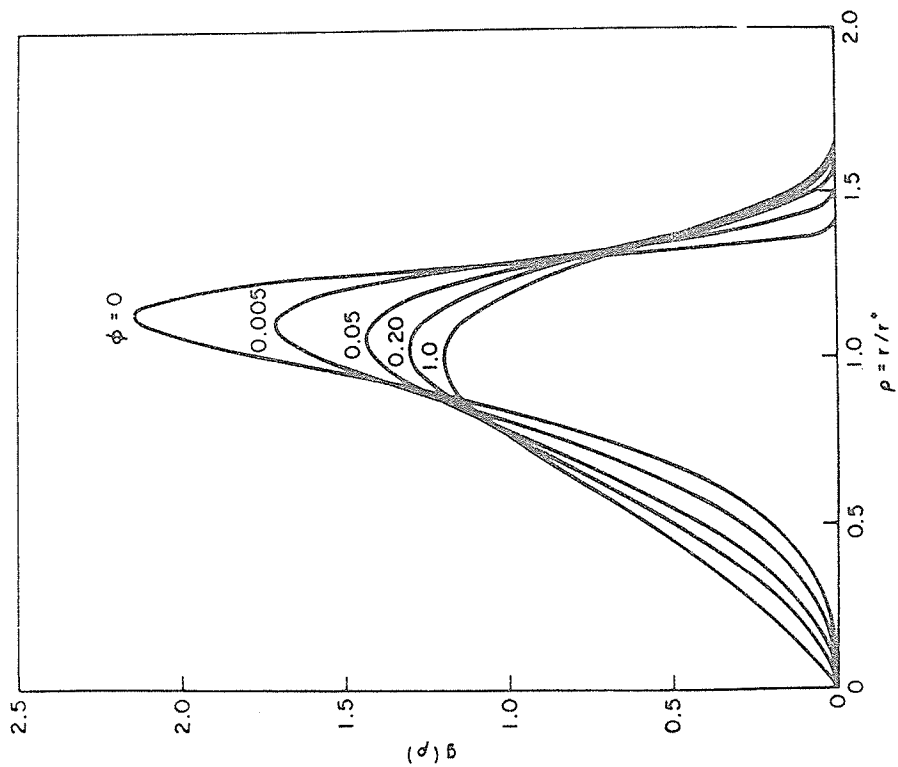
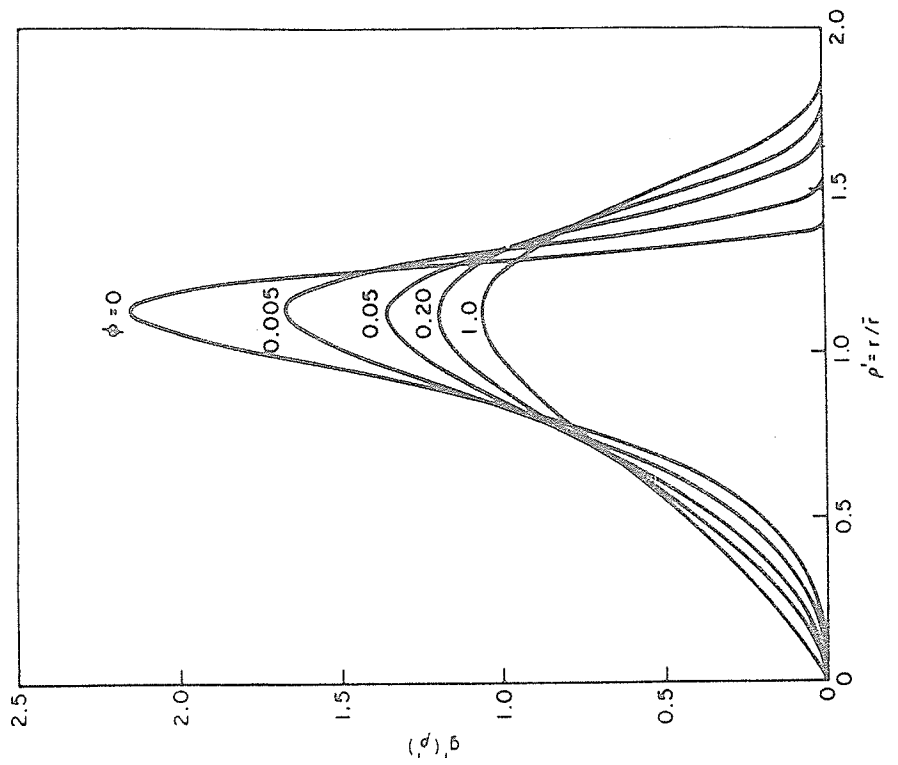


Figure 14. (a) Illustrating the dependence of the theoretical distribution of particle sizes on the volume fraction; ϕ ; (b) the particle size distributions redefined as functions of the variable $\rho' = r/\bar{r}$ ²³.

process in the following manner. In the case of appreciably large volume fraction, when a particle is growing its boundary expands outwards and may approach or even touch another one. Therefore very rapid diffusion will occur, which causes the two particles to coalesce and become one. It is seen that this effect will increase the growth rate and also broaden the particle size distribution. The coarsening rate equation of LSEM theory is as follows

$$\bar{r}^3 - \bar{r}_0^3 = K_e \frac{8}{9} \frac{D\sigma V_m C_e}{RT} t \quad (2.36)$$

where $K_e = \frac{K(Q)}{K(0)} = \frac{27}{4} \frac{\bar{R}_c^3}{\gamma}$ and \bar{R}_c, γ are functions of the volume fraction Q , usually $\bar{R}_c \approx 1$. When $Q=0$, $\gamma = \frac{27}{4}$ and $K_e = 1$, which is the case of the LSW theory.

Figure 15 shows the variation of K_e and γ with Q and Figure 16 shows the particle size distribution predicted by the LSEM theory.

Both the MLSW theory and LSEM theories still follow $t^{1/3}$ law of the LSW theory, the only differences being that they give the effect of the volume fraction on the growth rate constant and particle size distribution. Comparing Figure 13 with Figure 15, and Figure 14 with Figure 16, it is seen that for a given volume fraction of precipitates the growth

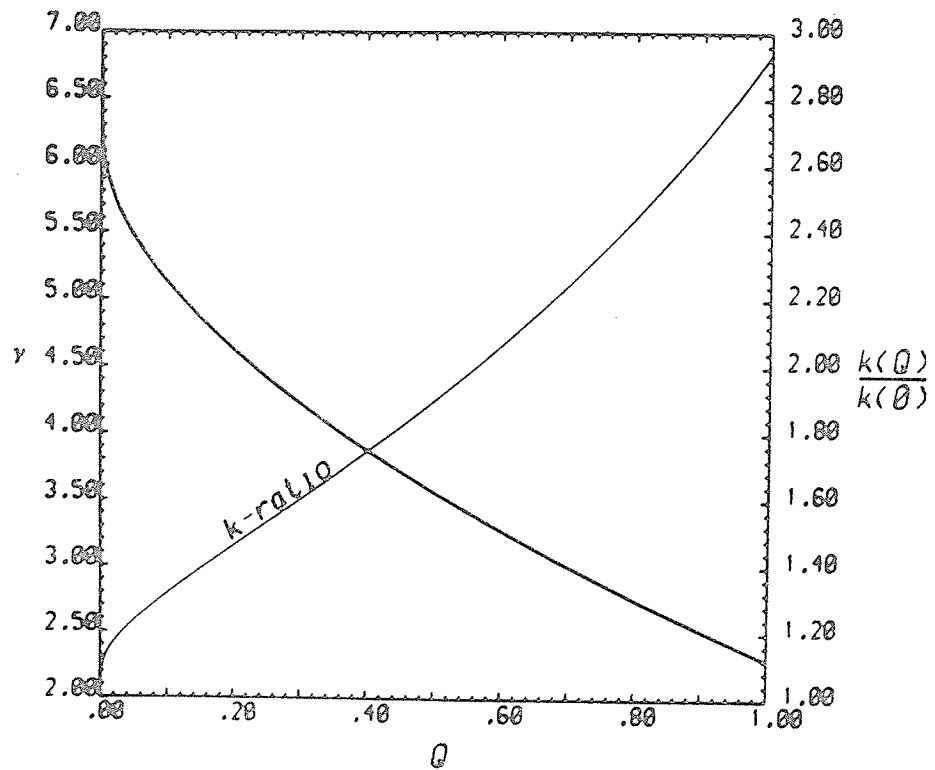


Figure 15. The effect of volume fraction Q , on the parameter γ and the ratio of the rate constant K_e at volume fraction Q to that at zero volume fraction²⁴.

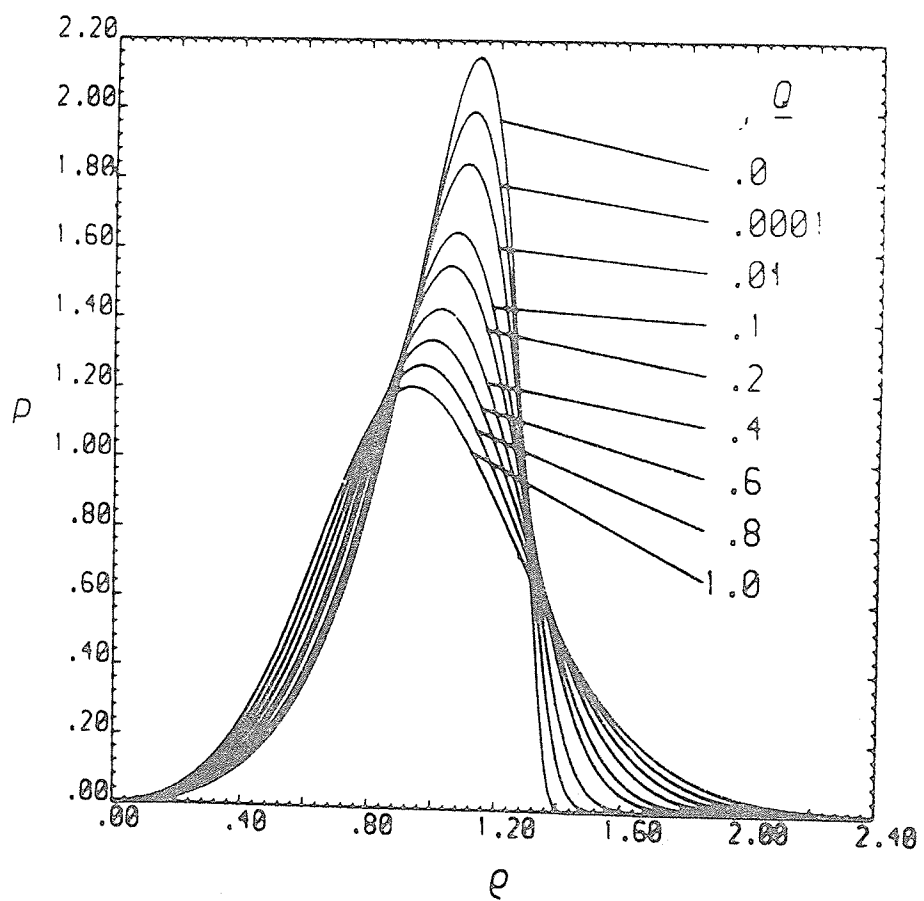


Figure 16. LSEM particle size distribution as a function of volume fraction of precipitate Q^{24} .

rate constant of LSEM is much smaller than that of MLSW theory and the former gives a broader particle-size distribution than the latter.

2.3 Experimental observations of precipitate coarsening

Many studies have been conducted on the coarsening behaviour of precipitates during the past twenty years^(1-6, 9-12). Most of the results have revealed that the coarsening behaviour follows the $t^{1/3}$ law, i.e., the LSW theory of lattice diffusion controlled coarsening, although the precipitates in different systems have various types of shapes and different mismatch between precipitates/matrix.

The coarsening behaviour of γ' precipitate in nickel base alloys has been extensively studied^(1-4, 25) as these alloys are widely used in high temperature parts of advanced engines and γ' is the most important strengthening phase in these alloys. Ardell⁽²⁵⁾ has studied the coarsening behaviour of γ' phase in Ni-Al, Ni-Ti and Ni-Si systems and concluded that despite the different shapes of γ' phase and a different γ - γ' misfit, the growth processes always followed the $t^{1/3}$ law of the LSW theory and the calculated values of activation energies from the coarsening processes in Ni-Al, Ni-Si systems were in agreement with the solute-diffusion-controlled process. Typical results for particle coarsening in Ni-Al alloy system⁽²⁵⁾ are shown in Figure 17.

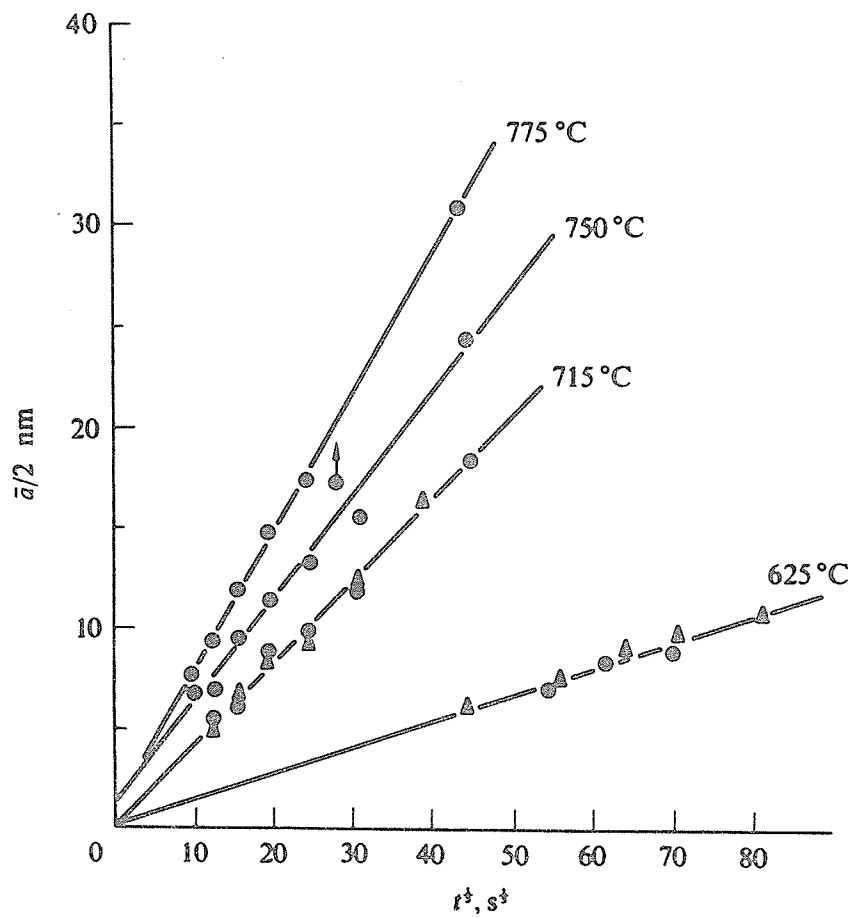


Figure 17. Typical experimental result of particle coarsening showing a linear variation of particle size ($\bar{a}/2$ for cube shaped particles) against the cube root of time for γ' precipitates in nickel-aluminium alloys: \blacktriangle = 6.35 wt. % Al
 \bullet = 6.71 wt. % Al²².

The coarsening behaviour of cubic-shaped γ' phase (Ni_3Ti) in 40 Co-38Ni-17Cr-5Ti superalloy has been studied by Chaturvedi et al⁽⁵⁾. They found that the coarsening kinetics of γ' precipitates in this system also follows the $t^{1/3}$ law at all the aging temperatures, and the calculated value of activation energy for the growth process was in good agreement with published data.

Some investigations of the coarsening behaviour of B.C.T. disc-shaped γ'' precipitates have been reported⁽⁹⁻¹²⁾ recently, which show that the growth of γ'' phase follows the $t^{1/3}$ law of LSW theory in some systems^(6, 9, 10), while it follows the $t^{1/2}$ law as predicted by interface-controlled growth in others⁽¹¹⁾. Other interesting and complex results were found in Ni-12.5 Ta systems⁽¹²⁾, which showed that the diameter of γ'' phase particles grow linearly with aging time while their thickness follows $t^{1/2}$ relationship.

The effect of volume fraction on the coarsening behaviour has been confirmed by experimental results. Both the MLSW and LSEM theories give the broader particle size distribution, which is in better agreement with the experimental results mentioned above. Also, the cut-off points have been observed to be between 1.6 and 2.4 rather than $\rho_c = 1.5$. On the other hand, the evidence of the effect

of volume fraction, ϕ , on the growth rate constant is poor. Ardell⁽²³⁾ found that although a large effect of ϕ_{Co} on the coarsening rate of Co-precipitates existed in the Cu-Co system, in many other systems^(1, 2, 19, 23, 25) there is no effect of ϕ on the growth rate constant even for a system containing up to 60% γ' precipitates. The LSEM theory predicts a reduced influence of ϕ on the coarsening rate constant, which is in somewhat better agreement with experimental results than the MLSW theory.

It should be pointed out that the lattice misfit between precipitate and matrix also seems to influence the particle-size distribution. As the misfit increases the particle-size distribution has been observed to become broader in some alloy systems^(3, 4, 26).

2.4 Precipitates in nickel-base superalloys

Nickel-base alloys are the most widely used for elevated temperature service since they have excellent high temperature tensile and creep rupture strengths (even up to $0.8 T_m$), good oxidation and corrosion resistances, adequate fatigue and thermal-fatigue resistances and acceptable room temperature yield strength and ductility.

The major contribution to the strength of precipitation hardened nickel base superalloys is provided by the formation of coherent stable intermetallic compounds, γ' [$\text{Ni}_3(\text{Al}, \text{Ti})$] and γ'' [$\text{Ni}_3(\text{Nb}, \text{Al}, \text{Ti})$]. Other phases, for example, carbide and boride, provide little additional strengthening at low temperature.

γ' phase is the most important strengthening phase in nickel and nickel-iron base alloys. This phase has L1_2 F.C.C. structure and precipitates coherently in the F.C.C. matrix with $\{100\}_{\gamma'}$ || $\{100\}_{\gamma}$, $\langle 001 \rangle_{\gamma'}$ || $\langle 001 \rangle_{\gamma}$ orientation relationship. In general, the shape of γ' phase is spherical when the misfit between γ matrix and γ' precipitate is 0 - 0.2%, then becomes cubical at a mismatch around 0.5 - 1.0% with increasing (Al + Ti) contents. When the mismatch is 1.25% the shape of γ' phase has been reported to be platelike⁽²¹⁾. The volume fraction of γ' increases with increasing amount of Al, Ti and Nb, and it changes from less than 10% in low (Al + Ti) content alloys to 67% in In-100 casting alloy.

B.C.T. (DO_{22}) phase has only been found in some alloys, such as Inconel 718, 706, René 62 and Udimet 630, which contains 2-6% niobium and a considerable amount of iron⁽²¹⁾. It is considered that γ'' (Ni_3Nb) phase can form only when

the concentration of valence electron $e/a > 8.65$.

The γ'' precipitate is usually disc shaped in appearance and has a $\{100\}_{\gamma''} \parallel \langle 100 \rangle_{\gamma}$, $\langle 001 \rangle_{\gamma''} \parallel \langle 001 \rangle_{\gamma}$ relationship with the matrix. γ'' phase containing nickel-iron-base alloys have excellent intermediate temperature strength and are used to approximately 1200° F (922 K) as extended service exposure at 1200 - 1400°F can cause γ'' to transform to δ phase, which is a brittle phase, in alloys such as Inconel 718.

CHAPTER 3

EXPERIMENTAL TECHNIQUES

3.1 Materials

The material used in this investigation was commercial Inconel 718 superalloy which was provided by the International Nickel Company of Canada. The starting material was 0.474 cm thick sheets whose chemical composition is listed in Table 1.

3.2 Rolling and heat treatment

The sheets were cold rolled to about 0.2 mm thick strips with intermediate annealing at 1473 K. Before each rolling, the surface of the sheets was cleaned using 600 grade abrasive paper. These strips were then used for various aging treatments. The final solution treatment of these strips was carried out at 1473 K for 1 hour in a sealed vycor capsule, partially filled with pure argon. Solution treatment was followed by quenching in cold water. The capsules were always broken under cold water to get a homogeneous supersaturated solid solution. The quenched specimens were aged in sealed evacuated vycor capsules in the temperature range of 973 K - 1023 K for various periods of time, then quenched in cold water.

Table 1
Chemical Composition of Inconel 718 (wt%)

C	Fe	Ni	Cr	Al	Ti	Mo	Cb + Ta	Mn	S	Si	Cu
0.03	19.24	52.37	18.24	0.52	0.97	3.07	4.94	0.19	0.007	0.30	0.04

3.3 Preparation of thin foils and electron microscopy

The aged strips were cleaned using 600 grade abrasive paper and then punched into discs of 3 mm diameter. These 3 mm discs were thinned with a jet electropolishing unit using 15% perchloric acid, 85% methanol bath at 223 - 233 K. The electric current used was 85 - 100 MA, which provided good quality thin foils. The thin foils were examined in a Philips EM-300 electron microscope.

It has been observed that in Inconel 718 the γ'' phase grows coherently into discs on {100} planes of F.C.C. matrix with the c axis of γ'' phase being perpendicular to the discs and the γ' phase also forms coherently on the {100} F.C.C. matrix planes⁽²⁸⁾. Due to the presence of large coherent strains around γ'' and γ' particles individual particles could only be observed in the dark field using their superlattice reflections. Therefore in order to determine the true sizes of γ'' and γ' particles their dimensions were measured only in dark field micrographs taken in {100} thin foil orientation.

3.4 Volume fraction determination

Since no electrochemical extraction solution has been found to separate γ'' and γ' particles the combined

volume fraction of ($\gamma'' + \gamma'$) phases was determined using electrochemical extraction of the precipitates by anodic dissolution of the γ matrix in 1% ammonium sulphate and 1% citric acid in distilled water with a current density of 50 - 80 mA/cm². After the matrix was completely dissolved in the solution, the solvent was removed and the precipitates were washed in distilled water, then in alcohol and dried in an oven at 340 K. The total weight of γ'' and γ' precipitates were then determined. Strictly speaking, this method can only give weight fraction of the precipitates. However, since the differences between the densities of matrix and precipitates is very small it could be considered that the weight fraction is approximately equal to the volume fraction.

By counting the number of γ'' and γ' particles and measuring the average particle sizes of γ'' and γ' in the same areas, the ratio of the volume fraction of γ'' and γ' was evaluated to be between 2.50 - 3.80 in this study, which is good agreement with the previously reported value of about 3.0⁽²⁸⁾.

3.5 X-ray diffraction technique

To obtain the lattice misfit between matrix and precipitates, the lattice parameters of γ' precipitate and γ matrix were determined by x-ray diffraction techniques. The lattice parameter of γ' was determined using the Debye-Scherrer powder method with a 114.6 mm Debye-Scherrer camera. The $\text{Cu K}\alpha$ radiation and nickel filter were used and the film was exposed for about 4 hours. In order to obtain clear diffraction lines in the film, a piece of aluminum thin foil was also mounted along with the film to filter some of the background radiation.

The lattice parameter of γ matrix was determined by a diffractometer using 1.0 mm thick flat specimen in the solution treated and quenched condition. $\text{Cr K}\alpha$ radiation with Vanadium filter and $\text{Cu K}\alpha$ radiation with Fe filter were used and scanning rates were $1/2^\circ/\text{minute}$ and $1/4^\circ/\text{minute}$, respectively.

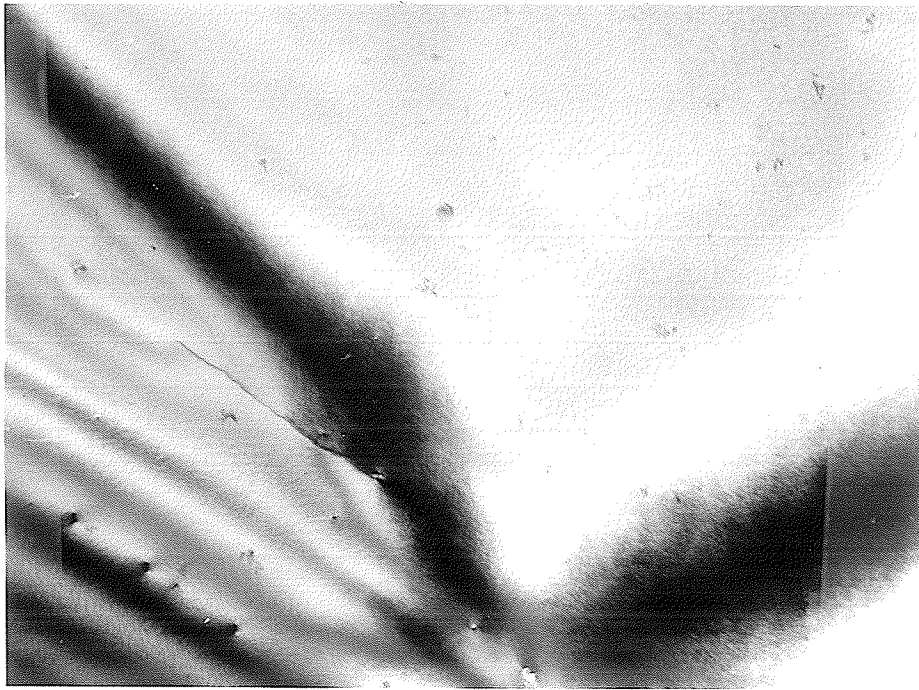
CHAPTER 4

RESULTS4.1 Precipitation behaviour of Inconel 718

As mentioned earlier, all the specimens were given a final solution treatment at 1473 K for 1 hour, then water quenched. During water quenching the vycor tube was broken under water to achieve a rapid cooling rate. The water quenched specimens were then resealed in a vycor tube and aged at 973, 998 and 1023 K for various periods of time.

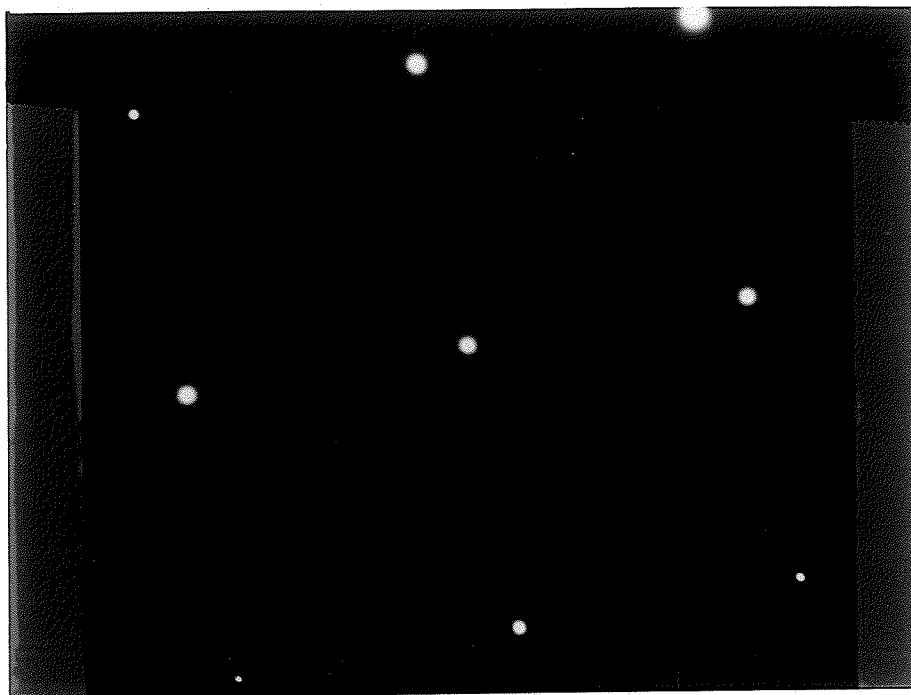
4.1.1 Microstructure of solution treated specimens

The thin foils of solution treated specimens were examined in the electron microscope and a typical bright field microstructure is shown in Figure 18. The selected area diffraction pattern is shown in Figure 19. It was observed that in the bright field structure most of the areas had a smooth surface, which suggests that the alloy is single phase solid solution whose crystal structure was found to be F.C.C. by electron and x-ray diffraction. However there exist some areas with rippled surface, as shown in Figure 18, suggesting that there could be very

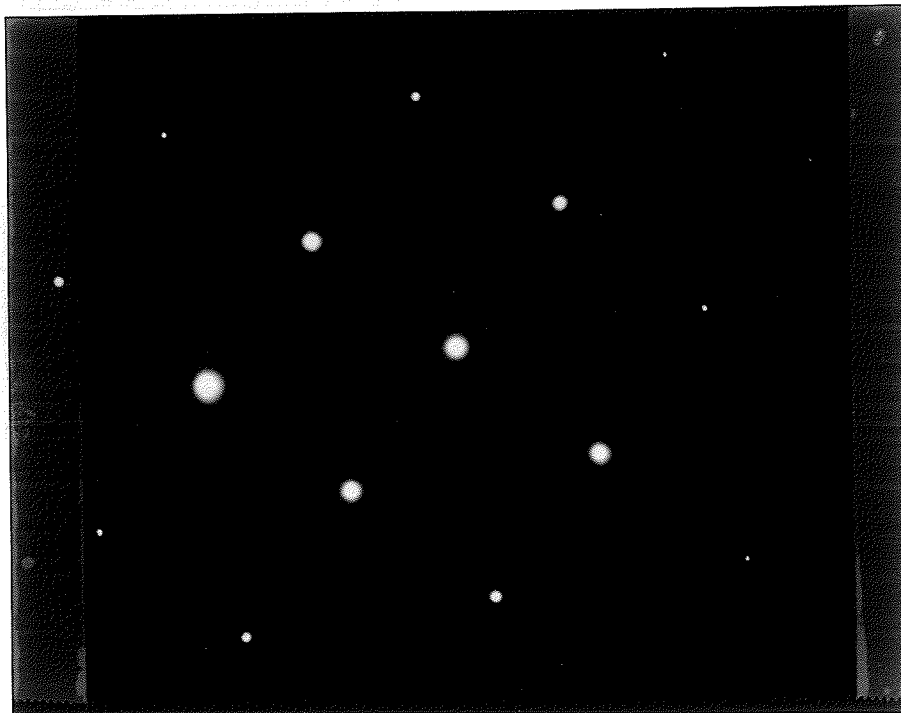


53000 x

Figure 18. Microstructure of solution treated Inconel 718 annealing for 1 hour at 1200°C and water quenching. bright field.



A



B

Figure 19. Selected area diffraction pattern of structure shown in Figure 18 (001) orientation
A. regular project lens current
B. reduced project lens current of A.

small precipitates or GP zones in the solution treated specimens. The SADP which has (001) orientation does not show any secondary diffraction spots due to the presence of either γ'' or γ' precipitates. The absence of secondary reflection could be due to the fact that the precipitates are too small and the total amount of precipitate is also small. However the x-ray diffractometer results did show the presence of a few peaks which could be due to the presence of γ'' and γ' precipitates, as shown in Table 2.

The lattice parameter of γ matrix was determined using the x-ray diffractometer. The solution treated specimen was given 50% deformation and annealed for 4 minutes at 1050°C followed by water quenching to get a very small grain size of 0.035 μ m. This specimen was then mounted on an x-ray diffractometer. The results are shown in Table 2. Only three diffraction peaks were available by using $Cu K_{\alpha}$ radiation, which arise from (111), (200) and (220) planes, as shown in Table 2A. To obtain more accurate a_{γ} the $Cu K_{\alpha}$ radiation with shorter wave length was also used for the determination of a_{γ} . The lattice parameter was calculated by using least square fit method and was found to be

Table 2

X-ray diffraction results of solution treated
Inconel 718 after 1473 K/1 hr + 50% deformation
+ 1323 K/4 minutes

A. Radiation Cr K α ($\lambda = 2.2909 \text{ \AA}$), Filter: V

2θ	$d(\text{\AA})$	I/I_0	Suggested Phase	$a(\text{\AA})$
66.76	2.0819	100	γ (111)	3.606
78.85	1.8036	57	γ (200)	3.607
128.0	1.2744	80	γ (220)	3.605

B. Radiation Cr K α ($\lambda = 1.5418 \text{ \AA}$), Filter, Fe

2θ	$d(\text{\AA})$	I/I_0	Suggested Phase
43.35	2.0869	100	$\gamma + \gamma'$ (111)
45.15	2.0076	12	γ'' (112)
50.47	1.8084	47	$\gamma + \gamma' + \gamma''$ (200)
66.05	1.4145	8	unidentified
74.30	1.2767	36	$\gamma + \gamma'$ (220)
79.40	1.2068	6	unidentified
90.13	1.0890	30	γ (311)
95.51	1.0414	10	γ (222)
117.50	0.9012	4	γ (400)
137.35	0.8272	21	γ (331)
138.05	0.8254	10	unidentified
145.0	0.8081	5	γ' (420)
145.82	0.8065	25	γ (420)
146.78	0.8047	15	unidentified

$a_{\gamma} = 3.606 \text{ \AA}$, which is slightly larger than the generally reported value of $a_{\gamma} = 3.60 \text{ \AA}$ ^(27, 29).

4.1.2 Structures of aged specimens

On aging in 973 - 1023 K range both γ' and γ'' precipitates exist simultaneously in the γ matrix. The precipitation behaviour of this alloy has been reported by Oblak et. al⁽²⁸⁾. These are two points of view about the precipitation behaviour of γ'' in the Fe and Nb containing nickel base alloys⁽²⁷⁾. One considers that γ' and γ'' form simultaneously at the beginning of the aging process, another argues that only γ' phase precipitates at the very beginning and then γ' transforms into γ'' phase. However, the results of the present investigation show that both γ'' and γ' phases exist in all the specimens aged between 973 to 1023 K temperature range. Furthermore, the diffraction peaks in the x-ray diffractometer results due to the presence of both γ'' and γ' have been observed in the water quenched solution treated specimen. This would suggest that γ' and γ'' form simultaneously in the present alloy.

Figure 20 shows a typical bright field structure of an aged specimen. This is the structure of a specimen that was aged for 200 hours at 998 K and its selected area



60000 x

Figure 20. Microstructure of 998 K, 200 hours aged Inconel 718 bright field.

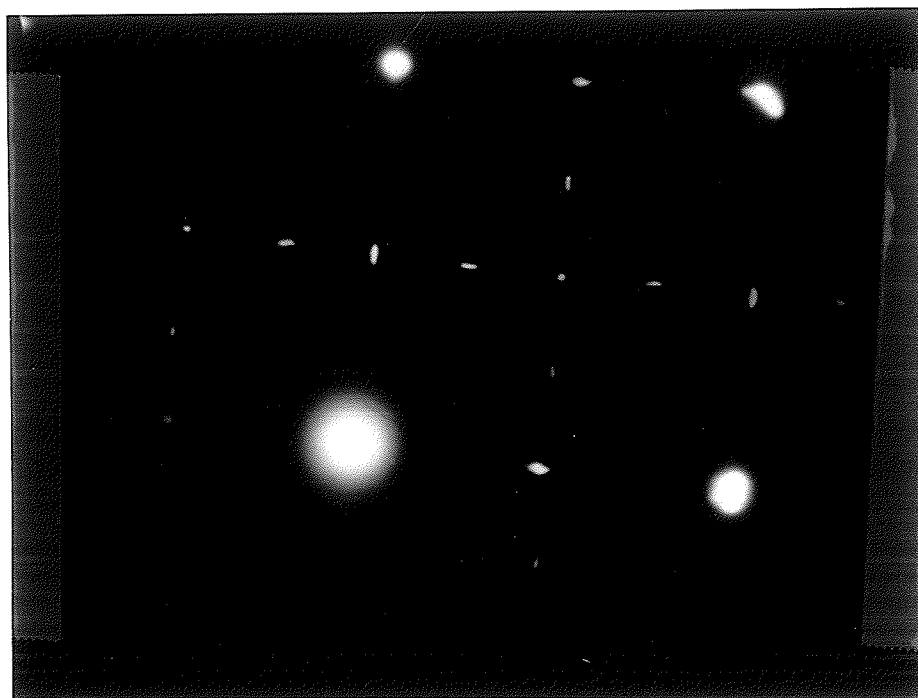


Figure 21. Selected area diffraction pattern of structure shown in Figure 20. (001) orientation.

diffraction pattern (SADP) is shown in Figure 21. The secondary diffraction spots in the SADP are due to the presence of ordered γ'' and γ' precipitates. The (100), (010) and (110) reflections are due to both γ'' and γ' phases, whereas $(\frac{1}{2} 10)$ and $(1 \frac{1}{2} 0)$ reflections only arise from the presence of γ'' phase. This is confirmed by the dark field microstructures shown in Figure 22. In Figure 22A and D using (100) and (010) reflections, the disc shaped γ'' and spherical γ' are observed, while in Figure 22B which is taken with $(\frac{1}{2} 10)$ reflection only disc shaped γ'' particles are visible. In the case of the dark field structure obtained with (110) reflection both γ'' and γ' phases are observed as shown in Figure 22C, but the particle size can not be measured easily. Therefore a number of dark field micrographs of areas in (001) orientation using (100), (010), $(\frac{1}{2} 10)$ and $(1 \frac{1}{2} 0)$ reflections were taken for the measurement of particle sizes of γ'' and γ' precipitates.

Similar to γ' phase in other alloys, the γ' phase in this alloy also has an ordered FCC LI_2 structure which is shown in Figure 23 and precipitates coherently in the FCC matrix, having an orientation relationship of $\{100\}_{\gamma'}$, $\parallel \{100\}_{\gamma}$, $\langle 001 \rangle_{\gamma'}$, $\parallel \langle 001 \rangle_{\gamma}$ with γ matrix. The lattice

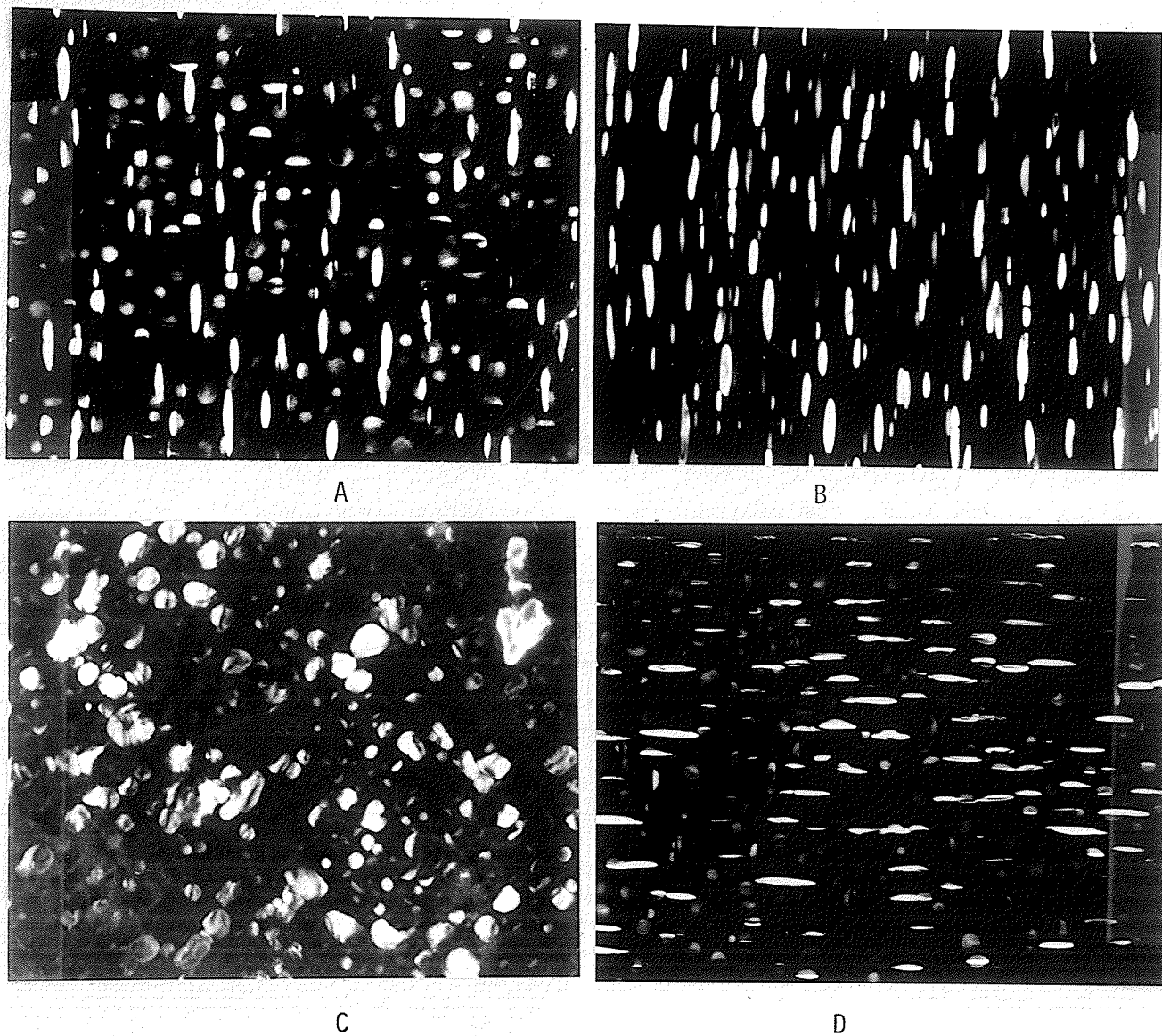


Figure 22. Microstructure of 1023 K, 30 hrs aged alloy 718. (001) orientation. Dark field micrographs 110,000 x. (a) $\bar{g} = 100 (\gamma' + \gamma'')$; (b) $\bar{g} = \frac{1}{2}10 (\gamma'')$; (c) $\bar{g} = 110 (\gamma' + \gamma'')$; (d) $\bar{g} = 010 (\gamma' + \gamma'')$.

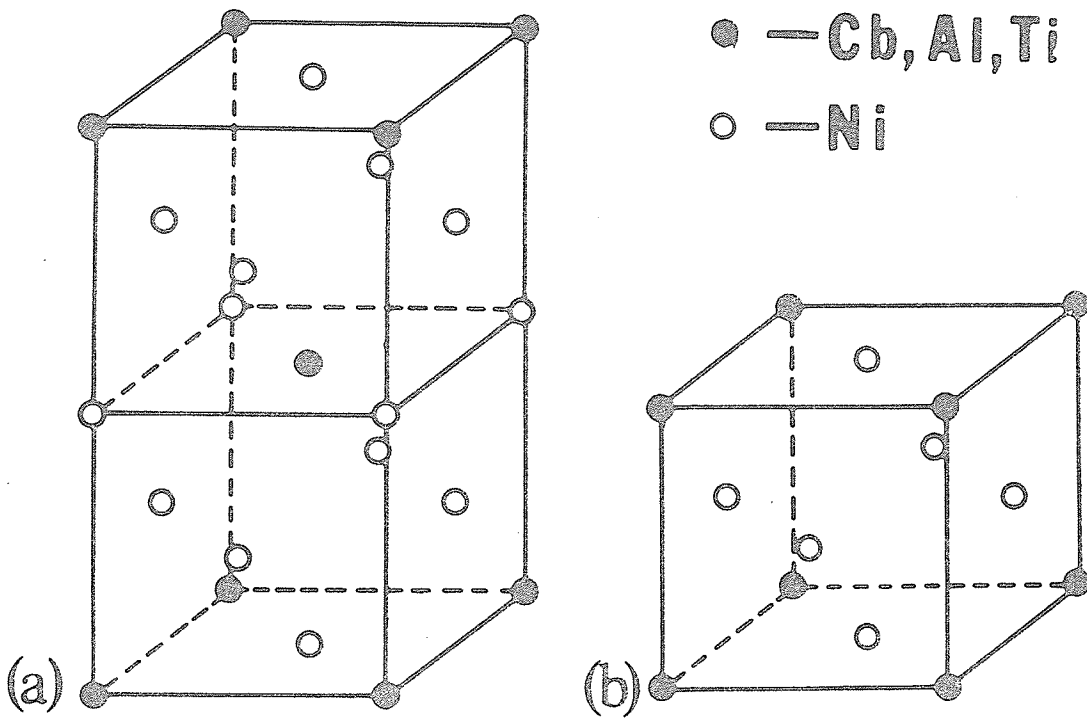
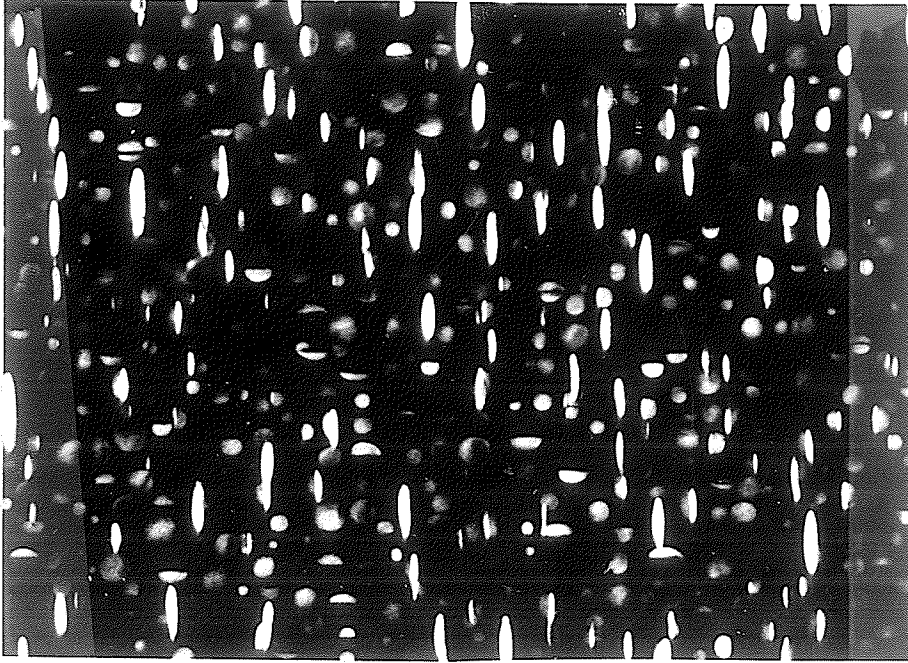


Figure 23. Unit cells showing ordering (a) BCT (DO_{22}) structure. (b) FCC (LI_2) structure^{28, 22}.

parameter of γ' phase in this alloy was determined by the Debye-Scherrer powder camera method using the electrochemically extracted powder. The calculated value of $a_{\gamma'}$ was found to be 3.622 \AA , hence the lattice misfit between γ' and γ matrix is about 0.4%. This is in agreement with the value reported elsewhere.^(27,30) The shape of γ' phase in this alloy was found to be spherical, as shown in Figure 24. The darker round particles in Figure 24 are γ' phase.

The γ'' phase has an ordered body-centered tetragonal (BCT) structure, which is also shown in Figure 23, and precipitates coherently with γ matrix with an orientation relationship of $\{100\}_{\gamma''} \parallel \{100\}_{\gamma}$ and $\langle 001 \rangle_{\gamma''} \parallel \langle 001 \rangle_{\gamma}$ with FCC matrix. The lattice parameters of γ'' phase were reported to be $a_{\gamma''} = 3.624 \text{ \AA}$, $c_{\gamma''} = 7.406 \text{ \AA}$ ^(28, 30) and hence the tetragonal distortion between γ'' phase and γ matrix is about 2.70%. Similar to other γ'' containing alloys γ'' precipitate in this alloy also has disc shaped morphology where the c axis is normal to disc plane. The typical shape of γ'' particles is also shown in Figure 24, where the higher contrast disc shaped precipitates are γ'' phase. The aspect ratio, i.e., the ratio of diameter to thickness, $q = d/h$, increases slightly with increasing aging time, as shown in Table 5. For example, at the aging temperature of 1023 K,



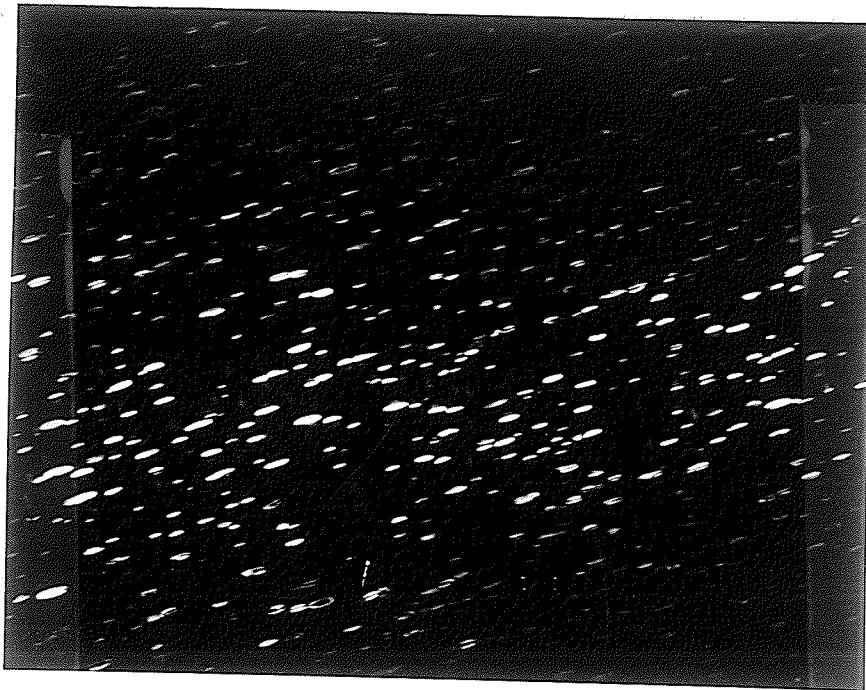
100000 x

Figure 24. Morphology of γ' and γ'' precipitates aged at 973 K for 300 hours.

$q = 3.56$ for aging time of 5 hours and $q = 3.89$ for 100 hours aging; for the case of 998 K, $q = 3.66$ at the aging time of 25 hours whereas $q = 4.03$ for 200 hours. This is shown in Figure 25.

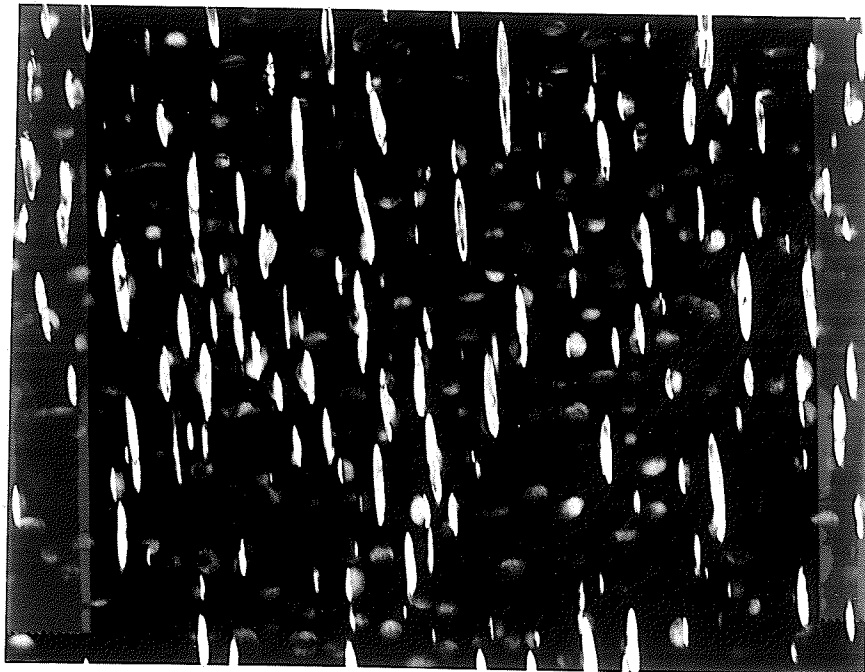
4.1.3 The volume fraction of precipitates

The total volume fraction of γ'' and γ' , $f(\gamma'' + \gamma')$, was determined by the electrolytical extraction method. The determined values of $f(\gamma'' + \gamma')$ for three aging temperatures after various aging times are shown in Table 4 and Figure 26. It is seen that at all three aging temperatures the volume fractions first increase with aging time and then remain constant after 5 hours at 1023 K, 10 hours at 998 K and 30 hours at 973 K. Since the particle size was measured only in those specimens aged for periods greater than 5 hours at 1023 K, 10 hours at 998 K and 30 hours at 973 K their growth can be assumed to have occurred at constant volume fraction. The proportions of volume fraction of γ'' and γ' and their individual values were evaluated by using electron micrographs. The results are listed in Table 3 which shows that the ratios of volume fractions of γ'' and γ' precipitates are in the range of 2.50 to 3.80.



A

$$q = 3.66$$



B

$$q = 4.03$$

90000 x

Figure 25. The difference in shape of γ'' particles aged at 998 K for different time. (001) orientation dark field micrographs

A) 25 hours;

B) 200 hours.

Table 3

Volume fraction of γ' and γ'' precipitates
measured by electron micrographs

aging temp.	aging time	$f_V(\gamma')$	$f_V(\gamma'')$	$f_V(\gamma'')/f_V(\gamma')$
973 K	100	3.75	12.80	3.41
	200	3.63	13.78	3.80
	306	4.09	13.00	3.18
998 K	25	3.38	12.42	3.67
	100	4.59	11.49	2.50
	300	4.60	12.13	2.64
1023 K	30	4.19	10.63	2.54
	100	3.81	11.79	3.09
	200	4.27	11.16	2.61

Table 4

Experimentally determined volume fraction $f(\gamma' + \gamma'')$ ¹

Aging temperature	Aging time (hours)	$f(\gamma' + \gamma'')$ (%)
973 K	2	6.0
	5	11.04
	10	13.97
	15	15.22
	20	16.03
	25	16.46
	30	17.31
	185	17.48
998 K	1	8.27
	2	12.50
	4	15.25
	7	15.44
	10	15.90
	15	15.84
	103	16.65
1023 K	0.5	11.01
	1	12.43
	2	13.60
	3	14.41
	5	15.06
	7	15.08
	88	15.30
718°C/8 hours + 620°C/18 hour AC (Standard heat treat of commercial Inconel 718)		16.81

¹All the specimens were given 1473 K/1 hr solution treatment

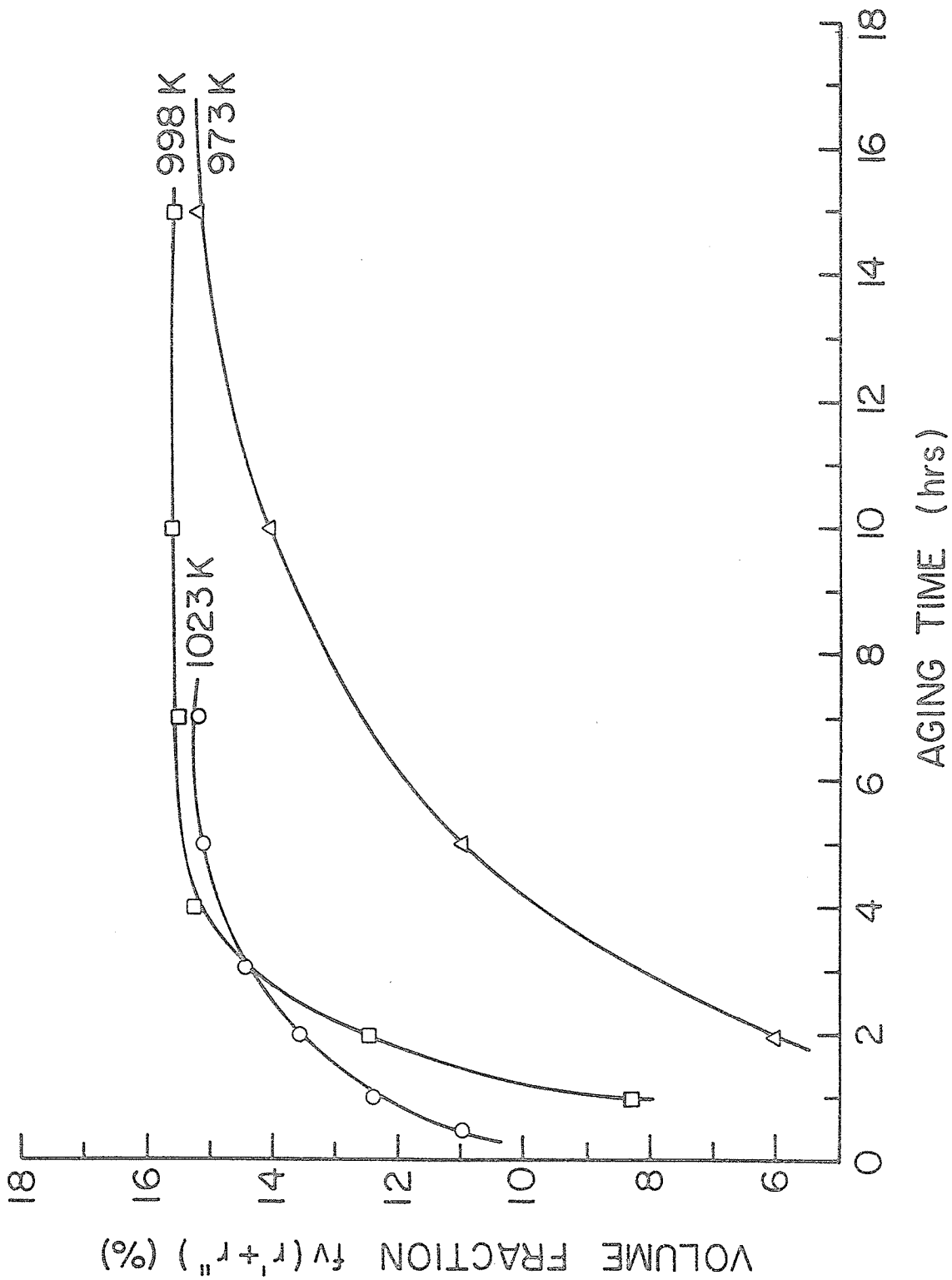


Figure 26. The variation in the total volume fraction, $f_v(\gamma' + \gamma'')$ with aging time for Inconel 718.

4.2 Growth rate of precipitates

A general equation for the variation of average particle size with time can be written as

$$\bar{r}^n - \bar{r}_0^n = Kt \quad (4.1)$$

where K is a rate constant and the exponent n is dependent on the mechanism of coarsening. Theoretically,

n = 2 for interface controlled coarsening

n = 3 for lattice diffusion controlled coarsening

n = 4 for grain boundary diffusion controlled coarsening.

The constant K is also different for the three cases, and the value of \bar{r} is given by $\Sigma r_i / N$ in the case of interface and diffusion controlled growth and

$$\bar{r} = \frac{1}{\Sigma(\frac{1}{r_i})/N}$$

in the case of grain boundary diffusion controlled growth.

In general r_0 is very small and can be neglected the equation (4.1) can be written as

$$\log \bar{r} = \frac{1}{n} \log K + \frac{1}{n} \log t . \quad (4.2)$$

Therefore n can be obtained from the slope of the $\log \bar{r} - \log t$ plot. As discussed earlier, when the growth of precipitates follows the LSW theory of lattice diffusion controlled growth, the kinetic equation for the growth of a spherical particles can be written as

$$\bar{r}^3 - \bar{r}_0^3 = \frac{8 \sigma DC_e V_m}{9RT} = K't \quad (4.3)$$

where \bar{r} is the average radius of the growing particles at time t and \bar{r}_0 is the average radius at the onset of the coarsening process, σ is the interfacial free energy of particle-matrix interface, D is the diffusion coefficient of the solute atoms in the matrix, C_e is the concentration of solute atoms in equilibrium with particle of infinite radius, K is the gas constant, T is the absolute temperature of coarsening and V_m is the molar volume of the precipitate.

For disc shaped particles equation (4.3) has been modified to

$$\bar{d}^3 - \bar{d}_0^3 = \frac{128 \sigma^{(p)} q DC_e V_m}{9\pi RT} = K''t \quad (4.4)$$

where \bar{d} is the average diameter of the disc shaped particles, $\sigma^{(p)}$ is the interfacial free energy of peripheral interface which is normal to the direction of measured d , q

is the aspect ratio, $q = d/h$, and h is the thickness of particles.

Therefore, to establish the coarsening kinetics of γ' and γ'' particles their sizes were first measured. It was observed that γ' particles precipitate on $\{100\}$ matrix planes and align themselves along $\langle 100 \rangle$ direction. Therefore, all the γ' particle size measurements were done on electron micrographs from areas in (100) crystallographic orientation. Similarly, the γ'' precipitate also forms on $\{100\}$ matrix planes, therefore the precipitate size measurements of these phase were also done only on micrographs from areas in (100) orientation. About 200-300 individual γ'' and γ' particles were measured for each aging heat treatment. The number of particles per unit volume, N_V , was calculated from the number of particles per unit area, N_A , using the expression $N_V = N_A/(\bar{d}+t)$, which was suggested by Cahn and Nutting⁽³²⁾, where \bar{d} is the average particle size and t is the thickness of the thin foil.

The measured values $\bar{d}_{\gamma''}$, $\bar{h}_{\gamma''}$ and $\bar{d}_{\gamma'}$, for three aging temperatures are listed in Table 5. According to equations (4.3) and (4.4), if the coarsening process of particles is lattice diffusion controlled the plot of \bar{d}^3

Table 5

Measured average particle size

Temp.	Time (hours)	\bar{d}_γ (Å)	$\bar{d}_{\parallel\gamma}$ (Å)	$\bar{h}_{\parallel\gamma}$ (Å)	$\bar{d}_{\parallel\gamma}/\bar{h}_{\parallel\gamma}$
1023 K	5		212	59	3.56
	15		334	88	3.79
	30	246	407	108	3.77
	50	285	513	134	3.83
	100	352	630	162	3.89
	200	429			
998 K	25	184	326	89	3.66
	50	230	424	111	3.82
	100	292	538	141	3.82
	200	360	702	174	4.03
	300	409	825	194	4.25
973 K	50	143	257	81	3.16
	100	187	321	101	3.18
	200	242	427	123	3.47
	306	281	506	146	3.47

against time t should be straight lines. Therefore the $\bar{d}_{\gamma''}^3$ vs. t and $\bar{d}_{\gamma'}^3$ vs. t have been plotted in Figures 27 and 28, which are straight lines in all cases, suggesting that both γ'' and γ' precipitates follow the lattice diffusion controlled growth. The rate constants, K'' and k' and \bar{d}_0 for the coarsening processes of γ'' and γ' particles are listed in Table 6. The volume diffusion controlled growth of γ'' and γ' particles was also established by plotting \log (particle size) vs. $\log t$ for various aging temperatures, as shown in Figures 29, 30 and 31. All these plots are straight lines and the slopes of these lines, as listed in Table 7, are close to $1/3$, which also suggests that both γ'' and γ' phase particles grow by lattice diffusion controlled process.

4.3 Activation energy

Another major requirement of the LSW theory of lattice diffusion-controlled growth is that the activation energy for the coarsening process should be equal to that for the diffusion of the solute atoms in the matrix. Therefore it is necessary to determine the activation energy for the coarsening process of γ'' and γ' phases in this alloy.

Table 6

Experimentally determined values of the rate constants K and the mean onset particle size \bar{d}_0

Temperature	γ''		γ'	
	$K'' (\text{\AA}^3/\text{s})$	$\bar{d}_0 (\text{\AA})$	$K' (\text{\AA}^3/\text{s})$	$\bar{d}_0 (\text{\AA})$
973 K	1.26×10^2	+28.6	0.213×10^2	-40
998 K	5.28×10^2	-35	0.627×10^2	-18
1023 K	6.94×10^2	-58	1.043×10^2	+110

Table 7

Slopes of log (particle size) vs. log (aging time) plots

temp. plots	973 K	998 K	1023 K
log $d_{\gamma''}$ - log t	0.377	0.370	0.352
log $h_{\gamma''}$ - log t	0.319	0.317	0.337
log $d_{\gamma'}$ - log t	0.356	0.322	0.295

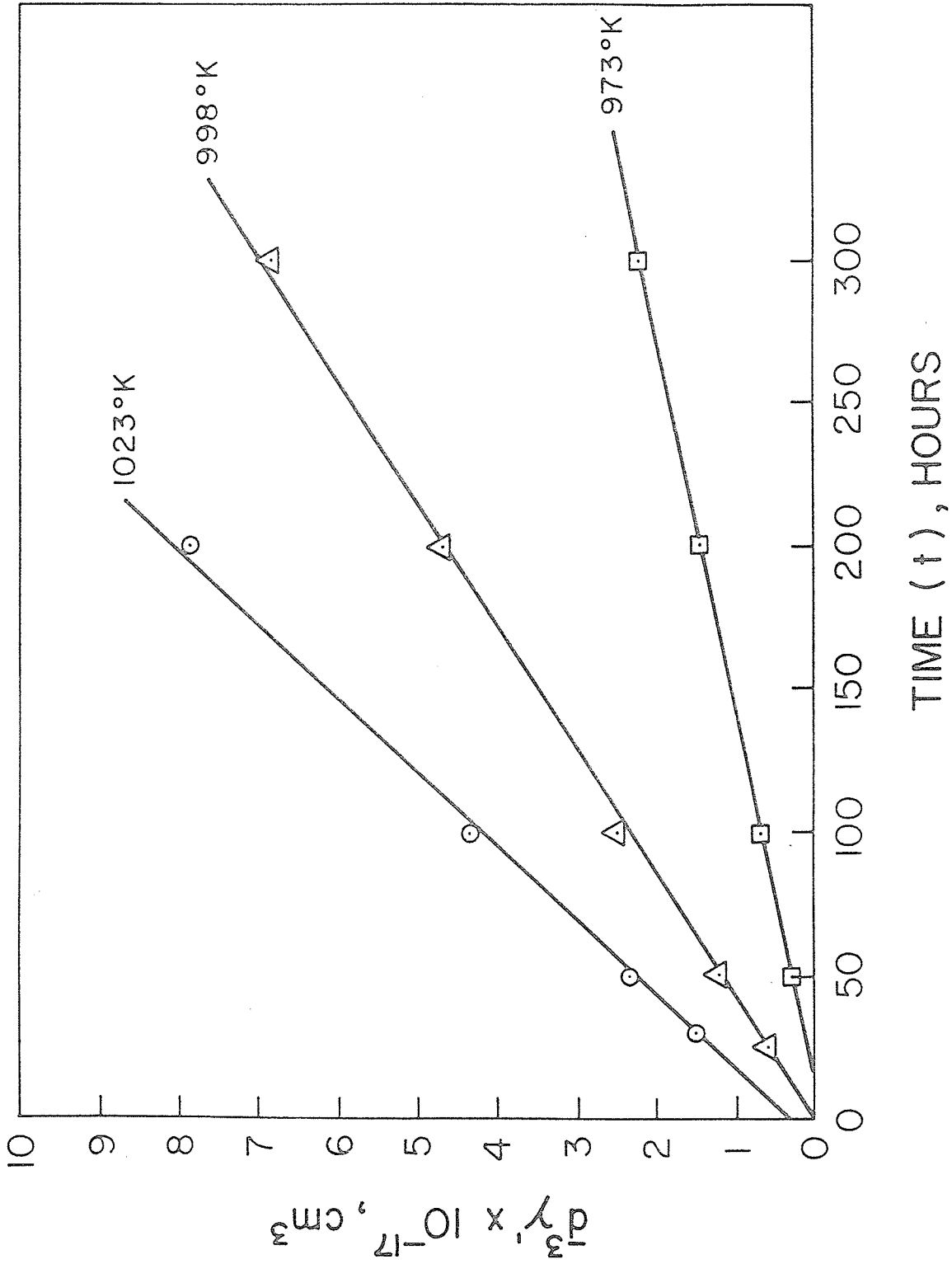


Figure 27. The variation in γ' (diameter)³ with aging time at different aging temperature.

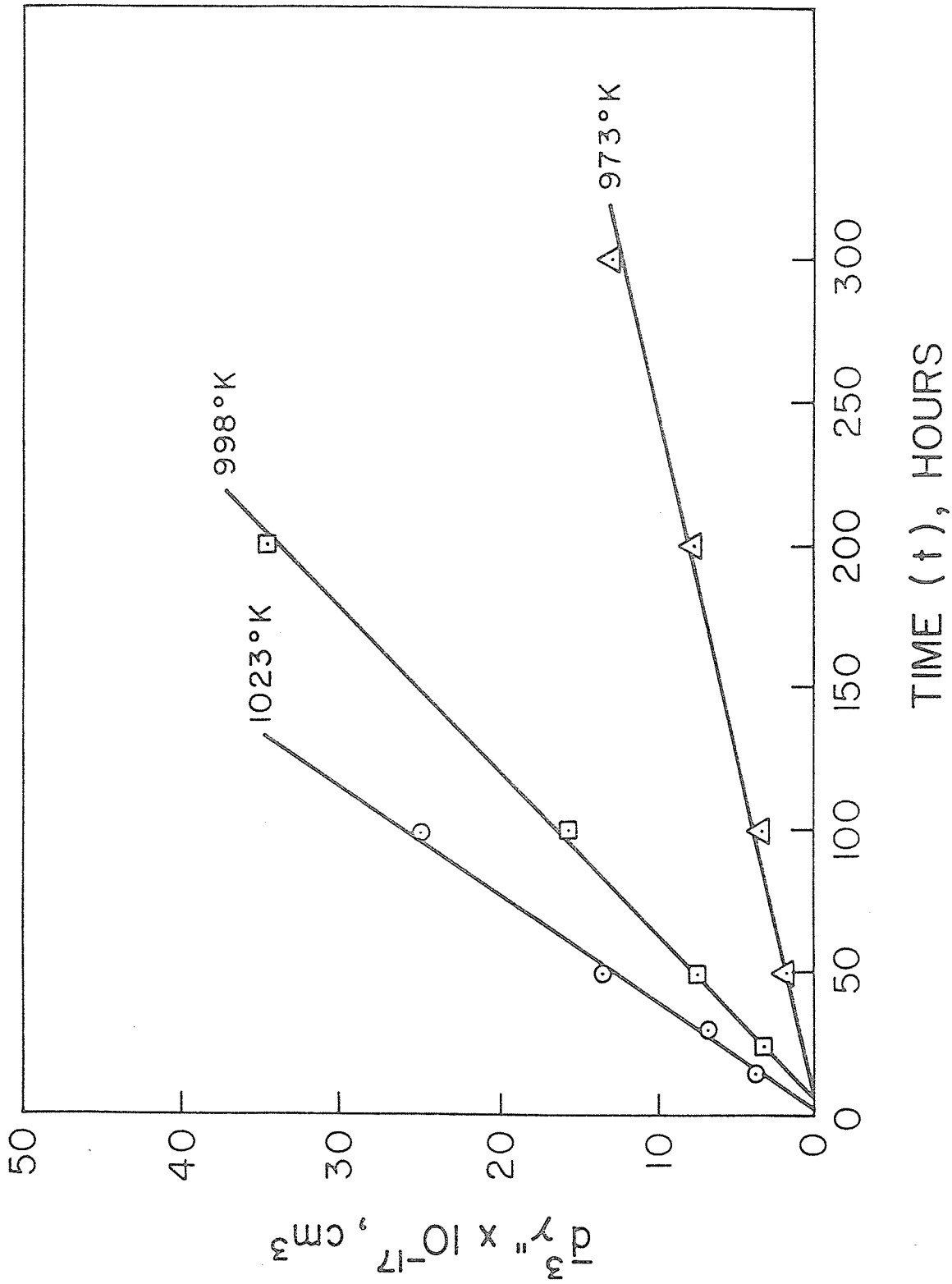


Figure 28. The variation in γ' (diameter)³ with aging time at different aging temperature.

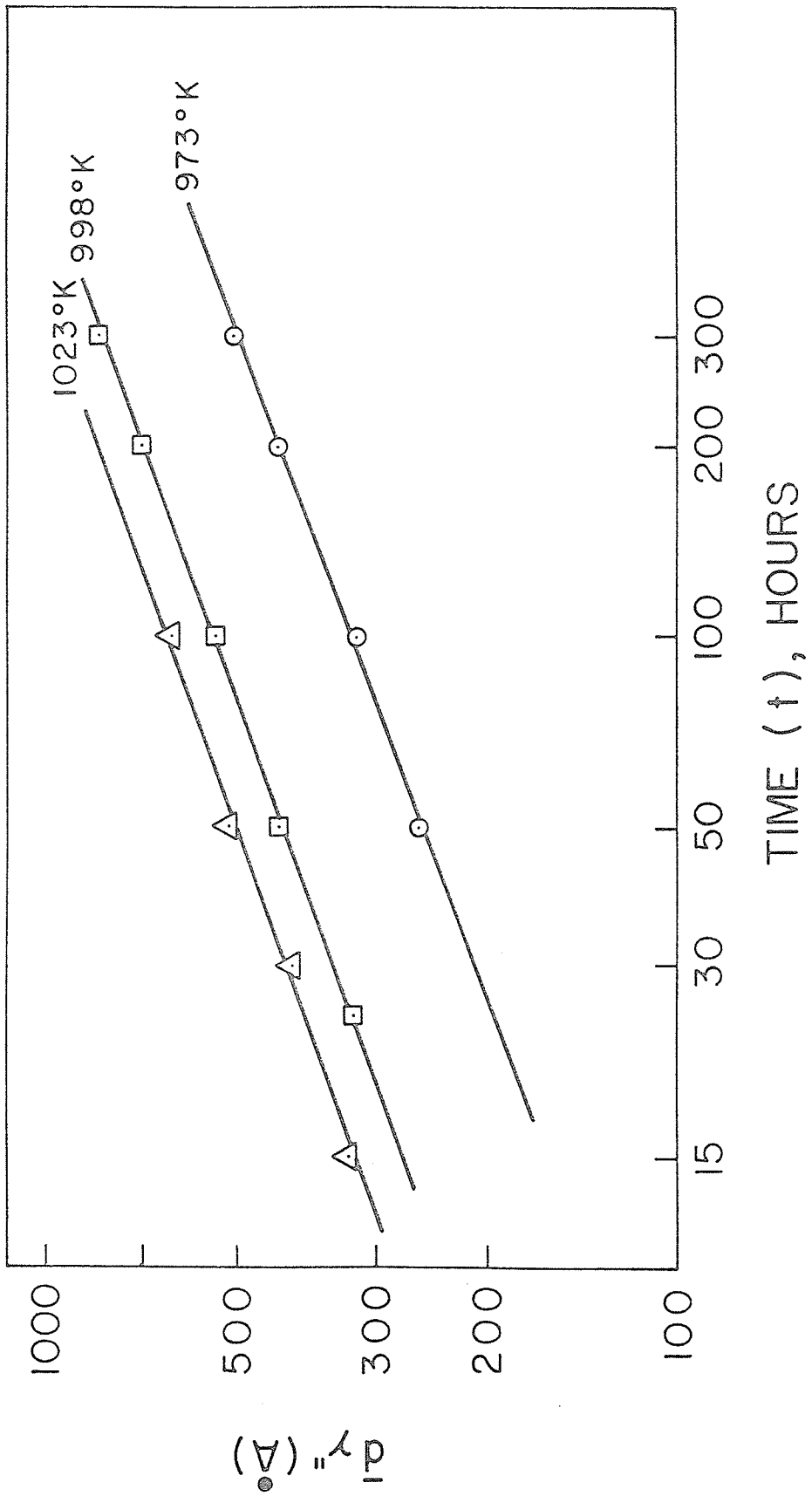


Figure 29. Log plots of mean diameter of γ'' vs aging time at different aging temperature.

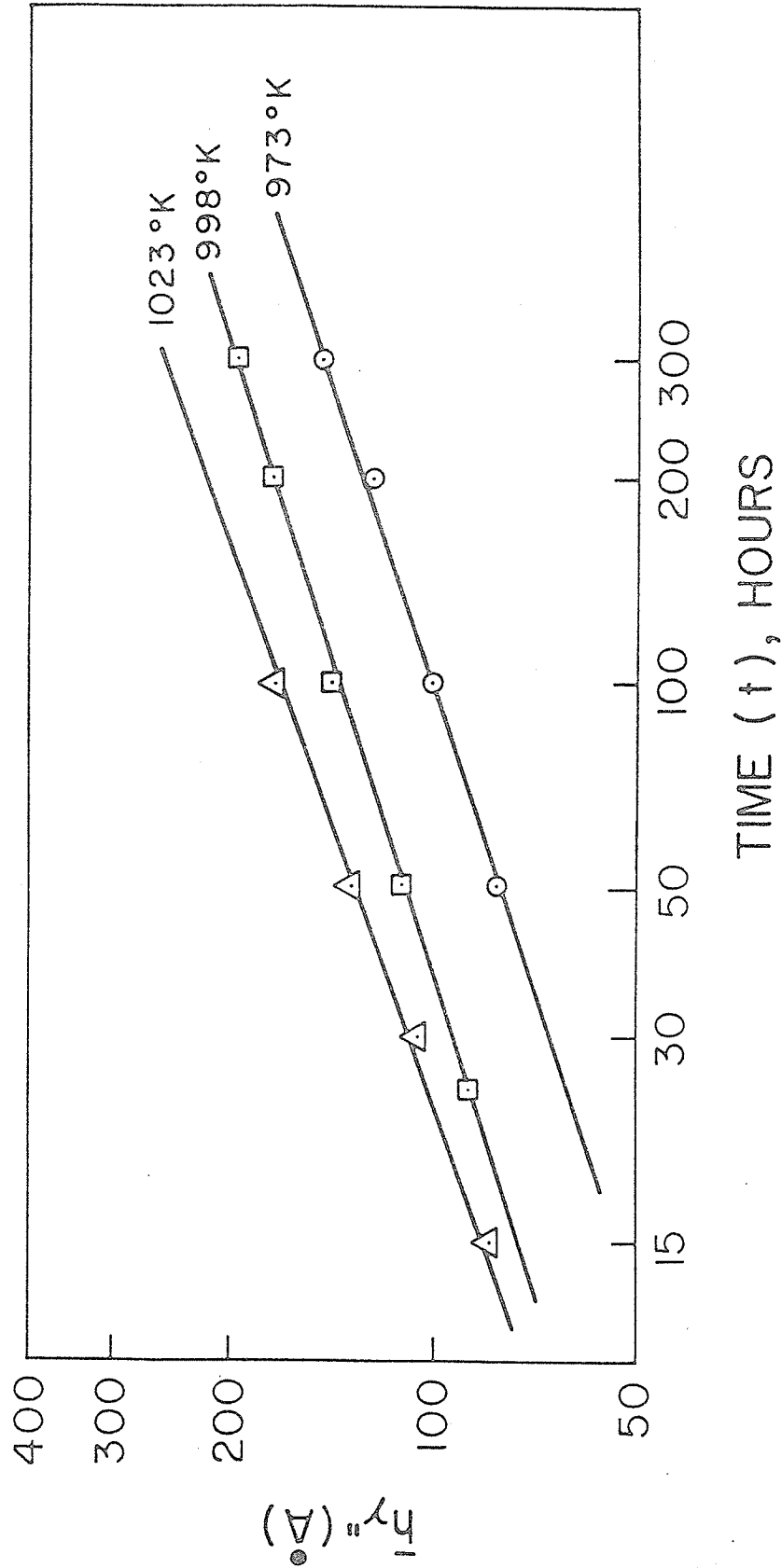


Figure 30. Log plots of thickness of γ'' vs. aging time at different aging temperature.

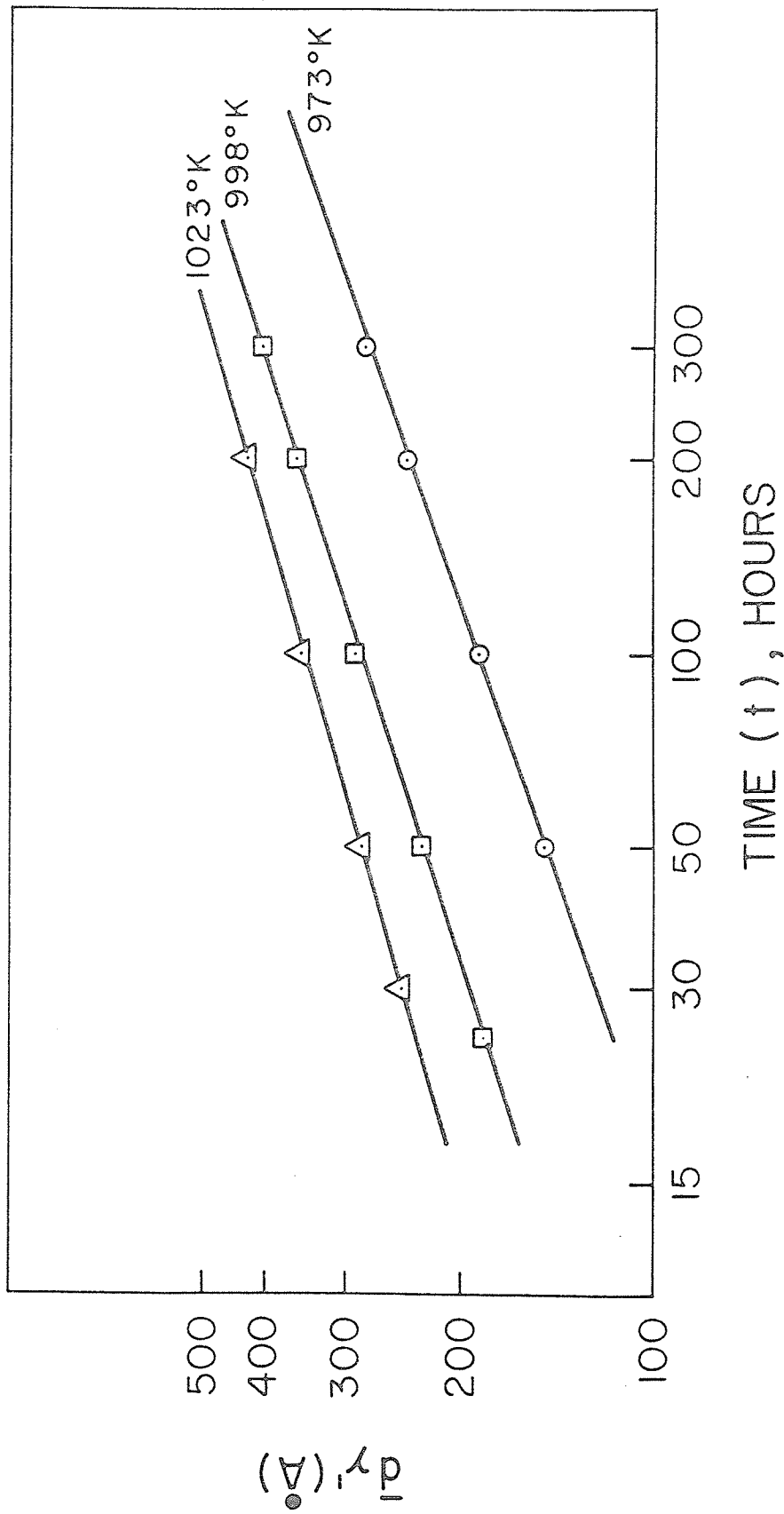


Figure 31. Log plots of mean diameter of γ' vs. aging time at different aging temperature.

The diffusion coefficient D in equation (4.3) and (4.4) is defined as $D = D_0 \exp(-Q/RT)$ where D_0 is the frequency factor and Q is the activation energy. The slope of the straight line in Figure 29, K'' , can be expressed from equation (4.4) as follows

$$K'' = \frac{128}{9} \frac{\sigma^{(p)} C_e V_m D_0}{\pi R} \cdot \frac{q}{T} \exp(-Q_{\gamma''}/RT) \quad (4.5)$$

In this expression, K'' , C_e , q and T are the only temperature dependent terms. Therefore, if their values at various temperatures are known the activation energy, $Q_{\gamma''}$, can be determined by the slope of $\ln(K''T/qC_e)$ vs. $1/T$ plot. It should be noted that unlike the case of a simple binary system, in this complex alloy some uncertainties exist regarding the partitioning of various elements in γ'' and γ' phases. For example, Nb can substitute for Ti and Al in γ' and Ti, Al can replace part of Nb in γ'' phase. Also the exact ratio of volume fraction of γ'' and γ' phases is unknown. Thus it is impossible to determine the activation energy for the coarsening process very accurately. However, it is observed that the total volume fraction of $(\gamma'' + \gamma')$ changes only by 2% over the temperature range used in the present investigation. Therefore the value of C_e may be considered

as constant and thus the activation energy $Q_{\gamma''}$ can be determined from the slope of $\ln (TK''/q)$ vs. $1/T$ plot. The data for the determination of activation energy is given in Table 8, and the $\ln (TK''/q)$ vs. $1/T$ plot is shown in Figure 32. It is seen that this plot is a straight line and the activation energy for the growth of γ'' precipitates by the least square fit method was obtained to be $298 \pm 41 \text{ KJ mol}^{-1}$. *Error limits are estimates of standing deviation.

Similarly, for γ' precipitate particles the slope of \bar{d}^3 , - t plots, shown in Figure 28 can be rewritten from equation (4.3) as follows

$$k' = \frac{8 \sigma C_e V_m D_0}{9R} \frac{1}{T} \exp (-Q_{\gamma'}/RT) \quad (4.6)$$

Thus the activation energy for the coarsening of γ' phase, $Q_{\gamma'}$, has been determined from the slope of the $\ln (TK')$ vs. $1/T$ plot, which is also shown in Figure 32. The relevant data for determining $Q_{\gamma'}$ are given in Table 8 as well and $Q_{\gamma'}$ was calculated to be $271 \pm 49 \text{ KJ mol}^{-1}$.

4.4 Distribution of precipitate particles

As discussed in Chapter 2, the Lifshitz-Wagner theory of lattice diffusion controlled coarsening predicted that

*Error limits are estimates of standard deviation.

Table 8

Data for the determination of activation energy Q

Temp.	$\frac{1}{T} \times 10^4$	γ''		γ'	
		$K'' (\text{Å}^3/\text{Sec})$	$\ln TK''/q$	$K' (\text{Å}^3/\text{Sec})$	$\ln T K'$
973 K	10.28	1.26×10^2	7.270	0.213×10^2	5.332
998 K	10.02	5.28×10^2	8.425	0.627×10^2	6.438
1023 K	9.775	6.94×10^2	9.074	1.043×10^2	6.973

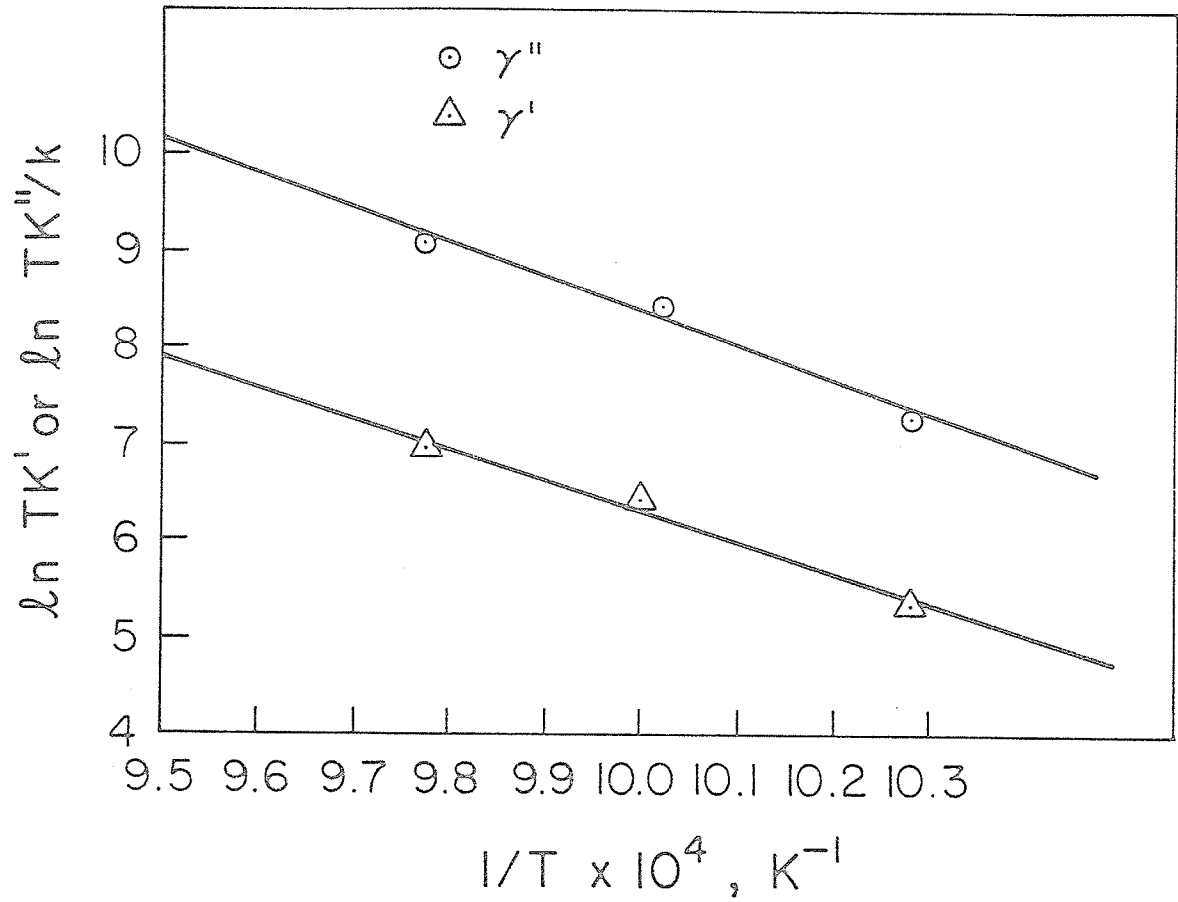


Figure 32. Arrhenius plots for the determination of the activation energy for coarsening of γ' and γ'' phases.

the particle-size distribution should approach a time-invariant function, i.e.

$$f(r,t) = f'(t) \rho^2 h_1(\rho) .$$

For comparing experimentally determined particle size distribution with theoretical distribution function $\rho^2 h_1(\rho)$, the distribution of γ'' and γ' particle size, after various aging times at three aging temperatures, were normalized according to the procedure suggested by Ardell and Nicholson⁽²⁾. The steady state distribution of particle size $f(d,t)$ can be obtained as follows

From equation (2.33) and (2.34)

$$g(d,t) = \frac{\rho^2 h_1(\rho)}{\frac{9}{8} \bar{d}}$$

$$f(d,t) = N_V g(d,t)$$

$$\text{therefore } f(d,t) = \frac{N_V}{\bar{d}} \cdot \frac{8}{9} \rho^2 h_1(\rho) . \quad (4.6)$$

Where N_V is the total number of particles per unit volume.

The number of particles, N_{Vj} , in each size class interval, Δ , is defined as⁽²⁾

$$N_{Vj} = f(r,t) dr \quad (4.7)$$

where $\Delta = D_{\max}/K$ and K is usually taken as 7-15, N_{Vj} denotes the number of particles having diameter between $(j-1)\Delta$ and $j\Delta$.

To evaluate the distribution function $[\rho^2 h_1(\rho)]$ in equation (4.5)] for oblate particles, dr in equation (4.7) has to be expressed in terms of their aspect ratio, $q = d/h$. It can be assumed that the oblate ellipsoidal particle is almost equal to the disc shaped particle when q is very small. Therefore equation (4.7) can be rewritten as⁽³³⁾

$$N_{Vj} = f(d,t) \frac{(2+q)\Delta}{6} \quad (4.8)$$

Then by combining equation (4.6) and (4.8) the distribution function for γ'' particles is given by

$$\rho^2 h_1(\rho) = \frac{27}{4} \frac{\bar{d}}{(2+q)\Delta} \frac{N_{Vj}}{N_V} \quad (4.9)$$

For γ' particles, the distribution function is given by

$$\rho^2 h_1(\rho) = \frac{9}{4} \frac{\bar{d}}{\Delta} \frac{N_{Vj}}{N_V} \quad (4.10)$$

The normalized histograms of γ' and γ'' particles were plotted against the reduced particle size, $\rho = d/\bar{d}$, after

various aging treatments. These plots are shown in Figure 33 for γ' particles and Figure 34 for γ'' particles. For comparison, along with the experimental distribution the theoretical distribution is also shown in these figures. Furthermore, the distribution of both γ' and γ'' precipitates were also plotted in the form of normalized distribution curves. These curves are shown in Figures 35 and 36.

It is seen that the experimental particle size distribution is much broader than the theoretical curve. For example at 973 K the cut-off point for γ' distribution curve is from 1.7 for specimen aged for 100 hours and increases to 1.9 when the aging time is increased to 300 hours. A similar behaviour is seen at 998 K and 1023 K aging temperatures. The maximum in the distribution curve occurs at the ρ value of about 0.8 - 0.9 instead of 1.135 at all the three aging temperatures. The observed values of maxima after various aging temperatures is nearly the same but considerably less than the theoretical value. The distribution curves of γ'' precipitates also show a very similar behaviour but their cut-off values are considerably larger than that of γ' , as shown in Figure 36.

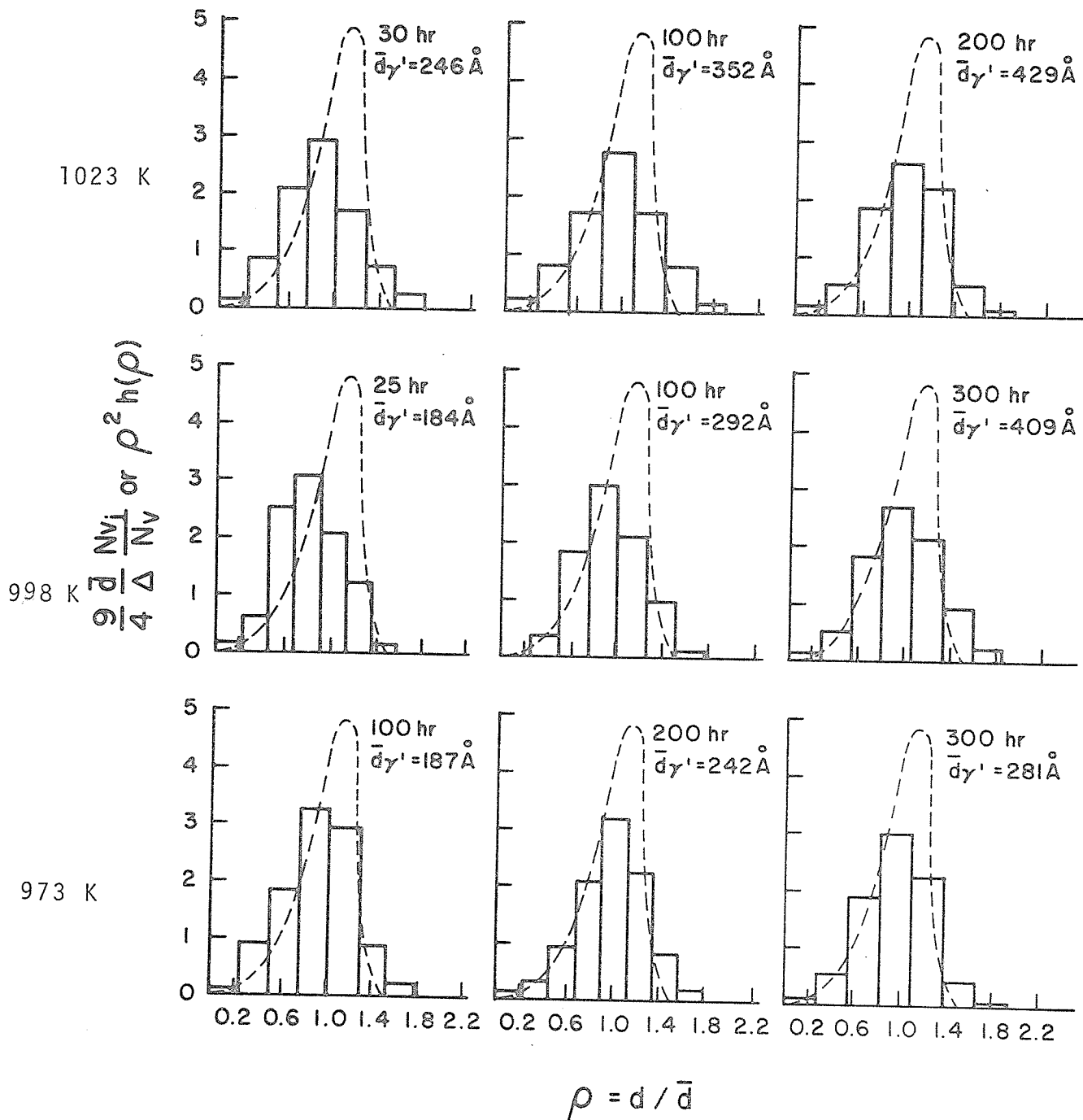


Figure 33. Experimentally determined distribution of γ' particle size, plotted as $(9/4) \bar{d} g$ (a.t.) for comparison with theoretical function $\rho^2 h(\rho)$.

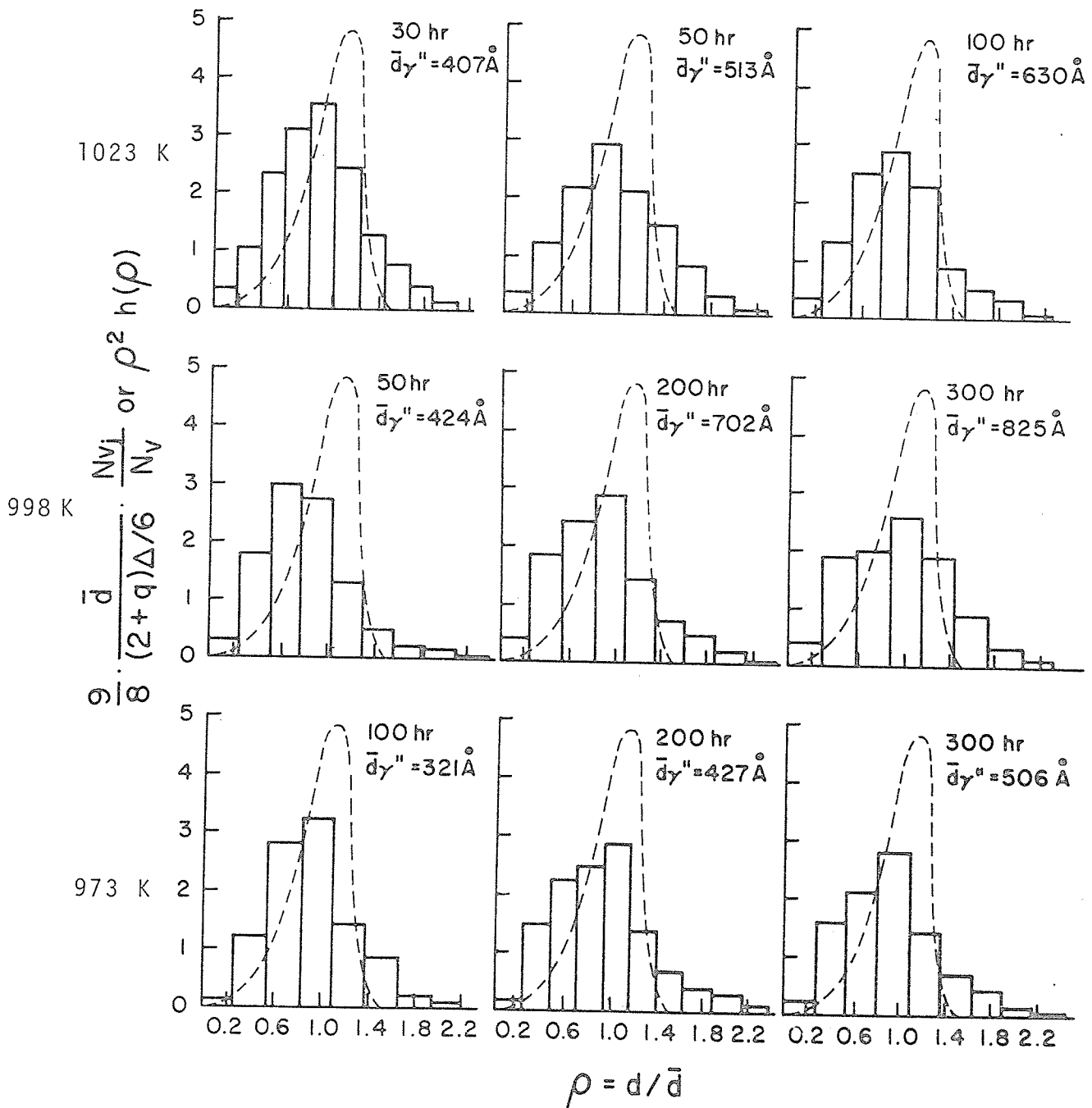


Figure 34. Experimentally determined distribution of γ'' particle size, plotted as $(9/4) \bar{a} g(a,t)$ for comparison with theoretical function $\rho^2 h(\rho)$.

Figure 35. Experimentally determined distribution curves of γ' particle size for comparison with theoretical function $\rho^2 h(\rho)$.

A. 973 K

B. 998 K

C. 1023 K

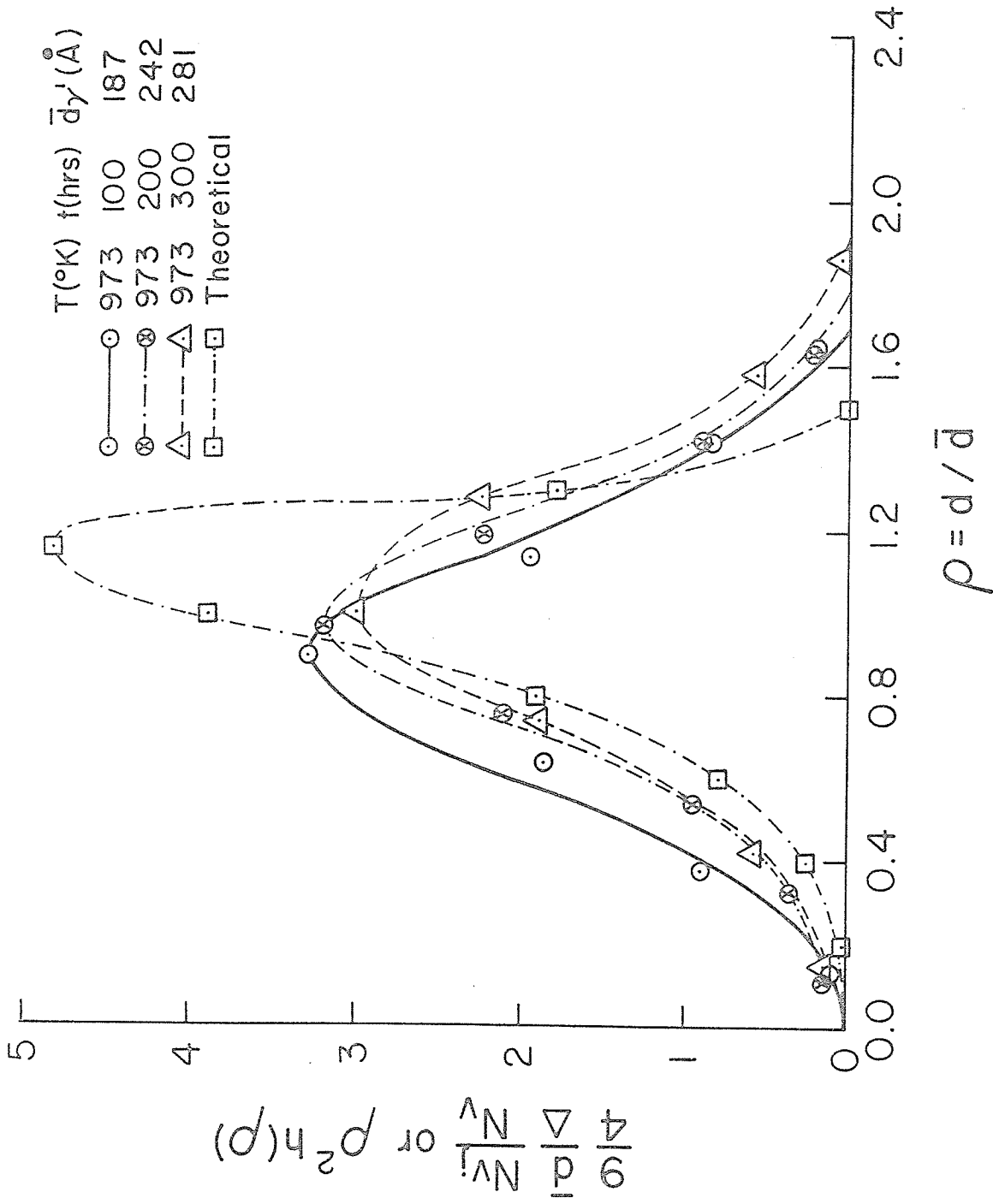


Figure 35A

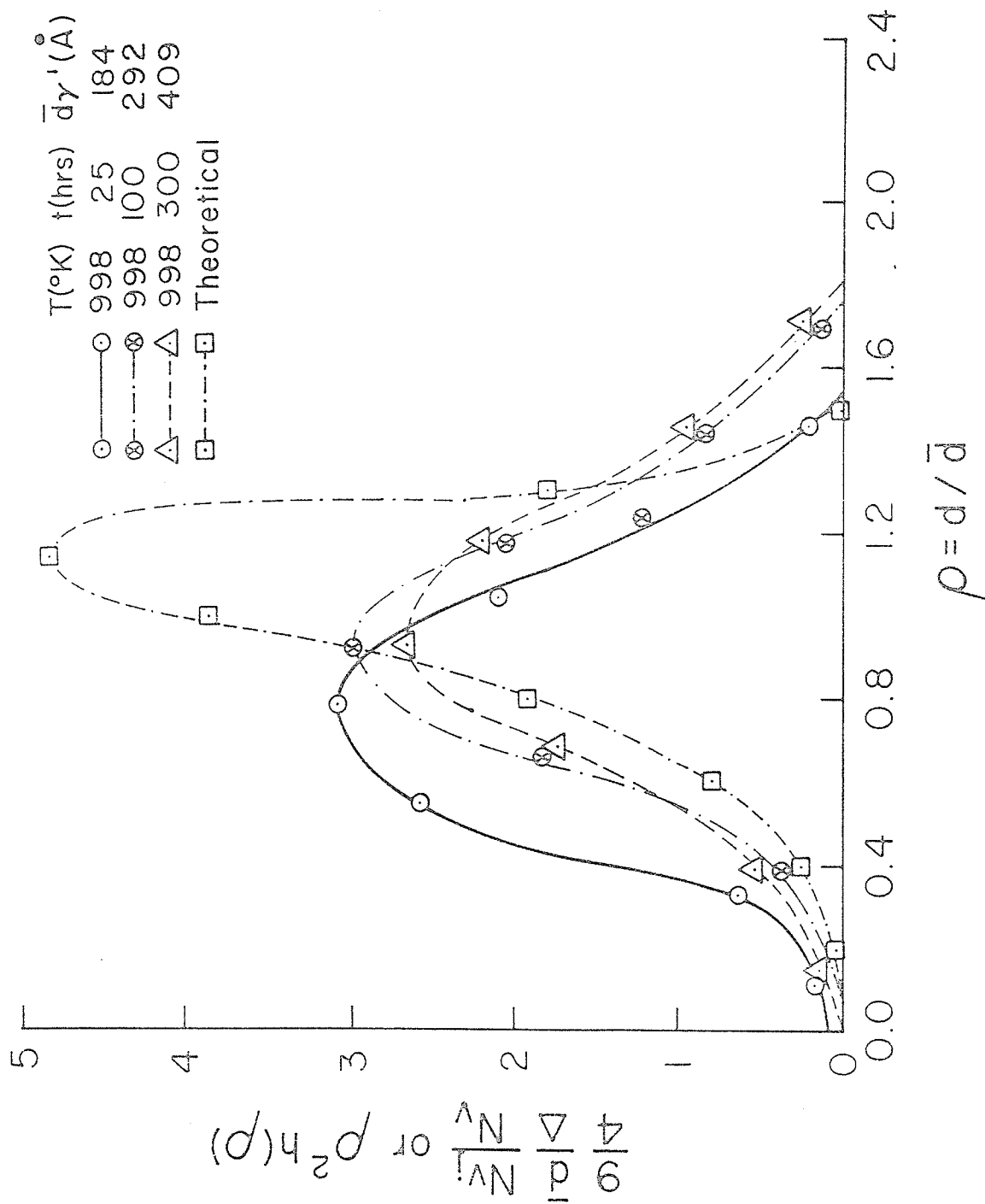
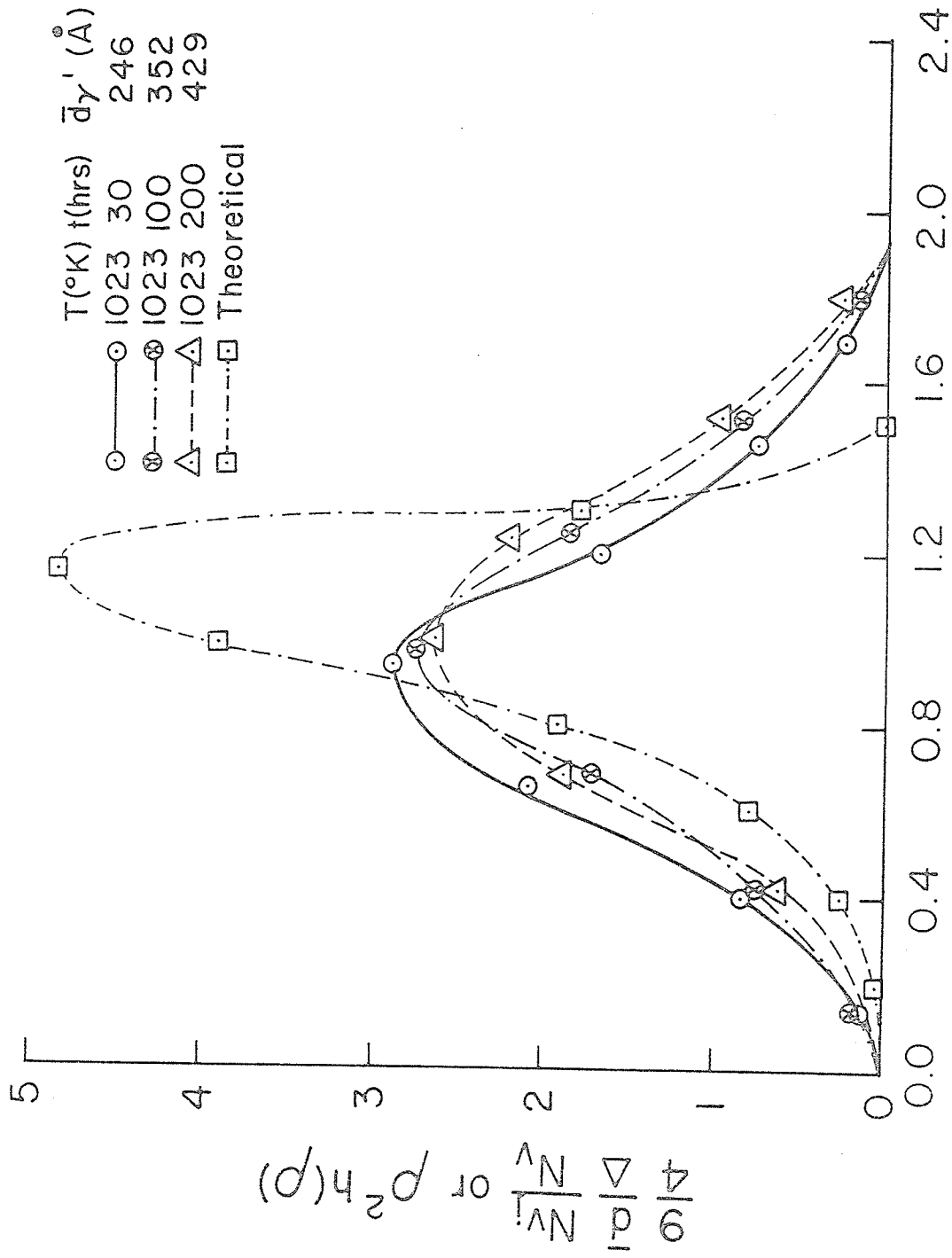


Figure 35B



$\rho = d/\bar{d}$

Figure 35C

Figure 36. Experimentally determined distribution curves of γ'' particle size for comparison with theoretical function $\rho^2 h(\rho)$.

- A. 973 K
- B. 998 K
- C. 1023 K

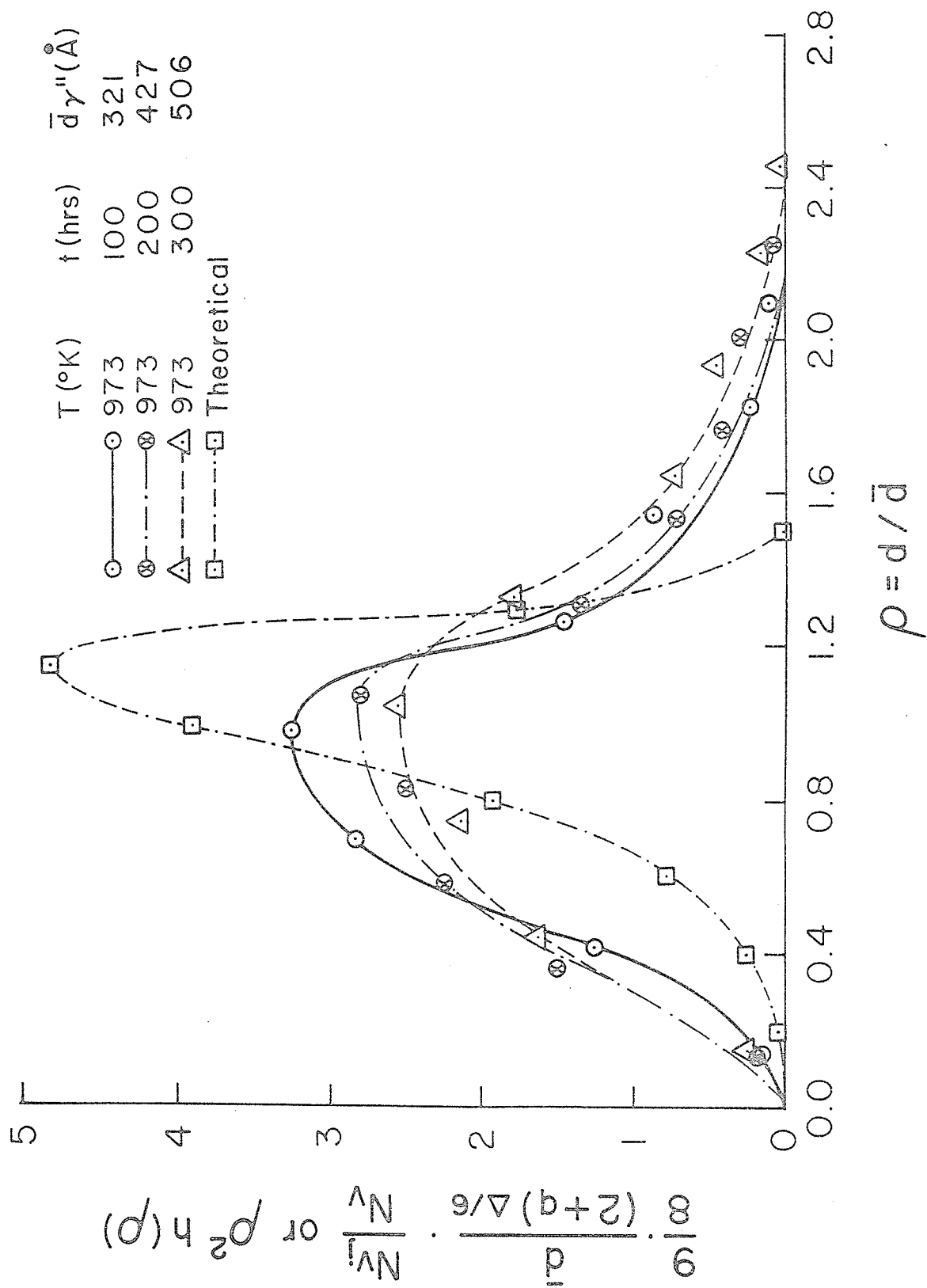
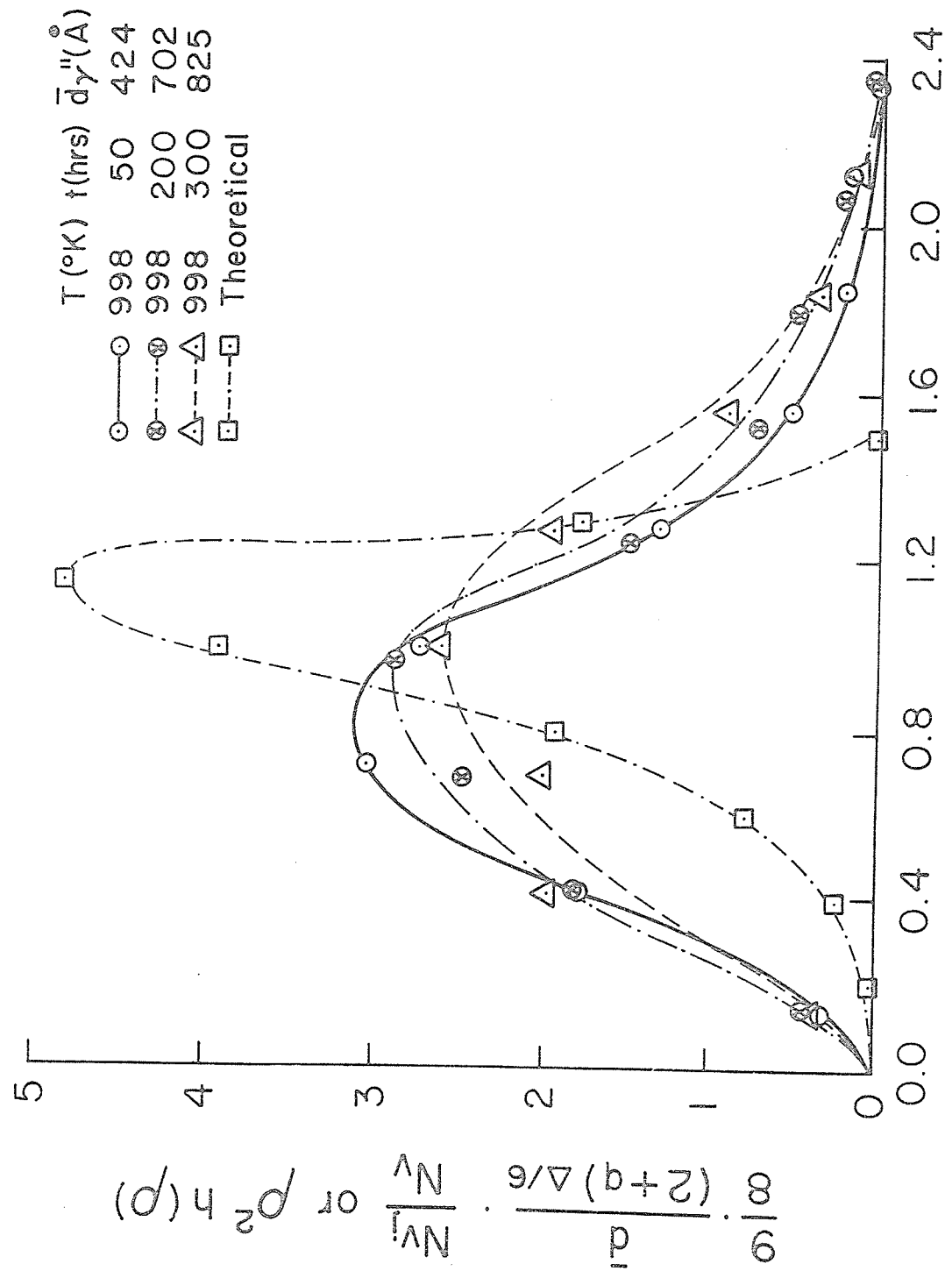


Figure 36A



$\rho = d/\bar{d}$
Figure 36B

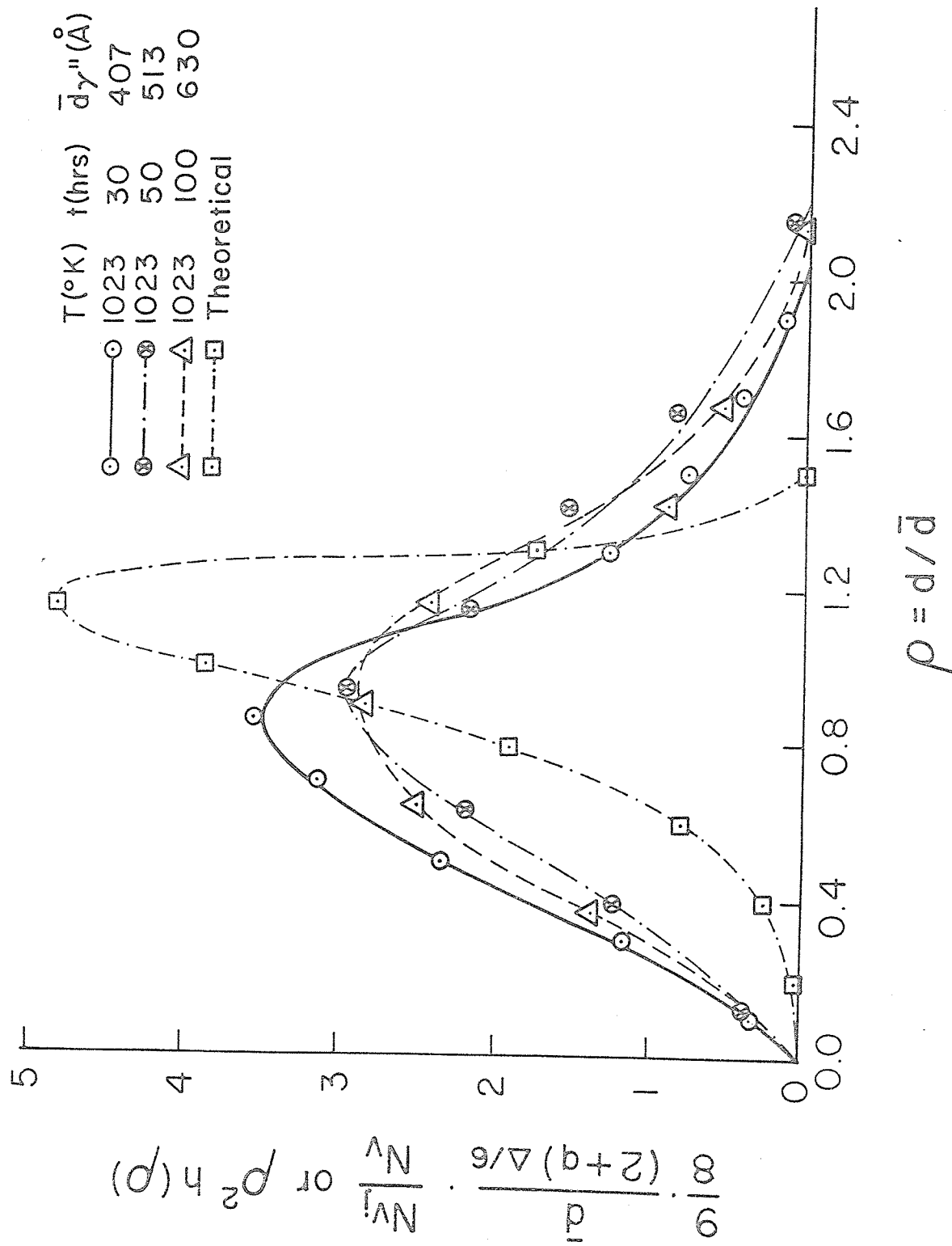


Figure 36C

CHAPTER 5

DISCUSSION

As observed in Chapter 4, the precipitation and growth behaviour of this alloy is a rather complex process since there are two major strengthening precipitates presented in it. Although they have different morphologies, i.e. γ' being spherical and γ'' being disc shaped, they have the same chemical formula, Ni_3X , as well as ordered structures. Therefore, not only the composition of these two phases is uncertain but also they may interact with each other during their precipitation and growth. In this chapter the results of the present investigation are discussed.

5.1 Precipitation behaviour5.1.1 The presence of precipitates in solution treated condition

As mentioned in Chapter 4, in the micrographs of solution treated condition there exist some rippled regions, which could be due to the presence of very fine precipitate particles or ordered G.P zones which are only few atoms in size and could have formed during the early stage of decomposition^(34, 35). Thermodynamically, the solubility

of solute atoms usually decreases with a decrease in temperature. Therefore, during quenching from high temperature (1473 K) the degree of supersaturation increases very rapidly, i.e., the free energy of the system increases greatly. This causes the precipitation process, which can decrease the supersaturation and hence cause a decrease in the free energy of the system to occur. Since diffusion distances for the nucleation and growth during the early stages of precipitation are very small, the short time available during the quenching process can be sufficient for the formation of new precipitates. These precipitate particles did not give rise to any extra diffraction spots in the electron diffraction patterns, which could be due to their small size and volume fraction. However, the x-ray diffractometer results did show the presence of a few strong peaks which could be due to the presence of γ'' and γ' phases in the solution treated specimen, as shown in Table 2. This would confirm the observation of bright field electron microscopy that a small amount of γ'' and γ' phases forms during quenching from the solution heat treatment temperature.

5.1.2 Lattice parameter of γ matrix

The lattice parameter of the solution treated supersaturated solid solution has been determined in this alloy to be 3.606 \AA , which is slightly higher than the reported value of $a_{\gamma} = 3.60 \text{ \AA}$ ⁽²⁹⁾ for Inconel 718. This small difference may be due to the difference in the compositions between the two materials. In solution treated condition the total number of solute atoms and their sizes will govern the lattice parameter. It is found that the atomic sizes of all the solute atoms in this alloy are larger than nickel itself⁽³⁶⁾, i.e., for the coordination number of 12 the values of atomic diameter of various solute atoms is as follows, $d_{Ni} = 2.49 \text{ \AA}$, $d_{Al} = 2.80 - 2.85 \text{ \AA}$, $d_{Ti} = 2.93 \text{ \AA}$, $d_{Nb} = 2.94 \text{ \AA}$, $d_{Cr} = 2.57 \text{ \AA}$, $d_{Mo} = 2.80 \text{ \AA}$ and $d_{Fe} = 2.54 \text{ \AA}$. Therefore it is reasonable that the more solute atoms the larger the lattice parameter, and the observed variation could imply a slightly greater number of solute atoms. A larger value of a_{γ} may also be due to the presence of coherent precipitates of γ' and γ'' whose lattice parameters are larger than that of the matrix.

5.1.3 Volume fraction of precipitates

The experimental results (Figure 26 and Table 4) show that during the early stage of aging, i.e., within 5 hours

at 1023 K, 10 hours at 998 K, 30 hours at 973 K, the volume fraction of precipitates increases with increasing aging time. This indicates that during this stage of the aging process the growth of precipitates involves precipitation of solute atoms from the supersaturated solid solution. The length of time required for this process to be completed increases with a decrease in aging temperature, suggesting that the process of growth of precipitates still involves lattice diffusion, since the higher the temperature the faster the diffusion process. The volume fraction of the precipitate in the equilibrium condition decreases with increasing aging temperature. This is attributed to the higher solubility of solute atoms at higher temperature, which has also been observed by other investigators⁽⁵⁾.

5.1.4 Interaction between γ' and γ'' phases

As shown in Figure 23, the structure of BCT (DO_{22}), γ'' phase and FCC (LI_2) γ' phase have similarities and some formula Ni_3X , suggesting that they have some proportion of Nickel atoms and Al, Ti or Nb atoms. Therefore transformation from γ' to γ'' or γ'' to γ' seems to be an easy process as it only needs to rearrange a portion of the atoms

inside the precipitate. The evidence of such an interaction between γ'' and γ' phases has been observed in many field micrographs during this investigation. A typical one with this kind of interaction is shown in Figure 37. In this micrograph, many γ' and γ'' precipitates can be seen to be in contact with each other. Some of them have even lost their interfacial boundaries between them, which suggests that they have good compatibility and could transform to each other under certain conditions. Another interesting feature seen in Figure 37 is that some particles have γ' morphology, i.e., spherical shape, but they have much stronger contrast than the normal γ' particles, which is similar to the γ'' particles contrast. This may be due to the presence of some BCT atomic arrangement of γ'' inside the high contrast γ' particles. Furthermore, it can be seen that some combined particles of γ' and γ'' consist of disc shaped γ'' and hemispherical γ' particles. The contrast of γ' phase in this situation is different, i.e., some of them are of very high contrast while the others are of normal low contrast. This could suggest a process of transformation of one precipitate particle to another. The interaction of γ' and γ'' particles makes the measurement of particle size difficult and could be one source of error in the particle size measurements.

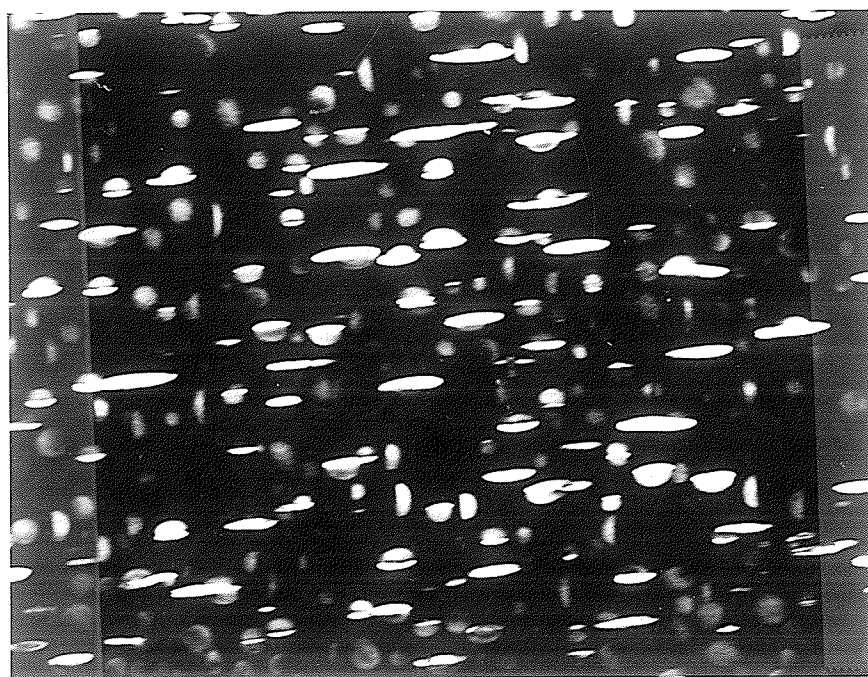


Figure 37. Microstructure of the specimen aged for 100 hours at 998 K, showing the interaction between γ' and γ'' . (001) orientation Dark field, 120000 x.

5.2 Growth kinetics

The results, as shown in Table 7 and Figures 30, 31 and 32, indicate that the precipitate size is proportional to the cube root of the aging time for both the γ' and γ'' precipitate in Inconel 718 at all the three aging temperatures, which is the basic and most important requirement of the LSW theory of lattice diffusion controlled growth.

The observed values of \bar{d}_0 obtained from the extrapolated lines are not exactly zero, which may be due to the presence of the precipitates before aging as suggested by electron micrograph shown in Figure 18. It is also possible that it is partly due to the error in the measurements of particle sizes. However, the values of \bar{d}_0 are very small in all cases for both γ' and γ'' phases, and they can be neglected during the subsequent analysis in this study.

Another requirement of LSW theory of lattice diffusion controlled growth is that the activation energy for the coarsening process should be equal to the activation energy of diffusion of solute atoms in the matrix. The activation energy for the growth of γ'' and γ' phases in this alloy is nearly the same, i.e., 298 and 271 KJ mol⁻¹, respectively.

The γ'' phase is based on Ni_3Nb and γ' is based on Ni_3 (Al, Ti). However, extensive amounts of other alloying elements such as Mo, Cr, Fe, etc., will also be present in both γ'' and γ' phases as has been observed in other alloys^(37, 38), and also the Nb atoms in Ni_3Nb γ'' phase can be replaced by Al and Ti atoms and Al, Ti atoms in Ni_3 (Al, Ti) can be replaced by Nb atoms. This means that the growth of both γ' and γ'' will require diffusion of similar type of alloying elements. Therefore, the activation energy for the growth of γ'' and γ' should be nearly the same and dependent on the activation energy for diffusion of Nb, Ti, Al, Fe, Cr and Mo atoms in Ni. The activation energies for diffusion of Ti and Al in Ni are found to be 257 and 270 kJ mol^{-1} , respectively⁽²⁹⁾, and that of Fe and Cr in Ni-Cr-Fe system^(39a) in the temperature range of 923 - 1673 K to be 276 - 288 kJ mol^{-1} and 283 - 293 kJ mol^{-1} , respectively. The activation energy for diffusion of Nb in Ni-Fe-Nb system^(39b, 39c) in the temperature range of 973 - 1373 K has been reported to be 252 - 280 kJ mol^{-1} . Therefore, the observed values of the activation energy for the growth of both γ'' as well as γ' phase in Inconel 718 are similar to that of the activation energy for the diffusion

of solute atoms in Ni and Nickel base alloys. This also suggests that the growth of γ' and γ'' phases follows the LSW theory of diffusion controlled growth.

5.3 The distribution of particle size

A major discrepancy between the results of the present investigation and prediction of the LSW theory has been observed in the distribution of both the γ' and γ'' phase particles at all the three aging temperatures. According to the LSW theory, during the steady-state coarsening process the distribution of precipitate particles is skewed towards larger particle size, i.e., the maximum occurs at $\rho = 1.135 \bar{d}$ as shown in Figures 33 - 36 and has a sharp cut-off at $\rho = 1.5 \bar{d}$. The experimental particle size distributions of both γ' and γ'' seem to be in a quasi steady-state but they are much broader than the theoretical distribution, especially for γ'' particles, i.e., the maximum cut-off size is about $1.7 \sim 2.0 \bar{d}$ for γ' phase and $2.2 \sim 2.4 \bar{d}$ for γ'' phase. The maxima in the distribution curves also occur at a small value of ρ , i.e., the experimental distribution curves are much flatter than the theoretical curves. It is also seen that the maxima in all the distribution curves is much smaller than the theoretically predicted value.

The distribution of both phases, however, is similar to that observed in other γ' and γ'' precipitation strengthening alloys^(1-6, 9-12).

Such a broad distribution could arise principally from two factors. Firstly, the volume fraction of precipitate may influence the particle size distribution. secondly, the lattice misfit between the precipitate and matrix may broaden the distribution.

It has been generally considered in many investigations that the broad distribution could be attributed to the presence of lattice misfit of precipitate/matrix, i.e., the larger the mismatch the larger is the deviation from the theoretical cut-off value of $1.5 \bar{d}$ ⁽⁴⁾. This trend has been found in many alloy systems^(5, 6, 8). For example, for the Ni-Cr-Al system⁽⁵⁾ with 0.1% misfit the deviation is nearly zero, whereas for the Ni-Ti system⁽⁴⁾ with 0.9% misfit, the deviation is about 40%. In the case of Co-Ni-Cr-Ti system⁽⁶⁾ where the mismatch is 1.3% the deviation in cut-off value was observed to be 36%. In the alloy used during this investigation the misfit between γ' and matrix is about 0.4% and the deviation is about 20%, while for γ'' precipitates with a tetragonal distortion of 2.7%, the

deviation is larger than 50%. It has been suggested that a large lattice misfit provides a large strain energy around the particles which increases the driving force for the coalescence of particles resulting in a large cut-off value⁽⁴⁾. This might explain a larger cut-off value of γ'' particles than that for γ' particles.

Another reason for the difference between the theoretical and experimental particle size distribution could be due to the effect of volume fraction on coarsening process suggested by Ardell⁽²³⁾ and Davies et. al⁽²⁴⁾, as discussed in Chapter 2. As seen in Figures 14 and 16, both the MLSW theory and LSEM theory predict that when volume fraction increases the maximum in the distribution curves becomes smaller and the value of the cut-off point ρ_c becomes larger. Therefore the distribution curve becomes flatter and more symmetrical. In this investigation, the volume fraction of $(\gamma' + \gamma'')$ is about 15.4 to 17.5% which is far from the assumed value of the volume fraction by the LSW theory, i.e., zero. The influence of volume fraction of precipitate particles in the form of "necks" between the growing particles has been observed in the present investigation. Examples of such necks are shown in Figures 22, 24 and 25. It is considered that the "necks" are the results of the "encounter" between two growing particles

suggested by the LSEM theory. It should also be noted that the "encounter" process may occur not only between two γ'' particles but also between γ'' and γ' particles since both γ' and γ'' phases contain nearly the same elements as discussed earlier. Therefore, although the volume fraction of γ' phase is relatively small, i.e., 3-5%, its coarsening process may also be influenced by "encounter" with neighbouring γ'' particles and vice versa. This is confirmed by the observed compact morphology which is a combination of γ'' and γ' particles in many dark field micrographs. The "encounter" effect should be expected to be more evident for γ'' because of its larger volume fraction and disc shape, which make the "encounter" process easier than for the γ' particles. This "encounter" mechanism is also suggested by the observation that the aspect ratio of γ'' , $q = d/h$, increases slightly with increasing aging time.

Therefore, the shape of the distribution curves of γ'' and γ' particles, which have large cut-off value, are symmetrical and have a significantly lower maxima than the theoretical curve can be explained better by the LSEM theory than by the LSW or the MLSW theory.

CHAPTER 6

CONCLUSIONS

1. The disc shaped ordered BCT γ'' precipitate and spherical ordered FCC γ' precipitate are present simultaneously in the FCC matrix when Inconel 718 is aged in the 973 - 1023 K temperature range. The precipitation process occurs very rapidly and some precipitates form during water quenching.
2. The lattice misfit of γ' /matrix is about 0.4% and the tetragonal distortion of γ'' /matrix is about 2.7%.
3. The total volume fraction of γ'' and γ' precipitates decreases with increasing aging temperature and the ratio of volume fraction of γ'' and γ' is between 2.5 - 3.8.
4. The particle size of γ'' and γ' are proportional to the cube root of aging time, t , and the activation energy for the coarsening process of both γ' and γ'' particles is in good agreement with that of diffusion of solute atoms in nickel and nickel base alloys. This indicates that the coarsening process of both γ'' and γ' precipitates in this alloy follows

the Lifshitz-Wagner theory of lattice diffusion controlled growth.

5. The particle size distribution of both γ'' and γ' phases at all the aging temperatures differs significantly from that predicted by Lifshitz-Wagner theory. This could be due to the effect of "encounters" between the growing particles and also due to the large lattice mismatch between the precipitates and matrix.

REFERENCES

1. A. J. Ardell and R.B. Nicholson, *Acta. Met.*, 1966, Vol. 14, p. 1295.
2. A.J. Ardell and R.B. Nicholson, *J. Phys. Chem. Solid*, 1966, Vol. 27, p. 1793.
3. P.K. Rastogi and A.J. Ardell, *Acta, Met.* 1971, Vol. 19, p. 321.
4. A.J. Ardell, *Met. Trans.*, 1970, Vol. 1, p. 525.
5. M. Chaturvedi and D.W. Chung, *J. of Metals*, 1973, Vol. 101, p. 253.
6. M.C. Chaturvedi and D.W. Chung, *Met. Trans.*, 1979, Vol. 10A, p. 1579.
7. M. Lifshitz and V.V. Slyozov, *J. Phys. Chem. Solids*, 1961, Vol. 19, p. 35.
8. C. Wagner, *Z. Electrochemi*, 1961, Vol. 65, p. 581.
9. M. Raghavan, *Met. Trans.*, 1977, Vol. 8A, p. 1071.
10. H.A. Moreen, R. Taggart and D.H. Polonis, *Met. Trans.*, 1974, Vol. 5, p. 79.
11. P.S. Kotoal, NASA Contract Rep. CR-52644, Dec. 1969, (Quoted in Ref. 10 above).
12. S.E. Axter and D.H. Polonis, *Mat. Sci. Eng.*, 1978, Vol. 36, p. 71.
13. P.M. Kelly, *International Metallurgical Reviews*, 1973, Vol. 18, p. 31.
14. L.M. Brown and R.K. Ham, 'Strengthening Mechanism in Crystals' (edited by A. Kelly and R.B. Nickolson), 1971.
15. H. Gleiter and E. Hornbogen, *Mat. Sci. Eng.*, 1967, Vol. 2, p. 285.
16. J. W. Martin, 'Micromechanicsms in Particle-hardened alloys', published by the press syndicate of the University of Cambridge, 1980.

17. D. Raynor and J.M. Silcock, *Met. Sci. J.*, 1970, Vol. 4, p. 121.
18. R.G. Davies and N.S. Scollof, *Trans. Met. Soc., AIME*, 1965, Vol. 233, p. 714.
19. M.C. Chaturvedi, D.J. Lloyd and D.W. Chung, *Met. Sci. J.*, 1976, Vol. 10, p. 373.
20. M.C. Chaturvedi and Y.F. Han, unpublished paper.
21. C.T. Sims and W.C. Hagel, 'The Superalloys', 1972.
22. J.W. Martin and R.D. Doherty, 'Stability of Microstructure in Metallic Systems', Cambridge University Press, 1976.
23. A.J. Ardell, *Acta Met.*, 1972, Vol. 20, p. 61.
24. C.K.L. Davies, P. Nash and R.N. Stevens, *Acta Met.*, 1980, Vol. 28, p. 179.
25. A.J. Ardell, 'The Mechanism of Phase Transformations in Crystalline Solids', published by the Institute of Metals, 1969, p.111.
26. E. Hornbogen and M. Roth, *Z. Metallkunde*, 1967, Vol. 58, p. 842.
27. 'The Superalloys', Textbook of Mat. Sci. Dept. Jiaotong, Univ., Shanghai, China, 1976.
28. D.F. Paulonis, J.M. Oblak and D.S. Duvall, *Trans. A.S.M.*, 1969, Vol. 62, p. 611.
29. R.A. Swalin and A. Martin, *Trans. Met. Soc. AIME*, 1956, Vol. 206, p. 567.
30. R. Cozar and A. Pineau, *Met. Trans.*, 1973, Vol. 4, p. 47.
31. J.D. Boyd and R.B. Nickolson, *Acta Met.*, 1971, Vol. 19, p. 1379.
32. J.W. Cahn and J. Nutting, *Trans. Met. Soc. AIME*, 1959, Vol. 215, p. 526.

33. P. Deb and M.C. Chaturvedi, 'Coarsening Behaviour of Cementite Particles in Ferrite in 101330 Steel', to be published.
34. M.V. Heimendahl, 'Electron Microscopy of Materials', published by John Wiley and Sons, Inc., 1962, p. 238.
35. Gareth, Thomas, 'Transmission Electron Microscopy of Metals', published by John Wiley and Sons, Inc., 1962, p. 238.
36. Z.Y. Xu, 'Physical Metallurgy', Science and Technology Edition Company, Shanghai, China, 1964, pp. 33-42.
37. J. Mihalism and D. Pasquine, 'Phase Transformation in Nickel-Base Alloy', International Symposium on Structural Stability in Super Alloys, Seven Springs, Pennsylvania, 1968.
38. O.H. Kruge and C.P. Sullivan, Trans. ASM, 1968, Vol. 61, p. 278.
39. Diffusion and Defect Data Journal,
 - 36a 1980, Vol. 22, p. 63
 - 36b 1975, Vol. 11, p. 73
 - 36c 1980, Vol. 22, p. 98.